Novel Ultra Wideband Antennas for Wireless Systems

Abdallah A. Alshehri

A Thesis

in

The Department

of

Electrical and Computer Engineering

Presented in Partial Fulfillment of the Requirements

for the Degree of Master of Applied Science (Electrical Engineering) at

Concordia University

Montreal, Quebec, Canada

July 2008

Your file Votre référence
ISBN: 978-0-494-45272-1
Our file Notre référence
ISBN: 978-0-494-45272-1

ABSTRACT

Novel Ultra Wideband Antennas for Wireless Systems

Abdallah A. Alshehri

This thesis focuses on Ultra Wideband (UWB) antenna designs and analysis. Studies have been undertaken covering the areas of UWB fundamentals and antenna theory. UWB wireless technology is being considered as the solution to overcome data rate bottlenecks in the wireless communications and applications. UWB is able to achieve high data transmission rates because it transmits data over a very large spectrum of frequencies from 3.1 GHz to 10.6 GHz (7.5 GHz). Consequently, it provides many challenges for design in the communications arena, including antenna design.

The main objective of this thesis is to study, design, analyze and implement novel UWB low profile printed patch antennas that satisfy UWB technology requirements. Several techniques are used for optimal UWB bandwidth performance of the UWB antenna designs in this thesis. The undertaken thesis focuses on planar antennas printed on PCBs. Therefore, this research introduces novel five designs of microstrip-fed, small, low-profile, printed microstrip UWB antennas using different bandwidth-enhancement techniques to satisfy UWB bandwidth. According to their geometrical shapes, they can be classified into two types: the first types are stepped UWB antennas which are namely: a stepped-trapezoidal patch antenna and a trimmed notch-cut patch antenna. The second

ones are beveled UWB antennas which are namely: an elliptical patch antenna, a double-beveled patch antenna, and a band-rejected elliptical patch antenna.

It has been demonstrated numerically and experimentally that the proposed antennas are suitable for UWB systems. They can provide satisfactory frequency domain performance, including ultra-wide bandwidth with nearly omni-directional radiation patterns, relatively flat gain and very good radiation efficiency. These features make them very suitable for UWB communications and applications, such as wireless personal area networks (WPANs) applications.

DEDICATION

This dissertation is dedicated in memory of Awadh Al-Shehri (my father) who passed away during the course of my graduate studies. He taught me discipline, hard work and sense of purpose, without which my studies would not have been accomplished.

ACKNOWLEDGMENTS

I am very thankful to God for giving me the strength and inspiration to do this work.

I owe my gratitude to all the people who have made this thesis possible and because of whom my graduate experience has been one that I will cherish forever.

First and foremost, I would like to express my deepest gratitude to my thesis supervisor, Professor Abdel Razik Sebak for his encouragement, guidance, valuable advice and endless support. He is the one who motivated and led me onto the research path. Without his encouragement, this work would not have been possible. Working with him has been a true privilege. He stimulated me to perform to the best of my ability as well as provided me with opportunities and exposure I never would have had if I had not joined him. For that, I am extremely grateful.

My sincere gratitude is also given to Professor Tayeb A. Denidni, Institut National de la Recherche Scientifique (INRS-EMT), Université de Québec, for devoting his laboratory and technician to perform my very necessary anechoic chamber measurements. He also provided a great amount of insight and advice.

I would also like to thank Mr. Jules Gauthier at the Poly-Grames Research Center, École Polytechnique de Montréal, for his professional job in fabricating the various antennas.

Special thanks goes out to my great colleagues and friends: S. Koodiani for his exceptional assistance in conducting the radiation experiments, Aidin M. for his stimulating discussions and technical suggestions, and Wadah M. for heartiest advice, goodwill and for boosting my morale at difficult times throughout my studies and

research.

I also gratefully acknowledge Saudi Aramco (my employer) for granting me a scholarship to pursue my Master degree. This work would not have been possible without the financial support provided.

Above all, I am forever genuinely thankful to my parents for their love and selflessness, for instilling in me the belief that anything is possible, and for working intensely during their entire life to provide to me and my brothers and sisters everything without asking for anything in return. This work is dedicated to my father who passed away during the course of my graduate studies.

I have immense appreciation for my brother, Mohammad, who I consider to be my second father. I thank him for his persistent support and encouragement in all aspects of my life including my educational life. I would not be who I am without his great guidance and inspiration.

Finally, I would like to express my sincerest gratitude to my wife who always provides support and walks this long journey with me. I thank her for sharing both the joys and burdens of this journey as well as for her unconditional love that has made all this possible.

TABLE OF CONTENTS

CHAPTER 5

LIST OF FIGURES

LIST OF TABLES

LIST OF ABBREVIATIONS

2D	Two-Dimensional
3D	Three-Dimensional
ABW	Absolute Bandwidth
AWGN	Additive White Gaussian Noise
BW	Bandwidth
CE	Consumer Electronics
DUT	Device Under Test
DVD	Digital Video Disc
EM	Electromagnetic
FBW	Fractional Bandwidth
FCC	Federal Communications Commission
FEM	Finite Elements Method
GPS	Global Positioning System
GSM	Global System for Mobile Communication
HFSS	High Frequency Structure Simulator
I/O	Input/Output
IEEE	Institute of Electrical and Electronics Engineers
LANs	Local Area Network
LTCC	Low-Temperature Cofired Ceramic
MP3	Moving Picture Experts Group Layer-3 Audio
PC	Personal Computers

PCB	Printed Circuit Board
PDAs	Personal Digital Assistants
PDE	Partial Differential Equation
PICA	Planar Inverted Cone Antenna
PSD	Power Spectral Density
RF	Radio Frequency
RL	Return Loss
RLC	Resonant Circuit
RT	Rogers Technology
USB	Universal Serial Bus
UWB	Ultra Wideband
VSWR	Voltage Standing Wave Ratio
Wi-Fi	Wireless Fidelity
WLAN	Wireless Local Area Network
WPAN	Wireless Personal Area Networks

LIST OF SYMBOLS

θ	Elevation Angle
ϕ	Azimuth Angle
π	Mathematical Constant Equal to 3.14159
η	Intrinsic Impedance
λ	Wavelength
ε_r	Relative Dielectric Of The Substrate
Γ	Reflection Coefficient
ε_{reff}	Effective Relative Permittivity
θ	Angle
θ_1	Angle of the First Bevel
θ_2	Angle of the Second Bevel
Ω	Ohm
V_0^-	Reflected Wave
V_0^+	Incident Wave
V_{max}	Amplitudes of the Maximum Standing Wave
V_{min}	Amplitudes of the Minimum Standing Wave
A	Very Sparse Matrix
a	Semi-Major Axes of the Ellipse
B	Channel Bandwidth
B	Known Matrix

b	Semi-Minor Axes of the Ellipse
C	Maximum Transmit Data Rate
C	Light Speed
D	Directivity
dB	Decibel
dBm	Power Ratio in Decibels Referenced to One Milliwatt
D_o	Maximum Directivity
E	Electric-Field
e_0	Total Efficiency
e_{cd}	Conduction and Dielectric Efficiency
e_r	Reflection Efficiency
f	Frequency
f_H	Upper Frequency
f_L	Lower Frequency
G	Gain
g	Feed Gap
GHz	Gigahertz
G_o	Maximum Gain
H	Magnetic-Field
h	Thickness of The Substrate
h	Feed Gap
h	Height of the Trapezoidal Patch
h_1	Height of the First Step

h_2	Height of the Second Step
J_1	Characteristic Mode 1
J_2	Characteristic Mode 2
J_3	Characteristic Mode 3
Jn	Characteristic Modes
L	Monopole Length
l	Height of the Cylindrical Wire
L1	Slot Parameter 1
L2	Slot Parameter 2
L3	Slot Parameter 3
L_g	Length of the Ground Plane
l_s	Length of the Notch Cut
L_{sub}	Length of the Substrate
MHz	Megahertz
mm	Millimeter
P_{rad}	Total Radiation Power
R	Resistance
r	Radius
r_a	Semi-Minor Axes of the Elliptical Patch
r_b	Semi-Major Axes of the Elliptical Patch
S_{11}	Forward Reflection
S_{12}	Reverse Transmission
S_{21}	Forward Transmission

S_{22}	Reverse Reflection
S_n	S Parameters
SNR	Signal-to-Noise Ratio
U	Radiation Intensity
U_{max}	Maximum Radiation Intensity
U_o	Radiation Intensity of Isotropic Source
W	Watts
W	Width of the Strip
W	Width of the Trapezoidal Patch Base
W_1	Width of the Trapezoidal Patch Base
w_1	Width of the First Step
w_2	Width of the Second Step
w_f	Width of the Feed
w_s	Width of the Notch Cut
W_{sub}	Width of the Substrate
X	Unknown Matrix
Z_{line}	Line Impedance
Z_{load}	Load Impedance
Z_o	Characteristic Impedance

CHAPTER ONE

Introduction

1.1 Introduction

Wireless communication technology plays a crucial role in our daily lives today. Actually, it has changed our lives during the past two decades. Satellite TV has allowed people around the world to instantly watch international events, World soccer, and any news. Cellular phones have given us more freedom such that we can communicate with each other without geographical location limitations. Wireless modem, walkie-talkie, and radio broadcasting have provided great services to our lives. Moreover, in homes and offices, cordless phones have freed us from the short-cabled handset. Furthermore, wireless local area network (WLAN) technology provides us with access to the internet without using cables. Also, the conventional wireless networking technologies, such as wireless personal area networks (WPAN), wireless fidelity (Wi-Fi) and bluetooth technology, have provided a great wireless lifestyle. However, they are not optimized for multiple high data rate streams [1,2]. Although they have supported data rates that can reach 54 Mbps for Wi-Fi, there are limitations in consumer electronics (CE) environments, such as power consumption and

bandwidth [2].

The admirable benefits of a wireless lifestyle have resulted in a huge demand for advanced wireless communication. In recent years, more worldwide interest has been paid into wireless personal area network (WPAN) technology since it reliably links wireless portable devices such as mobile phones, personal digital assistants (PDAs), media players, digital cameras and other consumer electronics in homes and offices. In addition, fast data storage and exchange between these devices have been desired. These multimedia applications require high-bandwidth usage which is much higher than what can be achieved through currently existing conventional wireless technologies [3].

Data communications are based upon the relationship discovered by Claude Shannon and Robert Hartley of Bell Labs. As shown in Equation 1.1, The maximum achievable data rate or capacity for the ideal band-limited additive white Gaussian noise (AWGN) channel is related to the bandwidth and signal-to-noise ratio (SNR) by Shannon-Nyquist criterion [4, 5].

$$C=B\log_2(1+SNR) \quad [\text{b/s}] \qquad (1.1)$$

Where, C is the maximum transmit data rate, B is the channel bandwidth and SNR is the signal-to-noise ratio.

Equation 1.1 designates that the transmit data rate can be increased by broadening the bandwidth occupation or increasing transmission power. In other words, it indicates that channel capacity increases linearly with bandwidth and decreases logarithmically as the SNR decreases. In conventional data communications and wireless applications, the frequencies of operation and bandwidth are fixed and strictly regulated. Therefore, higher speeds can only be attained with higher signal power. However, the transmission power is not easily increased since most of portable devices are battery-powered dependent and also

to avoid the potential interference generated form high transmitting power. Consequently, since the data rate scales linearly with bandwidth, a large spectrum frequency bandwidth will be the solution to achieve high data rate [3].

In February 2002, a wide new spectral band of 7.5 GHz was released for unlicensed use when the Federal Communications Commission (FCC) adopted the First Report and Order that permitted the commercial operation of ultra wideband (UWB) technology [6]. Since then, it has received high attention and has been considered as one of the most promising wireless technologies to revolutionize high data rate transmission such as through-wall radar and extremely fast bit rate wireless networking. UWB technology has offered important advantages not achievable by conventional narrowband technology. UWB radio technology for wireless communications has the capability of delivering a performance that can not be attained by conventional narrowband wireless technologies. In particular, UWB technology has many advantages, such as low power consumption, high speed transmission, immunity to multi-path propagation, and simple hardware configuration [8]. Therefore, it can support faster, high-quality, low cost and more power efficient wireless systems, and features more precise localization and positioning capabilities in comparion with conventional wireless technologies [7, 8]. Also, by using pulsed, broad spectrum, low power signals, UWB technology causes less interference than conventional narrowband wireless systems and can therefore coexist with other wireless technologies such as Wireless Local Area Network (WLAN) as well as other UWB systems. These unique advantages of UWB technology are very adequate for many communications systems like Wireless Personal Area Networks (WPAN) and Radars. UWB radar communication technology is a candidate for many applications like imaging, detection, mining, and positioning since UWB signals furnish the scene of fine range resolution, remote sensing,

low probability of interception, ground penetration and frequency spectrum sharing, among others [9].

UWB communication techniques have attracted a great deal of interest both in the academia and industry in the past few years because of the high merit of their advantages. Therefore, academic and industrial research has been devoted toward developing components and systems for UWB communications. All wireless systems and applications including UWB ones need a mean of transferring energy or signal from the apparatus to free space in the form of electromagnetic waves or vice versa which is an antenna. It has been recognized as a critical element of the successful design of any wireless device since the wireless systems are highly dependent on their antenna characteristics. Based on that, UWB antennas have been an important and active area of research and have presented antenna engineers with major design challenges.

1.2 Motivation

In recent years, many significant developments and high attention are being paid to UWB Technology since the FCC allocated 3.1 – 10.6 GHz of the frequency spectrum for commercial UWB communications and applications [11]. The potential of UWB technology is enormous due to its tremendous advantages such as the capability to provide extremely fast data rates at short transmission distances while requiring low power dissipation. The attractive nature of UWB coupled with the rapid growth in wireless communication systems has made UWB an outstanding candidate to replace the conventional and popular wireless technology in use today like Bluetooth and wireless LANs [10].

A lot of research has been conducted to develop UWB LNAs, mixers and entire front-ends but not the same amount of research has initially been done to develop UWB antennas. Later [11-14], academic and industrial communities have realized the tradeoffs between antenna design and transceiver complexity. In general, when new advanced wireless transmission techniques have been introduced, the transceiver complexity has increased. To maximize the performance of transceiver without changing its costly architecture, advanced antenna design should be used since the antenna is an integral part of the transceiver. Also, it has played a crucial role to increase the performance and decrease the complexity of the overall transceiver [10].

To maturate UWB technology, there are many challenges that must be overcome. One fundamental challenge is to design UWB antennas that can satisfy the requirements of this technology. UWB has a significant effect on antenna design. UWB has attracted a surge of interest in antenna design by providing new challenges and opportunities for antenna designers since UWB systems require an antenna that can accommodate UWB bandwidth and is capable of receiving on associated frequencies at the same time [15]. Consequently, the antenna behavior and performance have to be consistent and predictable across the entire band. The design of UWB antennas has required different considerations from those used in designing narrowband antennas. The main difference between narrowband antennas and UWB antennas is that UWB antennas radio signals are non-sinusoidal [16]. The hardest challenge in designing UWB antenna is attaining the wide impedance bandwidth while maintaining high radiation efficiency. UWB antennas have typically required achieving a bandwidth, which may reach greater than 100% of the center frequency to ensure sufficient impedance such that 10 % or less of incident signal is lost due to reflections at the antenna's input terminal [15]. A return loss of greater than 10

dB is necessary in obtaining high radiation efficiency. It is required since UWB transmission is very low power (below the noise floor level) and has a high sensitivity [10].

There are many classical broadband antenna configurations under consideration for use in UWB systems, such as a straight wire monopole that features a simple structure but has bandwidth of only around 10%. Also, a Vivaldi antenna is a directional antenna which accordingly is unsuitable for indoor wireless systems and portable devices [17]. A biconical antenna has a big size which makes its application very limited [18]. Spiral and log periodic antennas have drawbacks of severe ringing effect and dispersion [19]. The concurrent surge of wireless applications, with the high level of miniaturization and higher frequency of operation, has increased the interest in designing high performance antenna types. Therefore, the demand is rapidly growing for small and low cost UWB antennas that can provide satisfactory performance in both frequency and time domains.

In addition, the trend in modern wireless communication systems, including UWB based systems, are to build on small, low-profile integrated circuits in order to be compatible with the portable electronic devices. Therefore, one of the critical issues in UWB system design is the size of the antenna for portable devices, because the size affects the gain and bandwidth greatly. The use of a planar design can miniaturize the volume of the UWB antennas by replacing three-dimensional radiators with their planar versions. Also, their two-dimensional (2D) geometry makes the fabrication relatively easy. As a result, the planar antenna can be printed on a PCB and thus integrated easily into RF circuits [20].

In the last few years, this area of research has been very active, which is evidenced by the great number of published work since 2002. Several printed UWB antennas have been

designed however not all of them adequately meet the requirements for UWB communications [21]. So, great efforts are still ongoing in the antenna community to develop new UWB printed antennas having desired performance characteristics that are suitable for UWB communications and applications.

1.3 Objectives

The main objective of this thesis is to study, design, analyze and implement novel UWB low profile printed patch antennas that satisfy UWB technology requirements. The design and analysis of the proposed printed antennas for UWB communications and applications in the 3.1-10.6 GHz bandwidth are pursued using the commercially available full wave simulation software HFSS [22].

The undertaken thesis focuses on planar antennas printed on PCBs. They are desired in UWB wireless communications systems and applications, especially in portable devices and indoor applications because of their low cost, light weight and ease of implementation. However, it is a well-known fact that the bandwidth of patch antennas is narrow. Thus, many attempts have been made to broaden the bandwidth of printed antennas.

This research sets out to design five small, low-profile, printed microstrip UWB antennas using many bandwidth-enhancement techniques. Theses techniques are: a partial ground plane technique, an adjustment of the gap between radiating element and ground plane technique, steps technique or cutting two notches in the radiating element, a beveling radiating element technique and a notch cut technique. The notch cut from the radiator is also used to miniaturize the size of the planar antennas.

Therefore, the focus of this research is to introduce five novel designs of microstrip-fed printed antennas using different bandwidth-enhancement techniques to satisfy UWB bandwidth. According to their geometrical shapes, they can be classified into two types: the first types are stepped UWB antennas, which are namely: a stepped-trapezoidal patch antenna and a trimmed notch-cut patch antenna. The second ones are beveled UWB antennas, which are namely: an elliptical patch antenna, a double-beveled patch antenna, and a band-rejected elliptical patch antenna.

In designing these antennas, the thesis considers UWB frequency domain fundamentals and requirements, such as far field radiation pattern, bandwidth, and gain. The design parameters for achieving optimal operation of the antennas are also analyzed extensively in order to understand the antenna operation. It has been demonstrated numerically and experimentally that the proposed antennas are suitable for UWB communications and applications, such as wireless personal area networks (WPANs) applications that include home multimedia networks for data, video and music streaming.

1.4 Thesis Organization

This thesis is organized in five chapters, as follows:

Chapter one presents a general overview of the thesis. The introduction, motivation, objective and thesis organization are described.

The second chapter provides background theory and literature review. First, an introduction to UWB technology is presented in terms of its history, definition, advantages and applications. Then, the fundamental antenna theory is provided. After that,

microstrip antennas and their feeding techniques are discussed. Next, the major requirements for a suitable UWB antenna are discussed. Then, some general methods to achieve a wide bandwidth are presented. After that, an overview on UWB antennas is provided. Then, UWB Planar Monopole Antennas are reviewed. Finally, the UWB Printed Antenna is discussed.

The third chapter presents an introduction about the Finite Elements Method (FEM) and Ansoft's High Frequency Structure Simulator (HFSS) used to solve and analyze the proposed antennas. Then, design methodology is developed to be used in the antenna design. After that, two antennas are presented, which are the stepped-trapezoidal patch antenna and the trimmed notch-cut patch antenna. They are designed, simulated and tested. Then, their frequency domain performance is detailed in this chapter. After that, a parametric study on the important parameters which affect the antenna performance is pursued both numerically and experimentally to optimize the antenna and provide more information about the effects of the essential design parameters. Finally, the simulated and measured results, such as return loss, radiation pattern, gain and radiation efficiency are provided and discussed.

The fourth chapter presents three antenna designs, which are the elliptical patch antenna, the double-beveled patch antenna and the band-rejected elliptical patch antenna. They are designed, simulated and tested. Then, their frequency domain performance is described. After that, a parametric study on the important parameters which affects the antenna performance is pursued both numerically and experimentally to optimize the antenna and provide more information about the effects of the essential design parameters. Finally, the simulated and measured results, such as return loss, radiation pattern, gain and radiation efficiency are provided and discussed.

The fifth chapter concludes the research outlined within this thesis. Suggested future works are also highlighted.

CHAPTER TWO

Background and Literature Review

2.1 Introduction

UWB technology has been applied in many areas such as radar, sensing and military communications during the past 20 years. In recent years, many significant developments and high attention are being paid to UWB technology since the FCC allocated 3.1 – 10.6 GHz of the frequency spectrum for commercial UWB communications and applications in February 2002 [6]. It has received this attention due to its capability to provide a promising high data rate wireless communication for several applications.

This chapter provides background theory and literature review. First, an introduction to UWB technology is presented in terms of its history, definition, advantages and applications. Then, the fundamental antenna theory is provided. After that, microstrip antennas and their feeding techniques are discussed. Next, the major requirements for a suitable UWB antenna are discussed. Then, some general methods to achieve a wide bandwidth are presented. After that, overview on UWB antennas is provided. Then, the UWB Planar Monopole Antennas are reviewed. Finally, the UWB

Printed Antennas are discussed.

2.2 Ultra-Wideband History

Now, Ultra Wideband technology is a potentially viable-revolutionary approach to wireless communication however it is certainly not a new concept. UWB systems have been historically based on impulse radio since it has transmitted very high data rates by sending pulses of energy instead of using a narrowband frequency carrier. Typically, the pulses have very short durations (a few nanoseconds) that generate an ultra wideband frequency spectrum [3].

The concept of impulse radio dates back to the pulse-based spark-gap radio developed by Guglielmo Marconi in the late 1800's. This radio system induced pulsed signals which had very wide bandwidth [23]. It was used for several decades to transmit Morse code through the airwaves. But, it also caused strong emission and interference to narrowband (continuous wave) radio systems, which were developed in the early 1900's. Consequently, by 1924, the communications world abandoned wideband communication in preference of narrowband communication that were easy to regulate and coordinate [24, 25]. In 1942-1945, research in the UWB field continued and several patents were filed on impulse radio systems to reduce interference and enhance reliability. However, due to their potential military usage by the U.S. government, most of them were frozen for a long time [26].

In the 1960's, two very important advancements in UWB technology were created. First, Gerald F. Ross developed an impulse measurement technique, which was a time

domain electromagnetic method used to characterize the transient behavior of microwave networks through their characteristic impulse response. The second one was the development of the sampling oscilloscope by Hewlett-Packard in 1962. This equipment enabled the analysis, observation and measurement of the impulse response of microwave networks and catalyzed methods for sub-nanosecond pulse generation [25].

In the late 1960's, significant research was conducted by antenna designers, including Rumsey and Dyson [27, 28], who were developing logarithmic spiral antennas, and Ross, who applied impulse measurement techniques to the design of wideband, radiating antenna elements [29]. As a result of these antenna advances, the development of short pulse radar and communications systems had begun. In 1973, the first UWB communications patent was awarded for the short-pulse receiver [30].

In the mid 1980's, the FCC released the Industrial Scientific and Medicine (ISM) bands for unlicensed wideband communication use. Based on this revolutionary spectrum allocation, WLAN and Wireless Fidelity (Wi-Fi) have enormously grown. It also led the communication industry to consider and study the merits and implications of wider bandwidth communication [3].

Through the late 1980's, UWB was referred to as baseband, carrier-free, or impulse technology. Firstly, the term UWB was used by the U.S. Department of Defense in 1989. The advancement of technology in the 1990's allowed for the commercialization of UWB technology [15].

By 1989, UWB theory, techniques and many implementation approaches had been developed for a wide range of applications, such as radar, communications, automobile collision avoidance and positioning systems. However, much of the early UWB applications were permissible only under a special license by the US Government for

classified programs. In late 1990's, the development of UWB technology has greatly accelerated since it became more commercialized. For a further interesting and informative review of UWB history, the interested reader is referred to [9, 23, 25, 26]. For the nearly 40 year period of 1960-1999, over 200 papers were published in accredited IEEE journals and more than 100 patents were filed on topics related to ultra wideband technology [31].

On February14th, 2002, the Federal Communications Commission (FCC) adopted the First Report and Order that permitted the commercial operation of UWB technology [6]. After this official permission, research interest has exponentially grown with several researchers exploring RF design, circuit design, system design and antenna design related to UWB communications and applications. Also, several industrial companies have started investing in order to deliver revolutionary high-speed, short range data transfers and higher quality of services to the user [15].

2.3 Ultra-Wideband Definition

UWB is an emerging radio design standard that promises to deliver very high transmission rates where it transmits and receives pulse-based waveforms compressed in time instead of sinusoidal waveforms compressed in frequency. This enables transmission over a broad range of frequencies such that a very low power spectral density can be successfully received. Figure 2.1 depicts the equivalence of a narrowband pulse in the time domain to a signal of very wide bandwidth in the frequency domain. Also, it reveals the equivalence of a sinusoidal signal (essentially expanded in time) to a very narrow

pulse in the frequency domain [15].

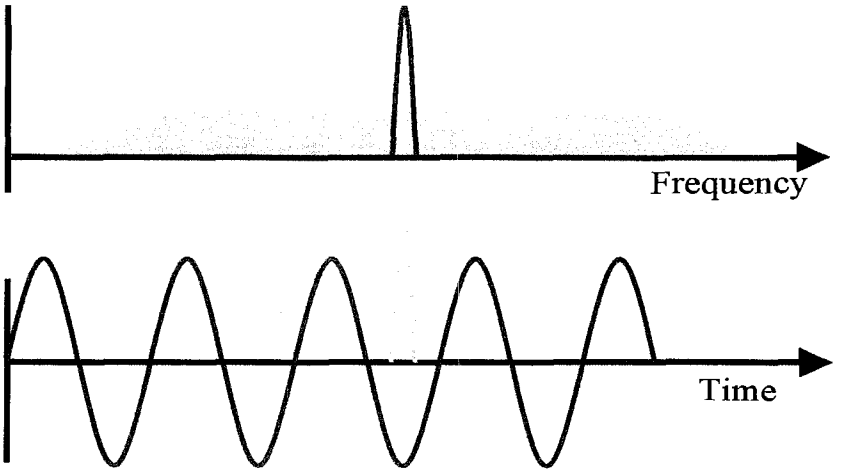

Figure 2.1: The equivalence of pulse-based waveforms compressed in time to a signal of very wide bandwidth in the frequency domain [15]

In February 14th, 2002, UWB technology changed significantly when the federal communications commission (FCC) issued UWB rulings that regulated the radiation limitations for UWB transmission, and also allowed the operation of UWB devices on an unlicensed basis. The FCC also allocated a bandwidth of 7.5GHz, i.e. from 3.1GHz to 10.6 GHz to UWB applications, which was the largest spectrum allocation for unlicensed use the FCC has ever granted [6].

According to the FCC rulings, UWB operation is defined as any transmission scheme that occupies a fractional bandwidth greater than or equal to 0.2, or a signal bandwidth greater than or equal to 500 MHz [6]. UWB bandwidth is the frequency band bounded by the points measured at -10 dB below the peak emission point, as based on the complete transmission system including the antenna. These points are the upper and the lower boundaries designated f_H and f_L, respectively. The fractional bandwidth FBW is then given in Equation 2.1 [3].

$$FBW = 2\frac{f_H - f_L}{f_H + f_L} \quad (2.1)$$

In order to avoid potential interference, UWB radio transmission has been mandated to legally operate in the range from 3.1 GHz to 10.6 GHz, with the power spectral density (PSD) satisfying a mandatory spectral mask emission assigned by the FCC. As shown in Figure 2.2, the outdoor emission mask is at the same level of -41.3dBm/MHz as the indoor mask is within the UWB band from 3.1 GHz to 10.6 GHz, and it is 10 dB lower outside this band to ensure sufficient interference protection for other wireless services [3].

An updated definition for UWB was given by the FCC in 2005. For indoor applications, the FCC defines UWB as any signal that occupies more than 500 MHz bandwidth in the 3.1 GHz to 10.6 GHz band and that meets the spectrum mask shown in Figure 2.2 [32]. That means UWB is no longer restricted to impulse radio, it also applies to any technology that uses 500MHz spectrum and complies with all other requirements for UWB.

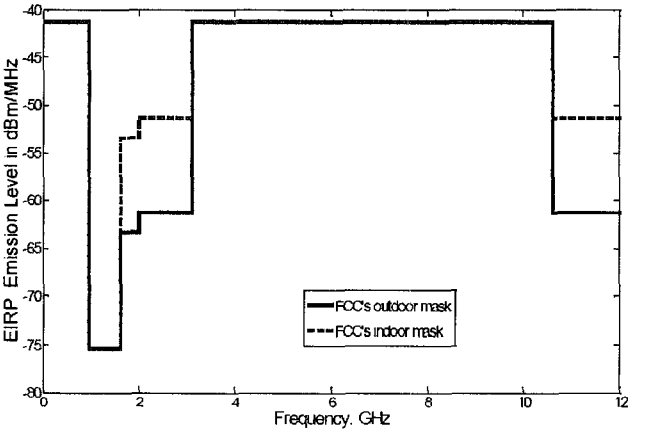

Figure 2.2: FCC's indoor and outdoor emission masks [3]

2.4 Ultra-Wideband Advantages

Due to the ultra wideband nature, UWB offers several motivating advantages that qualify it to be a more attractive solution to broadband wireless, radar communications and many applications than other technologies [3]. The key advantages of UWB are:

The extremely large bandwidth provided by UWB gives the potential of very high capacity resulting very high data rates. According to the Shannon-Hartley theorem discussed previously, channel capacity is proportional to bandwidth. Therefore, UWB can attain a very high capacity to support high speed wireless communications. It can provide hundreds of Mbps or even several Gbps with distances of 1 to 10 meters [33].

UWB communication systems transmit signals with extremely low spectral power density, at the level of parasitic emissions in a typical indoor environment (FCC part 15: -41.3 dBm/MHz). By splitting the power of the signal across UWB spectrum, the effect is below the acceptable noise floor on any frequency [34], as illustrated in Figure 2.3.

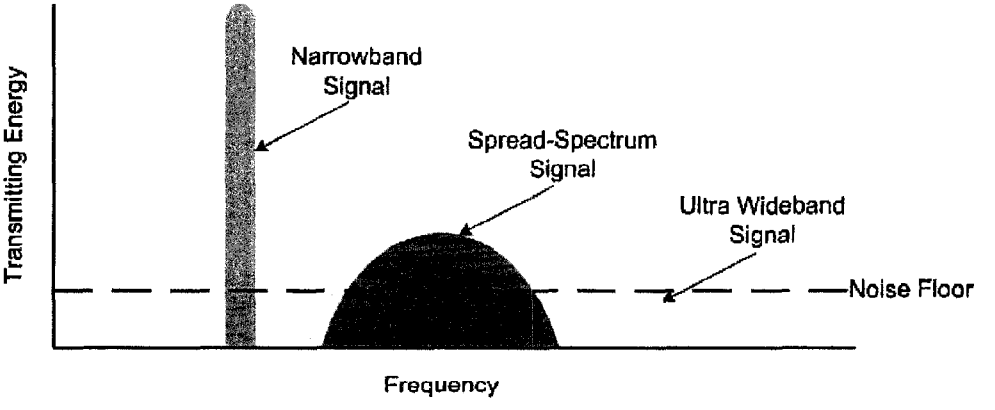

Figure 2.3: UWB transmitting energy across a wide spectrum of frequency [34]

For instance, one watt of power distributes over 1GHz of spectrum resulting in only

one nano-watt of power into each Hertz band of frequency. Consequently, UWB signals do not produce harmful interference to other coexisting wireless systems in the same frequency spectrum as depicted in Figure 2.4 [35].

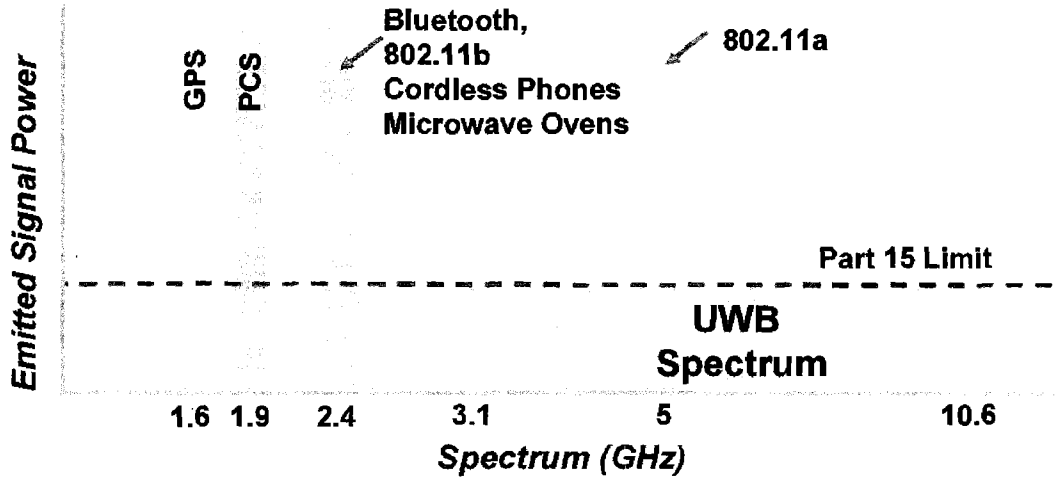

Figure 2.4: Spectrum of UWB and existing narrowband systems [35]

UWB provides highly secure and reliable communication solutions. Because of the low average transmission power, the UWB signal is noise-like that makes unintended detection rather difficult. Besides, this low power provides UWB communications systems with an inherent immunity to detection and interception since the eavesdropper has to be very close to the transmitter (about 1 meter) to be able to detect the transmitted information [36].

The UWB system is carrier-free, meaning that data is not modulated on a complex continuous waveform with a specific carrier frequency, as in narrowband and wideband technologies. Therefore, it requires fewer RF components than a carrier-based transmission that features low cost and low complexity [3].

Unlike narrowband technology, the ultra-short duration of UWB waveforms gives

the potential ability to provide high precision ranging and localization. Also, UWB signals can penetrate effectively through different materials. Based on these features, UWB signals offer opportunities for short range radar applications, such as rescue and anti-crime operations, as well as in surveying and mining industries [35].

2.5 Ultra-Wideband Applications

As mentioned in the previous section, UWB offers many elegant advantages and benefits that are very attractive for a wide variety of applications.

UWB is being targeted as a cable replacement technology since it has the potential for very high data rates using very low power at very limited range, which will lead to the applications well-suited for WPAN. UWB can remove the clutter around personal computers (PC) by wirelessly connecting PC peripherals such as storage, I/O devices and wireless USB (Universal Serial Bus) scanners and video cameras. Also, it can enable high data rate transmissions between computers and consumer electronics like digital cameras, video cameras, MP3 players, televisions and personal video recorders. In addition, UWB can simplify home entertainment systems setup by eliminating the need to use wires to connect all devices such as flat panel televisions and DVD players. Figure 2.5 depicts an example of a UWB network with some of possible UWB commercial applications [3, 10]. For example, Samsung and Freescale exhibited the world's first UWB-enabled cell phone in 2005 as illustrated in Figure 2.6. It features wireless connectivity to a PC and enables transferring data at very high data rate due to the use of the UWB technology. In 2006, Belkin introduced the first UWB-enabled CableFree USB hub in the U.S. market as

shown in Figure 2.7. It can immediately communicate to the PC providing a high-speed wireless connectivity for any USB device [3].

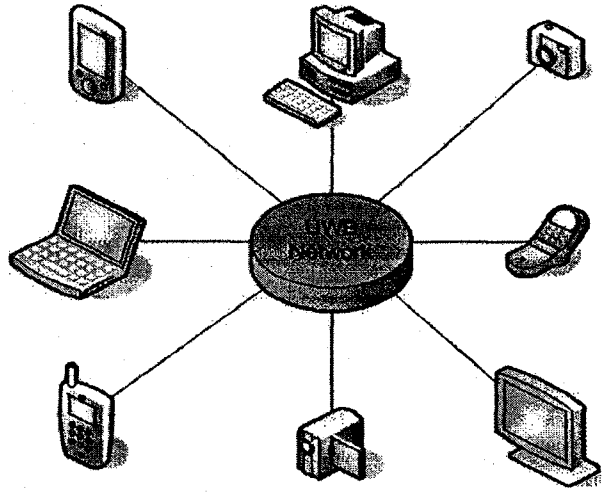

Figure 2.5: UWB network [10]

Figure 2.6:Samsung's UWB-enabled cell phone [3]

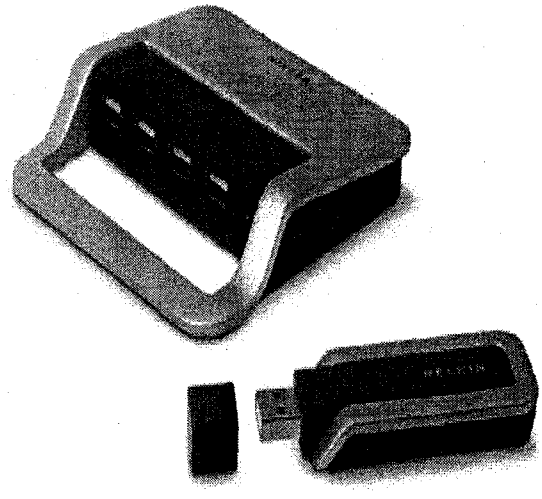

Figure 2.7:Belkin's four-port Cablefree USB Hub [3]

UWB technology could be beneficially and potentially used in all types of sensor networks [23]. Sensor networks consist of a large number of nodes spread over a geographical area to be monitored. Depending on the specific application, the sensor nodes may be static,

when used for securing home, tracking and monitoring, or mobile, if equipped on soldiers, firemen, automobiles, or robots in military and emergency response situations [7]. The key requirements for sensor networks, operating in challenging environments including low-cost, low-power and multi-functionality, can be well satisfied using UWB technology. High data rate UWB sensors networks can enable together and scatter or exchange a vast quantity of sensory data in a timely manner. The installation and maintenance cost can drop drastically by using UWB sensor networks as a result of eliminating wires. Furthermore, The UWB sensor network is very beneficial in medical applications since it frees patients from being trammeled by cables when extensive medical monitoring is applied [3].

UWB can be used in positioning and tracking applications. Due to the unique property of the high data rate characteristic in short range, UWB provides a high degree of accuracy for indoor locations compared with a GPS technology. In indoor environments, the tracking of moving objects can be precisely determined with an accuracy of several centimeters in case of using an advanced tracking mechanism [23]. Moreover, UWB positioning and tracking systems can run in cluttered places to allow effective communication between people. Consequently, it can help to locate missing people or objects in various situations, such as casualties in a collapsed, children lost in the mall or fire fighters in a burning building [3].

UWB can also be used in radar and imaging applications. It has been applied in military applications to determine the location of enemy objects behind walls and around corners in the battlefield [33]. It has also been applied in commercial applications such as rescue work, where UWB radars can detect a person's breath beneath rubble or medical diagnostics where X-ray systems may be less desirable. Besides, UWB vehicular radar is used to locate objects near a vehicle [3].

2.6 Fundamental Antenna Parameters

2.6.1 Antenna Bandwidth

The bandwidth *(BW)* of an antenna is defined as the range of frequencies within which the performance of the antenna is acceptable. From the impedance point of view, impedance bandwidth specifies a range of frequencies for which the antenna accepts more than 90% of the power applied to its input terminals [10]. Generally, in wireless communications, the antenna bandwidth is required to provide a return loss (RL) less than 10 dB or a voltage standing wave ratio (VSWR) of at most 2.0 over throughout the frequency band of interest. The return loss and the VSWR are both dependent on the reflection coefficient (Γ) [3, 10]. The reflection coefficient is defined as the ratio of the reflected wave to the incident wave at a transmission line load as shown in Figure 2.8. The transmission line model, and can be calculated by Equation 2.2 [15]:

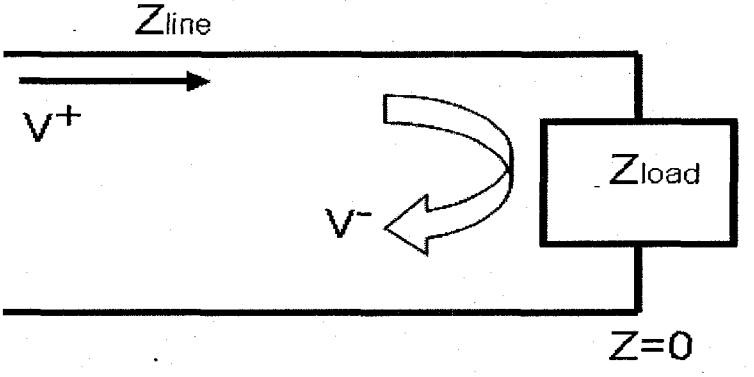

Figure 2.8: Transmission line model

$$\Gamma = \frac{V_0^-}{V_0^+} = \frac{Z_{Line} - Z_{Load}}{Z_{Line} + Z_{Load}} \qquad (2.2)$$

Z_{line} and Z_{load} are the transmission line impedance and the load (antenna) impedance,

respectively.

VSWR measures the ratio of the amplitudes of the maximum standing wave to the minimum standing wave, and can be calculated by the equation below:

$$VSWR = \frac{V_{max}}{V_{min}} = \frac{1+|\Gamma|}{1-|\Gamma|} \qquad (2.3)$$

The typically desired value of VSWR to indicate a good impedance match is 2.0 or less. This VSWR limit is derived from the value of Γ calculated above.

Return loss is another measure of impedance match quality, also dependent on the value of Γ, or S_{11}. Antenna return loss is calculated by the following equation:

$$Return\ Loss = -10log\ |S_{11}|^2,\ or\ -20log\ (|\Gamma|) \qquad (2.4)$$

The reflection coefficient Γ is equivalent to the S_{11} parameter of the scattering matrix. An antenna is can be analyzed like any other network component. For a general two-port device under test (DUT) as is shown in Figure 2.9, all four S parameters are shown.

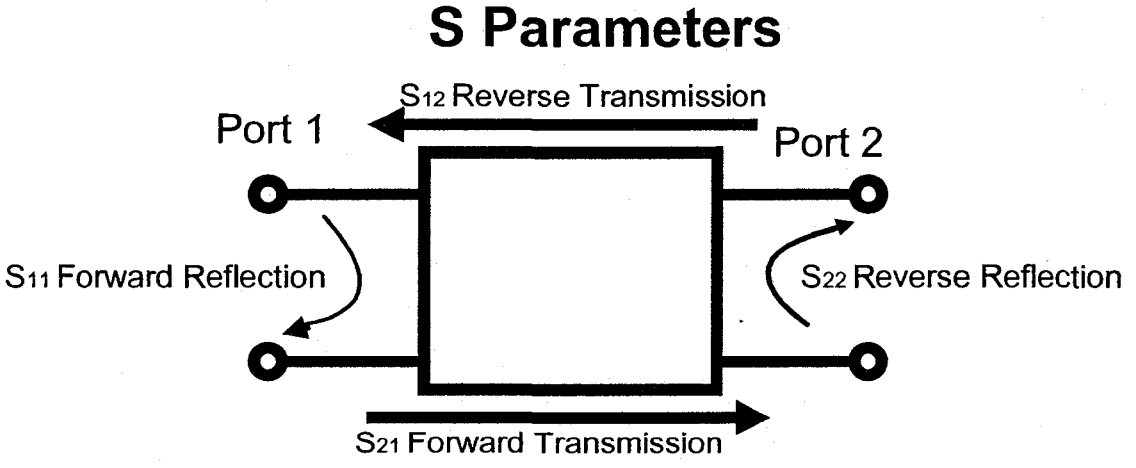

Figure 2.9: S Parameters for a two-port device

The S_{11} is the forward reflection coefficient and is identical to Γ. Hence,

$$S_{11} = \frac{Z_{Line} - Z_{Load}}{Z_{Line} + Z_{Load}} = \Gamma \qquad (2.5)$$

Although the reflection coefficient S_{11} is a vector, which has both magnitude and phase, it is commonly reported as a scalar value (as is the VSWR) which is the magnitude of S_{11}. All S_{11} values presented in this thesis will be given in dB [41].

In addition to being a measurement of the mismatch between the circuit and load impedance, the reflection coefficient S_{11} is also a measure of the power that is transferred to the device under test. In our case, since the device under test is an antenna, S_{11} is a measure of the power that is radiated by the antenna versus the power that is supplied to the antenna. This relationship is given by:

$$Percent\ \ of\ \ Power\ \ Transferred = \left(1 - |S_{11}|^2\right) * 100 \qquad (2.6)$$

For an antenna, the bandwidth is determined by the upper and lower frequencies where a VSWR = 2.0 corresponds to an S_n (dB) ~ -10 dB [18]. Although this is a somewhat arbitrary value, for an S_{11} below -10 dB, 90% of the power supplied to the antenna is transmitted.

The frequency bandwidth of an antenna can be expressed as either absolute bandwidth (ABW) or fractional bandwidth (FBW). f_H and f_L denote the upper edge and the lower edge of the antenna bandwidth, respectively. The ABW is defined as the difference of the two edges and the FBW is designated as the percentage of the frequency difference over the center frequency, as given in Equation 2.7 and 2.8 respectively [3].

$$ABW = f_H - f_L \qquad (2.7)$$

$$FBW = 2\frac{f_H - f_L}{f_H + f_L} \qquad (2.8)$$

2.6.2 Radiation Pattern

One of the main characteristics of an antenna is its radiation pattern. It is a graphical representation of the radiation properties of the antenna as a function of space coordinates. It describes a three dimensional angular variation of the field or power intensity as a function of the spherical coordinates θ and ϕ [38]. Mostly, it is evaluated in the far-field region where the spatial (angular) distribution of the radiated power does not depend on the distance. Typically, the pattern reports the normalized field values with respect to the maximum values [3].

In most cases, the radiation property is the two-dimensional or three-dimensional (2D or 3D) spatial distribution of radiated energy as a function of the position observation along a path or surface of constant radius. In some cases, the three-dimensional pattern is required and can be constructed in a series of two-dimensional patterns. In practical applications, a few plots of the pattern as a function of θ and ϕ for some specific values of frequency will provide most of the useful information needed, where θ and ϕ are the two axes in a spherical coordinate. The spherical coordinate system is used to define radiation patterns [3].

For a linearly polarized antenna, its performance is usually described in terms of its principal plane patterns which are *E*-plane and *H*-plane patterns. The *E*-plane can be defined as the plane containing the electric-field vector and direction of maximum radiation while the *H*-plane can be defined as the plane containing the magnetic-field vector and direction of maximum radiation [3, 38].

There are three common radiation patterns used to express an antenna's radiation property:

1. Isotropic: a hypothetical lossless antenna has equal radiation in all directions. It is merely valid for an ideal antenna and is frequently used as a reference to determine the directive properties of actual antennas.
2. Directional: an antenna has the property of radiating or receiving electromagnetic waves more effectively in some directions than in others. This is usually valid to an antenna where its maximum directivity is considerably greater than that of a half-wave dipole.
3. Omni-directional: an antenna has a basically non-directional pattern in a given plane and a directional pattern in any orthogonal plane [3].

2.6.3 Efficiency

An antenna can not radiate 100% of the delivered power to its input terminal because of the losses produced at the input terminal and within the structure of the antenna. The losses that are taken into account in the total antenna efficiency include conductive and dielectric losses and losses due to an impedance mismatch at the input port of the antenna. If the antenna has a reflection coefficient of Γ, then the antenna efficiency is given by [38]:

$$e_0 = e_r e_{cd} = e_{cd} = (1 - |\Gamma|^2) \qquad (2.8)$$

Where:

e_0 = total efficiency (dimensionless)

e_{cd} = conduction and dielectric efficiency

e_r = reflection efficiency = $(1 - |\Gamma|^2)$

However, the above equation can be applied at only a single frequency. This is adequate for narrowband systems but inadequate for UWB systems where the efficiency is a function of frequency. In UWB systems, the frequency should be considered in the radiation efficiency. Since the dielectric loss commonly dominates over the conductor loss, the radiation efficiency can be expressed as a function of frequency related to the dielectric loss as in Equation 2.9 [39]:

$$e_{rad}(f) = e_c e_d(f) \qquad (2.9)$$

2.6.4 Directivity and Gain

The directivity D is introduced to describe the directional properties of an antenna radiation pattern. The directivity is a parameter that measures the focusing ability of antenna energy in one direction compared to an isotropic radiator. Per IEEE standard definitions of terms for antenna, directivity is defined as the ratio of the radiation intensity in a given direction from the antenna to the radiation intensity average over all directions [18].

Directivity can be written as:

$$D = \frac{U}{U_0} = \frac{4\pi U}{P_{rad}} \qquad (2.9)$$

If not specified, the antenna directivity implies its maximum value;

$$D_{\max} = \frac{U_{\max}}{U_0} = \frac{4\pi U_{\max}}{P_{rad}} \qquad (2.10)$$

D = directivity (dimensionless)

D_o = maximum directivity (dimensionless)

U = radiation intensity (W/unit solid angle)

U_{max} = maximum radiation intensity

U_o = radiation intensity of isotropic source

Prad = total radiation power

The antenna gain *G* is closely related to the directivity that takes into account the radiation efficiency of the antenna. In other words, G is the directivity reduced by the losses on the antenna as given by [18]:

$$G = e_{rad} D \qquad (2.11)$$

Similarly, the maximum gain G_0 is related the maximum directivity D_0 by:

$$G_0 = e_{rad} D_0 \qquad (2.12)$$

2.7 Microstrip Antennas

The introduction of microstrip antennas has led to the development of a new innovation in antenna technology where new compact transceivers have been created. In 1952, Grieg and Engleman first realized the radiators that are compatible with microstrip transmission lines [40]. Nevertheless, the concept of microstrip antenna geometry that radiates electromagnetic waves, was first proposed by Deschamps [41] in 1953. The first patent of a microstrip antenna design was awarded to Gutton and Baissinot in France in 1955 [42]. The first practical antenna was created by Howell and Munson [40, 43]. After that, extensive research has been done to develop microstrip antennas. As a result, this technology has led to the development of compact, light weight, low profile conformal antennas that can be directly integrated to a variety of microwave circuits. Their low cost

and ease of fabrication on printed circuits (PCB) make them more attractive than the traditionally used lumped element antennas. Microstrip antennas may be made of any geometrical shape and dimension. However, there are three basic categories of microstrip patch antennas: microstrip patch antennas, microstrip traveling wave antennas and microstrip slot antennas [40].

The typical microstrip antenna geometry consists of a radiating patch, which is generally made from a metallic strip. The common metallic strip is copper or gold in some designs. The patch shapes can be designed to be any shape but the familiar shapes are square, rectangular, or circular shapes. They are common due to ease of analysis and fabrication [40]. The patch antennas are usually implemented in the upper side of the substrate and the lower side is used as ground plane [18, 44] as shown in Figure 2.10. The patch is usually fed by a microstrip line or a coaxial cable. A microstrip line is printed on the same side as the patch while a coaxial cable feed is attached to the patch antenna through the ground side. An array of microstrip elements with single or multiple feeds may also be used to generate more directivity [43]. There are many advantages and disadvantages of the microstrip antennas. Some of the principal advantages of microstrip antennas compared to conventional microwave antennas are [41]:

1. Light weight and low volume.
2. Low fabrication cost.
3. Can be made thin.
4. Low scattering cross section.
5. Easily mounted on missiles.
6. Microstrip antennas are compatible with modular designs (solid state devise such as oscillators , amplifiers, variable attenuators , switch modulators , mixers , phase

shifters etc.) that can be added directly to the antenna substrate board .

7. Feed lines and matching networks are fabricated simultaneously with the antenna structure.

On the other hand, microstrip antennas have some disadvantages compared to conventional microwave antennas including [41]:

1. Low efficiency due to losses in the dielectric substrate.
2. Relatively low power because of the size of the traces and different RF components.
3. Poor antenna pattern and polarization purity due to surface waves which travel within the substrate and scatter at surface discontinuities.
4. High Q due to the loss tangent of the substrate.
5. In most cases, the microstrip antennas show very low operational bandwidth.

There are numerous substrates that can be used for the design of microstrip antennas, and their dielectric constants are usually in the range of $2.2 < \varepsilon_r < 12$. A typical configuration of microstrip antenna is shown in Figure 2.10 below.

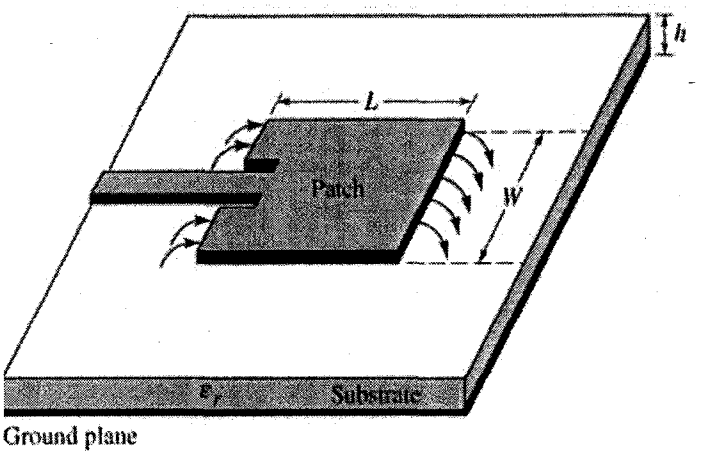

Figure 2.10: Typical microstrip antenna configuration [18]

2.8 Feeding Methods of Microstrip Antennas

In the past, microstrip antennas were fed either by a microstrip line or a coaxial probe through the ground plane. Since then a number of new feeding techniques have been developed. The most popular methods are the microstrip line, coaxial probe, aperture coupling, and proximity coupling [40, 45]. These feeding configurations with the corresponding equivalent circuits are depicted in Figure 2.11. In each of the equivalent circuits, an RLC circuit illustrates the resonant nature of the patch. The resistance (R) corresponds to an ohmic loss associated with the conductors (ground plane and patch) and substrate (loss tangent).

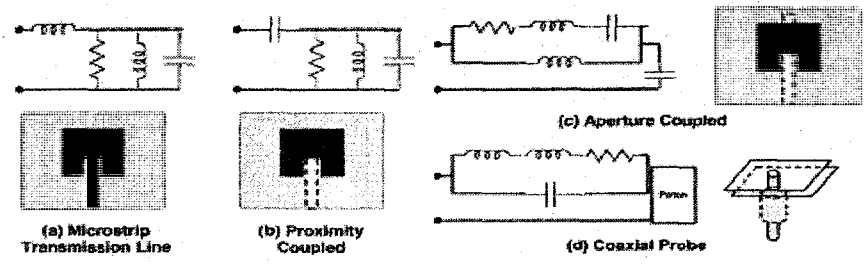

Figure 2.11: Equivalent circuits for feeds configurations [45]

The simplest feeding methods are the microstrip line and the coaxial probe as in (Figure 2.11a, d). Both configurations have direct contact with the patch to induce excitation. The point of excitation (contact point) is adjustable, which is a merit enabling the designer to control the impedance match between feed and antenna, polarization, mode of operation, and excitation frequency [45]. The formulas for calculating the desired characteristic impedance, Z_o, of the microstrip feed-line are derived using the Wheeler's method [46] as follows:

For wide strips (W/h>2):

$$Z_0 = \frac{377}{\sqrt{\varepsilon_r}}\left[\frac{W}{h} + 0.883 + \frac{\varepsilon_r + 1}{\pi\varepsilon_r}\left\{\ln\left(\frac{W}{2h} + 0.94\right) + 1.451\right\} + 0.165\frac{\varepsilon_r - 1}{\varepsilon_r^{\,2}}\right]^{-1} \qquad (2.13)$$

For narrow strips (W/h<2):

$$Z_0 = \frac{377}{2\pi\sqrt{\frac{\varepsilon_r + 1}{2}}}\left[\ln\left(\frac{8h}{W}\right) + \frac{1}{8}\left(\frac{W}{2h}\right)^2 - \frac{1}{2}\frac{\varepsilon_r - 1}{\varepsilon + 1}\left\{\ln\frac{\pi}{2} + \frac{1}{\varepsilon_r}\ln\frac{4}{\pi}\right\}\right] \qquad (2.14)$$

where

W = Width of the strip

h = Thickness of the substrate

e_r = Relative dielectric of the substrate

Similarly, the following formulas in terms of Z_0 and ε_r are derived for designing the strip width for desired characteristic impedance:

For wide strips (W/h>2)

$$\frac{W}{2h}\pi = \frac{377\pi}{2\sqrt{(\varepsilon_r)}Z_0} - 1 - \ln\left\{\frac{377\pi}{\sqrt{(\varepsilon_r)}Z_0} - 1\right\} + \frac{\varepsilon_r - 1}{2\varepsilon_r + 1}\left[\ln\left\{\frac{377\pi}{2\sqrt{(\varepsilon_r)}Z_0} - 1\right\} + 0.293 - \frac{0.517}{\varepsilon_r}\right] \qquad (2.15)$$

and for narrow strips (W/h<2):

$$\frac{2h}{W} = \frac{1}{4}e^x - \frac{1}{2}e^{-x}, where\ \ x = \left[\sqrt{\left(\frac{\varepsilon_r + 1}{2}\right)} + \frac{Z_0}{60} + \frac{\varepsilon_r - 1}{\varepsilon_r + 1}\left(0.226 + \frac{0.120}{\varepsilon_r}\right)\right] \qquad (2.16)$$

One disadvantage of the direct contact feeds is that they are inherently narrowband devices. These feeds are matched to specific impedances (in most cases 50 ohm) for a select range of frequencies. When the antenna operates outside this range of frequencies, the antenna performance will automatically be degraded due to the inherent mismatch between the antenna and the feed. To overcome the problem of the direct-coupled feeds, several non-contacting coupled feeds have been developed. The two main approaches are

the proximity-coupled (Figure 2.11 b) and aperture-coupled (Figure 2.11 c) feeds. The aperture-coupled configuration consists of two parallel substrates separated by a ground plane. Excitation of the patch is achieved by coupling energy from a microstrip line through a small aperture in the ground plane. By using this technique, the microstrip feed is designed on a thin high dielectric constant substrate which tightly binds the field lines, whilst the patch is designed on a thick low dielectric constant substrate. In this case, the ground plane isolates the feed from the patch and accordingly minimizes spurious radiation from the feed that would interfere with the antenna pattern [45]. Consequently, the design of the patch and the transmission line are independent. On the contrary, the proximity-coupled configuration operates in a similar way as that of the aperture-coupled technique but the ground plane is removed. Both non-contacting feeds have similar advantages except the thickness changes with removal of the ground plane in the case of a proximity-coupled configuration [40].

2.9 Ultra-Wideband Antenna Requirements

As is the case in conventional wireless communication systems, an antenna also plays a critical role in UWB systems. Therefore, all of the fundamental parameters described previously must be considered in designing UWB antennas. Moreover, there are further challenges in designing a UWB antenna as compared to a narrowband one [26].

A UWB antenna is different from other antennas in terms of its ultra wide frequency bandwidth. According to the FCC's definition, a suitable UWB antenna should provide an absolute bandwidth no less than 500 MHz or a fractional bandwidth of at least

0.2. This is the minimum bandwidth but generally the UWB antenna should operate over the entire 3.1-10.6 GHz frequency range resulting in spanning 7.5 GHz [3, 7].

The UWB antenna performance is required to be consistent over the whole equipped band. Ideally, antenna radiation patterns, gains and impedance matching should be stable across the entire band. In some cases, it is also needed that the UWB antenna provides the band-rejected characteristic to coexist with other narrowband systems operating in the same operational band [47, 48].

The radiation pattern of the UWB antenna is also a major characteristic that must highly be considered in antenna design. Directional or omni-directional radiation properties are desired depending on the antenna's practical application. A nearly omni-directional radiation pattern is desirable in mobile and hand-held systems since it enables freedom in the receiver and transmitter location. On the other hand, directional radiation characteristics are needed for directional systems, like radar systems, where high gain is required [3].

The radiation efficiency is another significant property of the UWB antenna. Thus, conductor and dielectric losses must be minimized in order to maximize radiation efficiency. Low loss dielectric must be used in order to maximize radiation efficiency. Since the transmit power spectral density is extremely low in UWB systems, high radiation efficiency is required because any unwarranted losses incurred by the antenna could affect the functionality of the system [3].

A suitable antenna should be physically compact and preferably planar to be compatible to the UWB unit, especially in mobile and portable devices. It is also greatly desired that the antenna attributes low profile and compatibility for integration with a printed circuit board (PCB). Besides, good design of the UWB antenna should be

optimized for the performance of the overall system [3].

Finally, a UWB antenna should achieve good time domain characteristics. In narrowband systems, an antenna has mostly the same performance over the entire bandwidth and fundamental parameters, such as gain and return loss, that have slight discrepancy across the operational band. Quite the opposite, UWB systems occupy huge operational bandwidth and often utilize very short pulses for data transmission. Consequently, the antenna has a more critical impact on the input signal. Indeed, minimum pulse distortion in the received waveform is a main concern of a suitable UWB antenna in order to provide a good signal to the system [48].

2.10 Methods to Achieve Wide Bandwidth

As discussed in previous section, operating bandwidth is one of the most essential parameters of an antenna. It is also the main characteristic that distinguishes a UWB antenna from other antennas. Historically, a lot of effort has been made toward designing broadband antennas such as the helical antenna, biconical antenna and log periodic antenna. Most of these antennas are designed for carrier-based systems however their bandwidth is still considered narrowband in the UWB sense. Nevertheless, the design theory and experience associated with these antennas are very useful in designing UWB antennas [49]. Accordingly, several methods have been employed to widen the operating bandwidth for different types of antennas [3]. Some of these methods are explained in the following sections.

2.10.1 The Concept of Frequency Independence

The pattern radiation and the impedance characteristic of any antenna can be determined by its specific shape and size in terms of wavelength at a given operating frequency. However, a frequency independent antenna is an antenna that does not change its properties when its size has changed. This was first introduced by Victor Rumsey in the 1950's [27]. According to Rumsey's principle, the impedance and pattern properties of any antenna will be frequency independent if the antenna geometry is specified only in terms of angles irrespective of any particular dimensions. This implies that the electrical characteristics of the antenna do not change with frequency [50].To enlighten more this definition, there are basically three principles accounting to achieve a frequency independent characteristics. They are smoothing, combining and self-complementarity principles.

2.10.1.1 Smoothing Principle

This principle is based on the definition of frequency independent antennas. It suggests that the antenna shape is specified entirely by angles irrespective of any dimensions. The antenna shape must form a smooth geometry change from the feed point to the radiation part. As shown in Figure 2.12, the biconical antenna is a good example of a frequency independent antenna based on this smoothing principle [51]. Ideally, the biconical antenna has impedance and radiation characteristics that are independent of frequency. However, the biconical antenna has bandwidth limitations due to the finite length constraint. Besides, the three dimensional structure is undesirable in modern wireless communications where compact size is preferable [3, 49].

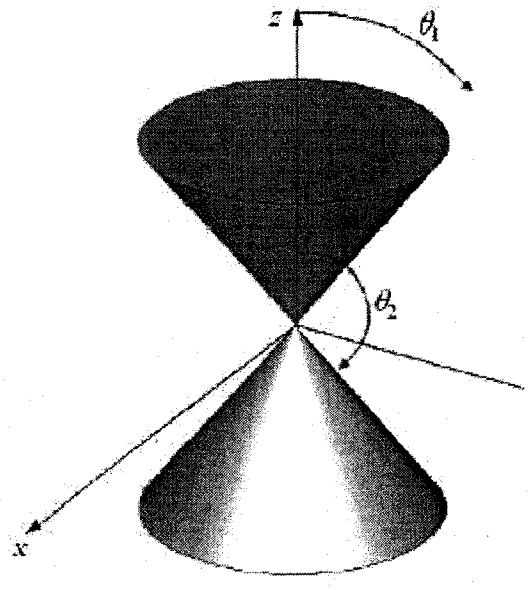

Figure 2.12: The biconical antenna [3]

2.10.1.2 Combining Principle

This principle suggests that the antenna is composed of a combination of various antennas at different lengths where each one resonates at a different frequency corresponding to its own length and has its own bandwidth. The summation of the individual bandwidths results approximately in the overall bandwidth. The log-periodic antenna is a good example of a frequency independent antenna based on the combining principle [51]. As depicted in Figure 2.13, it is actually a combination of dipole antennas with different lengths. It is a good broadband antenna in a carrier-based system but its performance in UWB is not that good due to the extremely short duration UWB pulses generated from different path delays in different dipole branches [49].

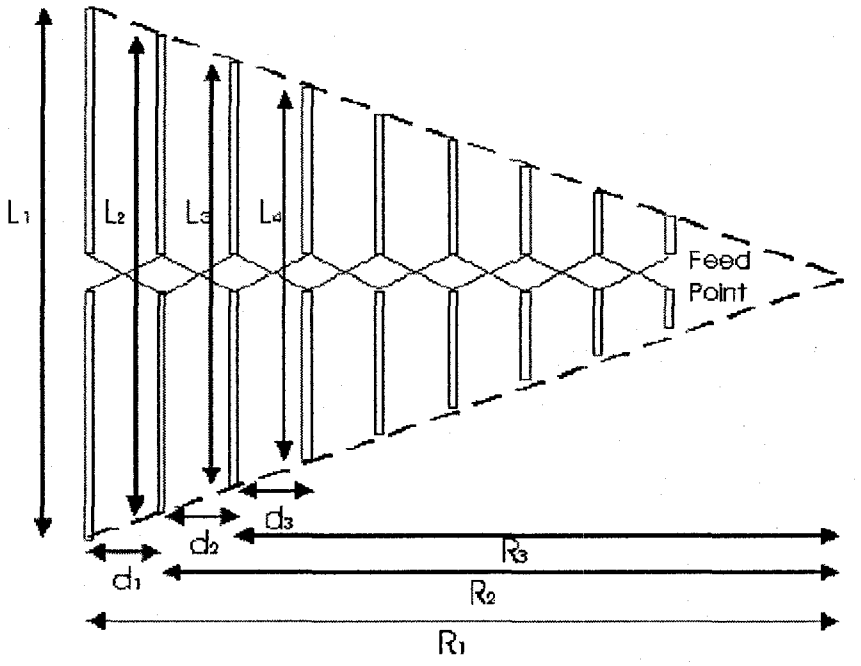

Figure 2.13: The log-periodic antenna [3]

2.10.1.3 Self-complementarity Principle

This principle was introduced by Yasuto Mushiake in the 1940's [52, 53]. He discovered that the product of input impedances of a planar electric current antenna (plate) and its corresponding "magnetic current" antenna (slot) is the real constant $\eta^2/4$, where η is the intrinsic impedance (377 Ohms for free space). Thus, frequency independent impedance response can be attained if an antenna is its own complement. The self-complementary antenna has a constant impedance of $\eta/2$ which is equal to 188.5 ohms. As shown in Figure 2.14, the spiral antenna is self-complementary if the metal and the air (slot) regions of the antenna are equal. In this case, the input impedances of the metal and slot are the same and their product will always be a constant regardless of the frequency [3].

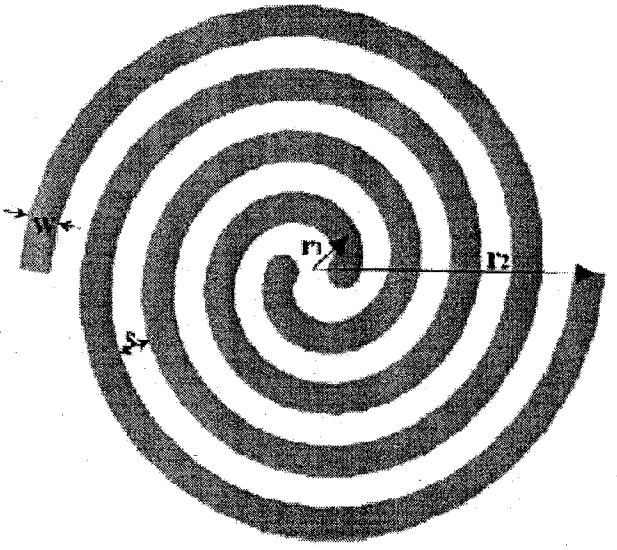

Figure 2.14: The spiral antenna

Although frequency independent antennas can function over an enormously wide frequency range, they still have some limitations. The antenna design has to be infinite in principle, though its size is practically truncated. This makes frequency independent antennas rather large in terms of wavelength. Moreover, frequency independent antennas have a tendency to be dispersive due to their radiation of different frequency components from different parts of the antenna. Accordingly, the received signal suffers from severe ringing effects and distortions. Owing to this drawback, the frequency independent antennas can merely be used when the level of signal dispersion is accepted [3].

2.10.2 The Concept of Overlapping Resonances

In general, a resonant antenna has narrow bandwidth since it has only one resonance. However, the combination of two or more resonant parts, each one operating at its own resonance while living closely spaced together, may generate overlapping of

multiple resonances resulting in multi-band or broadband performance. Actually, the two resonant parts technique has been broadly applied in antenna design, especially for mobile handset antennas that are required to operate at diverse wireless bands. The two resonant parts can be combined either in parallel [54, 55], or one works as the passive radiator and the other as parasitic element [56, 57].

For example, a stacked shorted patch antenna is designed for the GSM1800 (1710 MHz-1880 MHz) handset application as depicted in Figure 2.15. It is composed of two patches printed on a low-loss dielectric substrate and has a common shorting wall. The lower patch serves as the passive radiator and is directly fed by a probe feed and the upper patch is parasitically coupled to the lower one. This design results in two well-overlapping resonant modes due to the combination of the two patch radiators. Hence, this overlapping leads to a broad bandwidth ranging from 1688 MHz to 1890 MHz [57]. However, there is a main disadvantage of this design, i.e. using two different radiating elements. It can not provide constant radiation patterns over the operational bandwidth since the patterns differ from each other at different frequencies.

In theory, an ultra wide bandwidth can be attained by using a sufficient number of resonant parts provided that their resonances can be well-overlapped. Nevertheless, it is more difficult to practically obtain impedance matching over the entire bandwidth when there are more resonant parts. Furthermore, the antenna structure will be further complicated and expensive to fabricate. In addition, it is hard to have constant radiation characteristics when using multiple radiating elements [3].

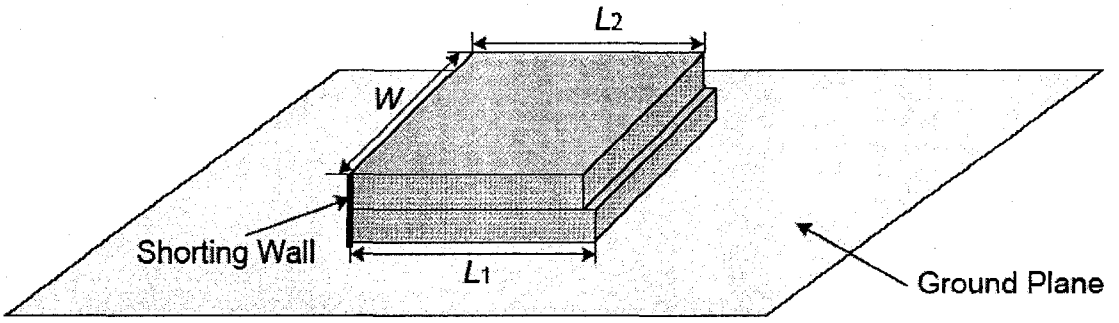

Figure 2.15: The geometry of the stacked shorted patch antenna [3]

2.10.3 The Concept of Increasing the Radiator Surface Area

The conventional monopole is well-known antenna. It is composed of a straight wire perpendicular to a ground plane as illustrated in Figure 2.16. It is one of the main antennas used widely in wireless communication systems due to its great advantages. These advantages include simple structure, low cost, omni-directional radiation patterns and ease for matching to 50Ω [18]. The -10dB return loss bandwidth of straight wire monopole is naturally around 10 %– 20 %, based on the radius-to-length ratio of the monopole [3].

The bandwidth of the monopole antenna increases with the increase of the radius-to-length ratio. This means that when the radius increases, the bandwidth will increase. In other words, the larger surface area (i.e. thicker monopole) will lead to a wider bandwidth due to the increase of the current area and thus the radiation resistance is increased [58]. This can be verified by simulating straight wire monopole for different radius-to-length ratios. In this simulation, the monopole length (*L)* and the feed gap (*h)* are fixed at 12.5 mm *and* 2 mm respectively, as illustrated in Figure 2.16. As shown in Table 2.1, it is found that the bandwidth increases with the increase of the radius-to-length ratio. However, when the monopole radius extremely increases and becomes very large compared to the feeding line,

the impedance mismatch will significantly occur and the bandwidth can no longer increased [3].

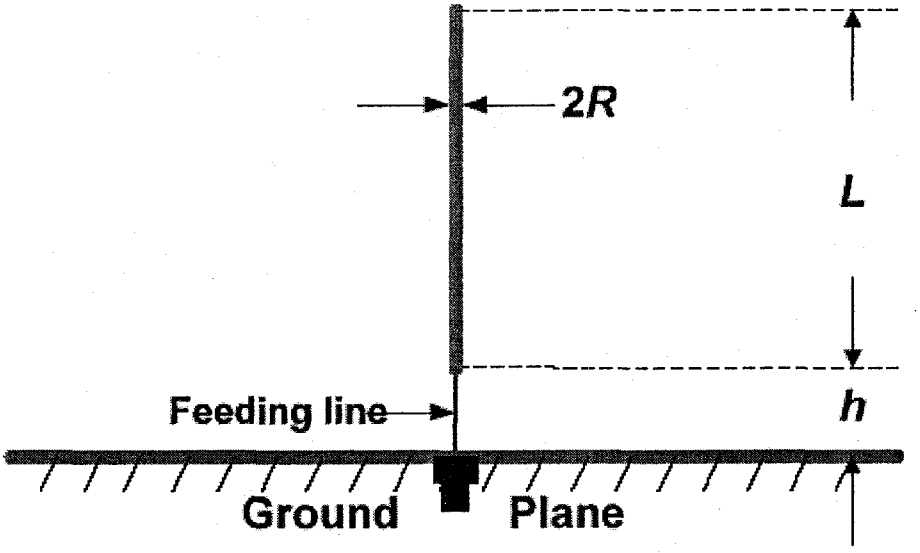

Figure 2.16: The geometry of the straight wire monopole [3]

Radius-to-length ratio *R/L* (%)	Lower edge of bandwidth (GHz)	Upper edge of bandwidth (GHz)	Absolute bandwidth (GHz)	Fractional bandwidth (%)
0.8	4.95	5.64	0.69	13.03
2.0	4.86	5.85	0.99	18.49
4.0	4.67	5.64	0.97	18.82
6.4	4.65	5.94	1.29	24.36

Table 2.1: Simulated -10dB impedance bandwidth of straight wire monopole [3]

Based on the concept of increasing the radiator surface area, instead of enlarging the radius of the conventional monopole, the wire is replaced with a planar plate yielding a planar monopole. By using this technique, the bandwidth can be greatly enlarged. This planar plate can be designed using several shapes such as square [59, 60], circle [61], triangle [62], trapezoid [63], "Bishop's Hat" [64] and so on [65-67], as shown in Figure 2.17.

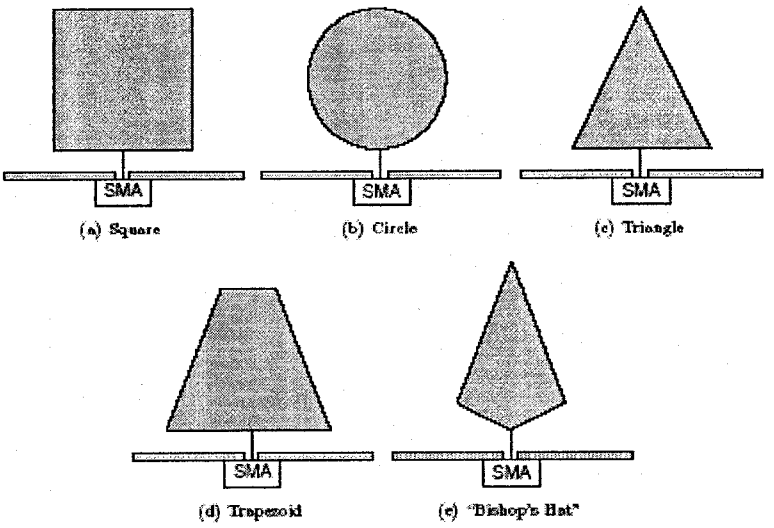

Figure 2.17: Various configurations of planar monopole antennas [3]

Also, what is applied on the monopole antenna is valid for the dipole antenna since the monopole antenna initiates from the dipole antenna by eliminating one element and operating the residual one against a ground plane. Thus, it is explicable that thicker dipoles such as the bow tie antenna [67], the diamond antenna [68], the elliptical disc dipole [69] and the circular disc dipole [70], can also reveal UWB characteristics. These UWB dipoles are demonstrated in Figure 2.18.

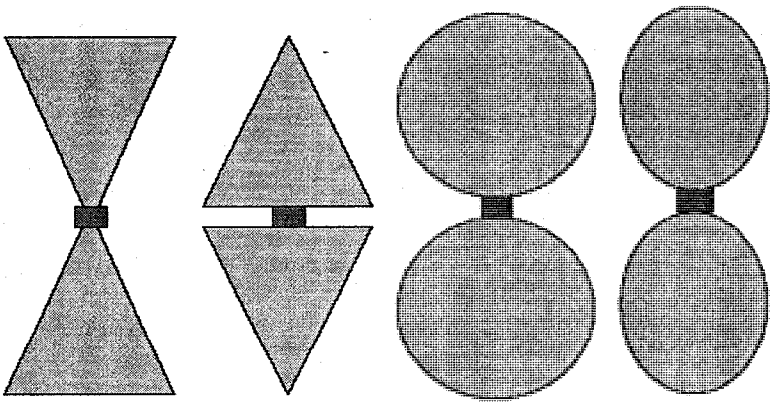

Figure 2.18: UWB dipoles with various configurations [3]

It is well-known that planar monopole antennas exhibit really charming physical features, such as simple structure, small size and low cost. Additionally, planar monopoles are compact broadband omni-directional antennas, and are also non-dispersive. Because of all these remarkable characteristics, planar monopoles are used in UWB communications and thus great efforts have been made on the planar shape that can provide wider bandwidth. Therefore, a number of planar monopoles with various configurations have been experimentally characterized and automatic design methods have been developed to attain the optimum planar shape [71].

Moreover, many studies and analyses have been performed on the various shapes of the planar monopole antennas in order to understand their physical performance and to acquire enough knowledge of their operating principles. One study used the Theory of Characteristic Modes, introduced by Harrington and Mautz in the seventies, to determine how the planar monopole shape affects the input bandwidth performance of the antenna. Characteristic modes (Jn) are the real current modes on the surface of the antenna that depend on its shape and size but are independent of the feed point. These current modes produce a close and orthogonal set of functions that can be used to develop the total current. To characterize the electromagnetic behavior of electrically small and intermediate size antennas, only a few modes are needed, so the problem can be simplified by only considering two or three modes [71].

Using the Theory of Characteristic Modes, different planar monopole geometries such as square, reverse bow-tie, bow-tie and circular shapes have been analyzed [71]. The current distributions of the first three characteristic modes (Jn) of these planar monopoles were studied at their resonance frequency. It was noted that mode J_1 shows vertical current flow along the monopoles with intense currents in the feeding strip. On the contrary, mode

J_2 revealed horizontal currents flowing nearly parallel to the ground plane. Mode J_3 is a higher order mode that presents vertical currents like mode J_1. As a result of this analysis, the first characteristic mode J_1 was found to be similar to that of a traveling wave mode and its influence on the antenna impedance matching extends to high frequencies. Then, to obtain broad input bandwidth performance, it is necessary to obtain a well-matched traveling mode which can be achieved by reinforcing the vertical current distribution (mode J_1) and minimizing horizontal current distributions (mode J_2). This can be accomplished by using different techniques as will be discussed later [71].

A few simple formulas have been reported to predict the frequency corresponding to the lower edge of the -10 dB return loss impedance bandwidth for different shapes of the monopole antennas [61, 72]. However, the prediction of the upper edge frequency requires full-wave analysis. Also, it is found that the upper edge frequency depends on the part of the planar element near to the ground plane and feed probe where the current density concentrates. Thus, different techniques are proposed to control the upper edge frequency such as beveling the square element on one or both sides of the feed probe [73].

2.10.4 Techniques to Improve the Planar Antenna Bandwidth

As previously discussed, the upper edge frequency depends on the part of the planar element near to the ground plane and feed probe where the current density concentrates. Also, some shapes like the square and circular planar monopole antennas have a drawback of a relatively small impedance bandwidth [74, 75]. Consequently, several techniques have been suggested to improve the antenna bandwidth. In Figure 2.19, various typical planar

monopoles are depicted [76]. All of them are originated from a rectangular radiator, which is able to achieve a bandwidth of about 60% for VSWR = 2:1. In order to enhance the impedance bandwidth, some techniques have been proposed.

First, the radiator may be designed in different shapes. For instance, the radiators may have a bevel or smooth bottom or a pair of bevels to obtain good impedance matching, as shown in Figure 2.19 (a). The optimization of the shape of the bottom portion of the antenna can lead to the well-matched traveling mode. In other words, it can improve the impedance bandwidth by attaining smooth impedance transition [77, 78].

Secondly, a different type of slot cut may be inserted in the radiators to improve the impedance matching, particularly at higher frequencies, as shown in Figure 2.19 (b) [79], [80]. The effect of slots cut from the radiators is to vary the current distribution in the radiators in order to change current path and the impedance at input point. Besides, using an asymmetrical strip at the top of the radiator can decrease the height of the antenna and improve impedance matching [81].

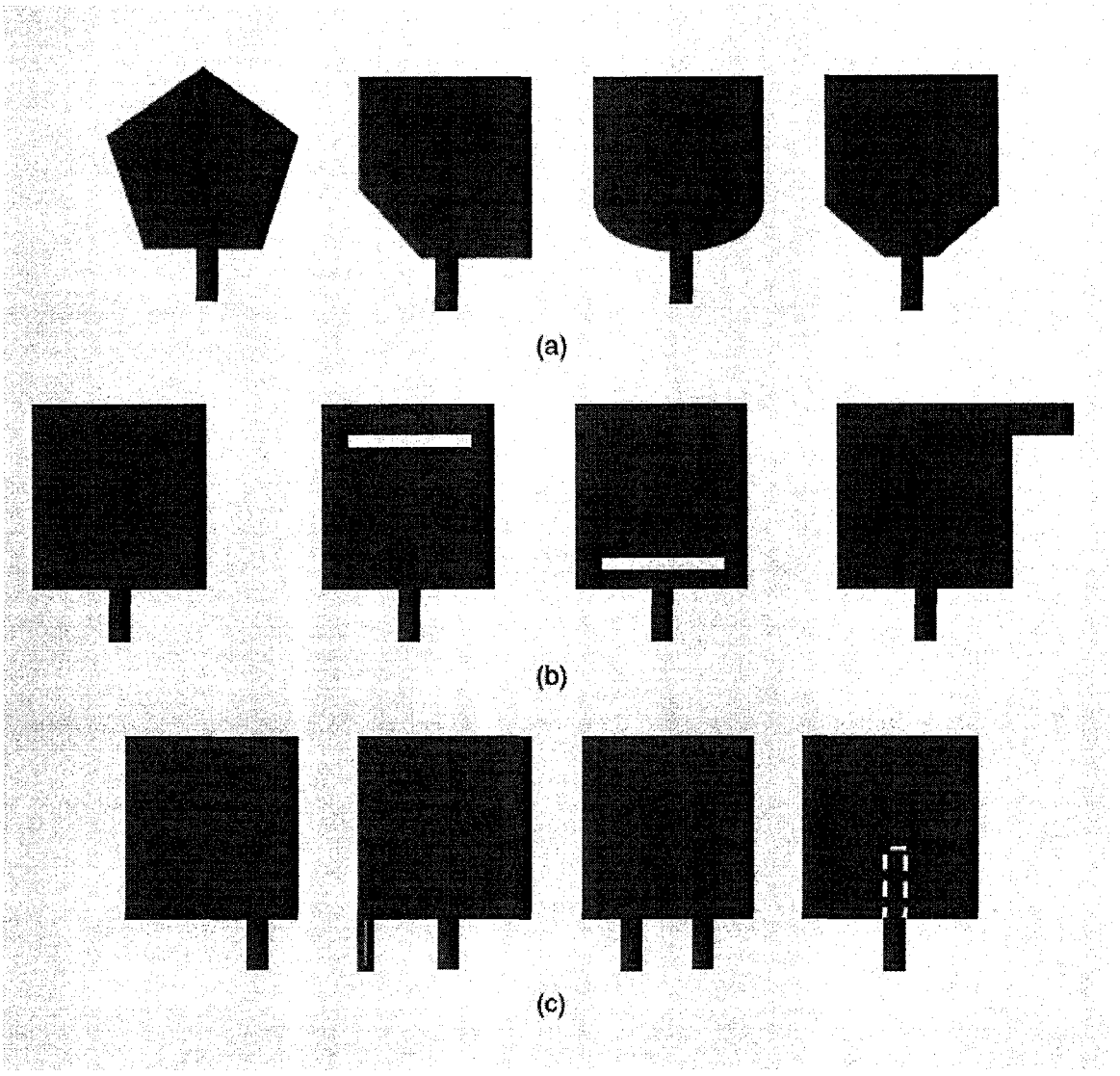

Figure 2.19: Planar antenna

Thirdly, a partial ground plane and feed gap between the partial ground plane and the radiator may be used to enhance and control the impedance bandwidth. The feed gap method is crucial for obtaining wideband characteristics and it particularly affects mode J_1 (the vertical current distribution) resulting in the well-matched traveling mode [61]. Also, a cutting slot in the ground plane beneath the microstrip line can be used to enhance the bandwidth [82]. In addition, a notch cut from the radiator may be used to control impedance matching and to reduce the size of the radiator. The notch cut significantly

affects the impedance matching, especially at lower frequencies. It also reduces the effect of the ground plane on the antenna performance [20].

Fourthly, cutting two notches in the bottom portion of rectangular or square radiators can be used to further improve impedance bandwidth since they influence the coupling between the radiator and the ground plane. Also, transition steps may be used to enhance the bandwidth by attaining smooth impedance transition between the radiator and feeding line [83, 84].

Finally, several modified feeding structures may be used to enhance the bandwidth, as shown in Figure 2.19 (c). By optimizing the location of the feed point, the antenna impedance bandwidth will be further broadened since the input impedance is varied with the location of the feed point [74]. A shorting pin can be used to reduce the height of the antenna as used in a planar inverted L-shaped antenna [85]. A double-feed structure highly enhances the bandwidth, especially at higher frequencies [86].

2.11 Overview on Ultra-Wideband Antennas

Different kinds of wideband antennas are designed, each with its advantages and disadvantages. The history of wideband antennas dates back to those antennas designed by Oliver Lodge in 1897. Later, they led to some of the modern ultra-wideband antennas. These antennas were early versions of bow-tie and biconical antennas which had significant wideband properties. Biconical antennas are the earliest antennas used in wireless systems designed by Oliver Lodge. In the 1930's and 1940's, more types of wideband antennas were designed, such as spherical dipole and coaxial, conical and

rectangular horn antennas. Biconical antennas were also redesigned [37].

In the 1960's, other classes of wideband antennas were proposed. These classes include wideband notch antennas, ellipsoid mono and dipole antennas, large current radiator antennas, magnetic UWB antennas, spiral and helical antennas, bow-tie antennas, microstrip antennas and tapered slot and Vivaldi-type antennas. Also, frequency independent antennas were applied to wideband design. A typical design includes the self-complementary log periodic structures, such as planar log-periodic slot antennas, bidirectional log-periodic antennas, log-periodic dipole arrays, two/four-arm log spiral antennas, and conical log-spiral antennas. Besides, there are other types of antennas which do not belong to the classes of antennas previously cited. For example, they include printed and stepped fat-dipole, fractal, dielectric wedge, disk and half disk and quasi-horn microstrip antennas [37].

The wideband characteristics of all of the above-mentioned antennas depend on two main antenna features, which are the geometry shape and the dielectric material type, if any. The antenna bandwidth is affected by the impedance match between the feeding circuit and free space. This is a consequence of the currents flowing in the antenna. The currents flowing in the antenna are varied by adapting the shape and dielectric properties of the antenna. Thus, these adaptations will drive the antennas to radiate with varying degrees of efficiency. The bandwidth of these antennas fluctuates significantly inside each class of antenna as well as between the different classes and types of antennas. So, the range of the bandwidth is from hundreds of MHz to tens of GHz based on the antenna design [37].

However, the antennas mentioned above are rarely used in portable devices and are difficult to be integrated in microwave circuits because of their bulky size or directional radiation. However, many of them are widely used in electromagnetic

measurements. Alternatively, planar monopoles, dipoles or disc antennas have been introduced due to their wide bandwidths and small size. The earliest planar dipole is the Brown-Woodward bowtie antenna, which is a planar version of a conical antenna. Some of these antennas will be reviewed within the following subsections [76].

2.11.1 Ultra-Wideband Planar Monopole Antennas

Planar monopole antennas [25, 59, 61, 68, 69, 85-89, 90-101] are constructed from a vertical radiating metallic plate over a ground plane fed by a coaxial probe. It can be formed in different shapes such as rectangular, triangular, circular or elliptical, as illustrated in Figure 2.17. The main features of these shapes are their simple geometry and construction. Planar monopole antennas have been explored numerically and experimentally and have shown to exhibit very wide bandwidth [25, 59, 61, 69, 85-89, 90-94]. They provide wide impedance bandwidth because their radiators can support multiple resonant modes. The radiator can be designed so that the resonant frequencies are closely spaced together to combine properly the multiple resonances to yield, as a total, a very wide impedance bandwidth response [85, 89]. In addition, excited modes that correspond to the multiple resonances can be modified by changing the geometry and the size of the radiator as previously mentioned. This can be done by using enhancement techniques like beveling and through the addition of shorting pins to obtain and adjust the impedance bandwidth and performance of planar monopole antennas [59, 85, 90].

One of the most interesting planar monopole antennas is the planar inverted cone antenna (PICA). Its design provides more than 10:1 matching impedance bandwidth and

radiation patterns similar to the monopole disk antennas but it has smaller dimensions [16]. A second version with two circular holes covers a wider range of operating frequencies and improves the omni-directional radiation pattern bandwidth [102].

Another type is a square planar monopole antenna, which provides a bandwidth of 1.98 - 12.74 GHz with a quasi-omni-directional radiation pattern [84]. To improve the matching impedance bandwidth in a square planar monopole antenna, several techniques have been suggested, as mentioned in earlier section. These include double feed, semi-circular base, beveling technique, shorting pin, and notch technique. In this design, the notch from the bottom portion of the radiator technique is used. Also, here is another design of rectangular monopole antenna using a beveling technique. Thus, the matching impedance bandwidth increases from 6:1 to 10:1 (1.65 - 20 GHz) and provides a quasi-omni-directional radiation pattern that is frequency dependent, such as similar planar monopole antenna designs [103].

A circular monopole antenna yields a broader impedance bandwidth as compared to a rectangular monopole antenna with similar dimensions. This is because the circular planar monopole is more gradually bent away from the ground plane than the rectangular monopole. This provides smooth transition between the radiator and feed line resulting in a wider impedance bandwidth [21]. The circular monopoles are proposed to give wider matching impedance bandwidth and omni-directional radiation patterns as in [87, 88]. Following that, elliptical shapes are proposed [61, 82, 66, 102]. It can provide high matching impedance bandwidth by optimizing the major and minor axes of the ellipse as well as feed gap between the bottom of the ellipse and ground plane. As in the case of the circular shape, the broadband characteristics are due to the smooth transition between the radiator and feeding strip. Also, the elliptical radiator can be modified to reduce the size

and enhance the impedance bandwidth as shown [76].

Another interesting planar antenna is the Bi-Arm Rolled Monopole antenna. Its radiator is implemented by wrapping a planar monopole. This antenna has a matching impedance bandwidth from 3.1 to 10.6 GHz with an omni-directional radiation pattern [104].

From the above, one can conclude that planar monopoles, suspended in space against ground plane, are not suitable for printed circuit board applications due to their vertical configuration. However, they can be well matched to the feeding line over a large frequency band (2 - 20 GHz) with gain of 4 - 6 dBi. But they suffer from radiation pattern degradation at higher operation frequencies. The size of monopole can be small (approximately 30 × 30 mm^2), but at the same time such monopole requires a ground plane with dimensions of around 150 × 150 mm^2 [76]. It makes the monopole a 3-D dimensional antenna which is not well suitable for printed circuit board applications and is difficult to be integrated into RF circuits as well as embedded into UWB devices. Therefore, some efforts have been made to develop the low-profile planar monopoles with desirable return loss performance in the 3.1 - 10.6 GHz frequency range. So, the antenna can be integrated to a PCB for use in UWB communications, which will be discussed in the following sections.

2.11.2 Ultra-Wideband Printed Antennas

The UWB antennas printed on PCBs are further practical to implement. The antennas can be easily integrated into other RF circuits as well as embedded into UWB

devices. Mainly, the printed antennas consist of the planar radiator and ground plane etched oppositely onto the dielectric substrate of the PCBs. In some configurations, the ground plane may be coplanar with the radiators. The radiators can be fed by a microstrip line and coaxial cable [76].

In the past, one major limitation of the microstrip or PCB antenna was its narrow bandwidth characteristic. It was 15 % to 50 % of the center frequency. This limitation was successfully overcome and now microstrip antennas can attain wider matching impedance bandwidth by varying some parameters like increasing the size, height, volume or feeding and matching techniques [40]. Also, to obtain a UWB characteristic, many bandwidth enhancement techniques have been suggested, as mentioned earlier.

Numerous microstrip UWB antenna designs were proposed. For instance, a patch antenna is designed as a rectangular radiator with two steps, a single slot on the patch, and a partial ground plane etched on the opposite side of the dielectric substrate. It provides a bandwidth of 3.2 to 12 GHz and a quasi-omni-directional radiation pattern [105]. A clover-shaped microstrip patch antenna is designed with the partial ground plane and coaxial probe feed. The measured bandwidth of the antenna is 8.25 GHz with gain of 3.20 -4.00 dBi. Also, it provides a stable radiation pattern over the entire operational bandwidth [106]. Another design is a printed circular disc monopole antenna fed by a microstrip line. The matching impedance bandwidth is from 2.78 to 9.78 GHz with an omni-directional radiation pattern and it is suitable for integration with printed circuit boards [107].

In addition, several elliptical shaped-based antennas have been designed. For example, three printed antennas are designed starting from elliptical shape, namely the elliptical patch antenna, its crescent-shaped variant and the semi-elliptical patch. These antennas have revealed good performance characteristics of wide impedance bandwidth

(2.8 - 12 GHz), consistent radiation pattern and a gain variation between 2.5 to 10.4 dB. The semi-elliptical patch antenna is the miniaturized one among the three antennas proposed while providing the same desired performance characteristics [108]. A small printed antenna with a notch cut is designed. The radiator and ground plane of the antenna are etched oppositely on a piece of PCB. A notch is cut from the radiator while a strip is asymmetrically attached to the radiator. This design attains a broad operating bandwidth of 2.9–11.6 GHz. The antenna is characterized by omni-directional radiation patterns with a high radiation efficiency of 79 % - 95 % across the UWB bandwidth. The ground-plane effect on impedance performance is highly reduced by introducing the notch from the radiator since the electric currents on the ground plane are significantly suppressed at the lower edge operating frequencies [20]. Another type of printed antenna is a slot antenna. As an example, the elliptical antenna is designed on low-temperature cofired ceramic (LTCC) technology. This antenna can share the ground plane with other radio circuitry. It provides a matching impedance bandwidth from 3 to 10.6 GHz with a quasi-omni-directional radiation pattern at low frequencies [109].

Another promising type of printed antenna is the Vivaldi antenna. Theoretically, the vivaldi antenna can exhibit an infinite bandwidth but the only limitation is its physical size and fabrication capabilities. In fact, one of the major bandwidth limitations is the microstrip-to-slotline transition. There are many methods proposed to solve this problem, which include a broadband balun, a microstrip-to-printed-twinline or two side slotline transitions [110]. Vivaldi antennas are considered directional microstrip UWB antennas that can provide an operational bandwidth between 1 to 5 GHz. Moreover, an antipodal Vivaldi antenna provides a bandwidth from 1.3 to 20 GHz [111].

A UWB printed antenna fed by coplanar waveguide (CPW) is another type of the

printed antenna. For instance, one trapezoidal design is proposed to operate from 3.1 to 8.3 GHz. It shows an acceptable radiation pattern and gain [83]. This design has later been modified and improved to possess the frequency notch function. The modified antennas cover the entire UWB band (3.1 - 10.6 GHz) and have a notch for the IEEE 802.11a frequency band (5.15 - 5.825 GHz). The frequency notch function is obtained by inserting different slot shape into the antenna. The notch frequency can be adjusted by varying the slot length. The antennas show good radiation patterns as well as good gain flatness except in the IEEE 802.11a frequency band [112].

Another type of frequency-notched antenna is a CPW-fed planar antenna having hexagonal radiating elements with an inserted V-shaped thin slot. It provides a frequency band notch for wireless local area network (WLAN) at a frequency of 5.25 GHz, which can be adjusted by varying the length of the V-shaped slot. It operates on a frequency bandwidth from 2.8 to 10.6 GHz without using the V-slot [113]. Also, a frequency notched UWB microstrip slot antenna with fractal tuning stub is proposed. The antenna without fractal tuning stub is similar to a conventional microstrip slot antenna, but by introducing a fractal tuning stub, a frequency-notched function is obtained to avoid interfering with nearby WLAN systems. It provides the operation bandwidth of 2.66 to 10.76 GHz but with a frequency notched band from 4.95 to 5.85 GHz. Also, it achieves good omni-directional radiation performance over the entire frequency band [114].

CHAPTER THREE

Stepped Ultra-Wideband Antennas

3.1 Introduction

As discussed in chapter two, the UWB antennas printed on PCBs are greatly preferred since they can be easily integrated into other RF circuits as well as embedded into UWB devices such as mobile and portable devices. Thus, in this thesis, following the main requirements of the UWB antennas covered earlier and through the use of antenna design techniques described in the privous chapter, several small, low-cost and efficient UWB printed microstrip antennas, satisfuing UWB frequency domain requirements, are designed. Two of them are presented in this chapter and the others are discussed in the next chapter.

In this chapter, two designs of UWB antennas are proposed and investigated. Before we discuss these antenna designs in greater detail, we will first introduce the numerical technique and its software package utilized to calculate the electromagnetic performance of the proposed antennas. The designs, optimizations, and simulations are conducted using the Ansoft High Frequency Structure Simulator (HFSS™). It works based

on the Finite Element Method (FEM). Then, the design methodology developed to design the antennas is outlined. After that, the design and fabrication of two novel UWB printed antennas are presented in detail. They are namely: the stepped-trapezoidal patch and the trimmed notch-cut patch antennas. The structural properties and performance characteristics of these antennas are investigated via numerical simulations and verified by measurements. The design process, parametric study, optimization as well as simulated and measured results, such as return loss, radiation characteristics, gain and radiation efficiency, are provided.

3.1.1 Finite Elements Method (FEM)

The finite element method (FEM) is created from the need to analyze and solve complex structure analysis. The FEM is a partial differential equation (PDE) based method. It was first mathematically treated by Courant in the 1940's for structural analysis. However, FEM applications were not applied to electromagnetic (EM) problems until 1968. After that, the method has been used in several areas, such as microwave circuits, antennas, waveguides, scattering, semiconductor devices, electric machines, microstrip, and absorption of EM radiation by biological bodies [115].

FEM is a powerful numerical technique since it has the flexibility to model complex geometries with arbitrary shapes and inhomogeneous media. It builds general-purpose computer programs for solving a wide range of problems due to its systematic generality. Thus, programs generated for a specified field can effectively be applied to solve problems in another discipline after little modification [115].

The FEM begins with discretizing the computational domain into smaller elements

called finite elements. These finite elements differ for one-, two-, and three-dimensional problems. The next step is to implement the wave equation in a weighted sense over each element, apply boundary conditions and accumulate element matrices to form the overall system of equation as in Equation 3.1:

$$[A]\,[X]=[B] \qquad (3.1)$$

where A is a very sparse matrix of size $N \times N$, B is known, and X is the unknown vector.

To sum up, the finite element analysis of any problem involves basically four steps [115]:

- discretizing the solution region into a finite number of subregions or elements
- deriving governing equations for a typical element
- assembling all elements in the solution region
- solving the system of equations obtained.

3.1.2 High Frequency Structure Simulator (HFSS™)

Ansoft's High Frequency Structure Simulator (HFSS) is a commercially available and state-of-the-art electromagnetic simulation package. HFSS is one of the industry leading 3D EM software tools for radio frequency (RF) applications. It employs the finite element method (FEM) to simulate any arbitrary three-dimensional structure by solving Maxwell's equations based on the specified boundary conditions, port excitations, materials, and the particular geometry of the structure. In HFSS, each problem is similarly developed as follows:

- Indicating the solution type

- Constructing the geometry
- Setting up the materials for the structures
- Setting up the boundary conditions of the problem
- Setting up the solution:
  - Adaptive frequency
  - Number of adaptive passes and convergence criteria
  - Frequency sweep
- Solving the solution
  - Post process analysis
  - S-parameters
  - field antenna patterns, gain, current distributions

In order for HFSS to perform all necessary calculations using FEM for any geometry, it has to create an enclosed and suitable volume which is defined in HFSS as a radiation box. HFSS applies precise radiation boundary conditions on all its sides in order to imitate infinite space. The trade-off between accuracy and computer ability depends on the size of the radiation region comparative to the design structure. Ansoft Corporation recommends that the sides of the radiation box should be kept about one quarter wavelength at the lowest frequency away from any radiating interfaces of the design structure [22].

3.1.3 Design Methodology

In order to satisfy UWB requirements mentioned previously in chapter two, the following design methodology is developed:

- Choosing the appropriate substrate.
- Choosing candidate radiator geometry.
- Calculating the initial geometrical parameters based on the empirical formulas which predicts the lower edge frequency, if any.
- Simulating the antenna behavior over a slightly extended bandwidth and detailed analysis of results.
- Changing the parameters according to intuition and iteration of the previous step until getting generally satisfactory results for the performance over the entire band but especially for the lower band or deciding to change the candidate geometry.
- Applying the proper bandwidth-enhancement techniques to obtain UWB characteristics.
- Trying to miniaturize the geometry by cutting off parts that do not radiate after checking the current distribution.
- Conducting parametric studies to find out which parameters affect the antenna performance and hence starting the optimization process.
- After successful simulation, obtaining the results, such as impedance and radiation patterns and gain.
- Fabrication of the antenna, measuring the impedance and radiation patterns to confirm simulated results.

In Figure 3.1, the following chart demonstrates this design methodology.

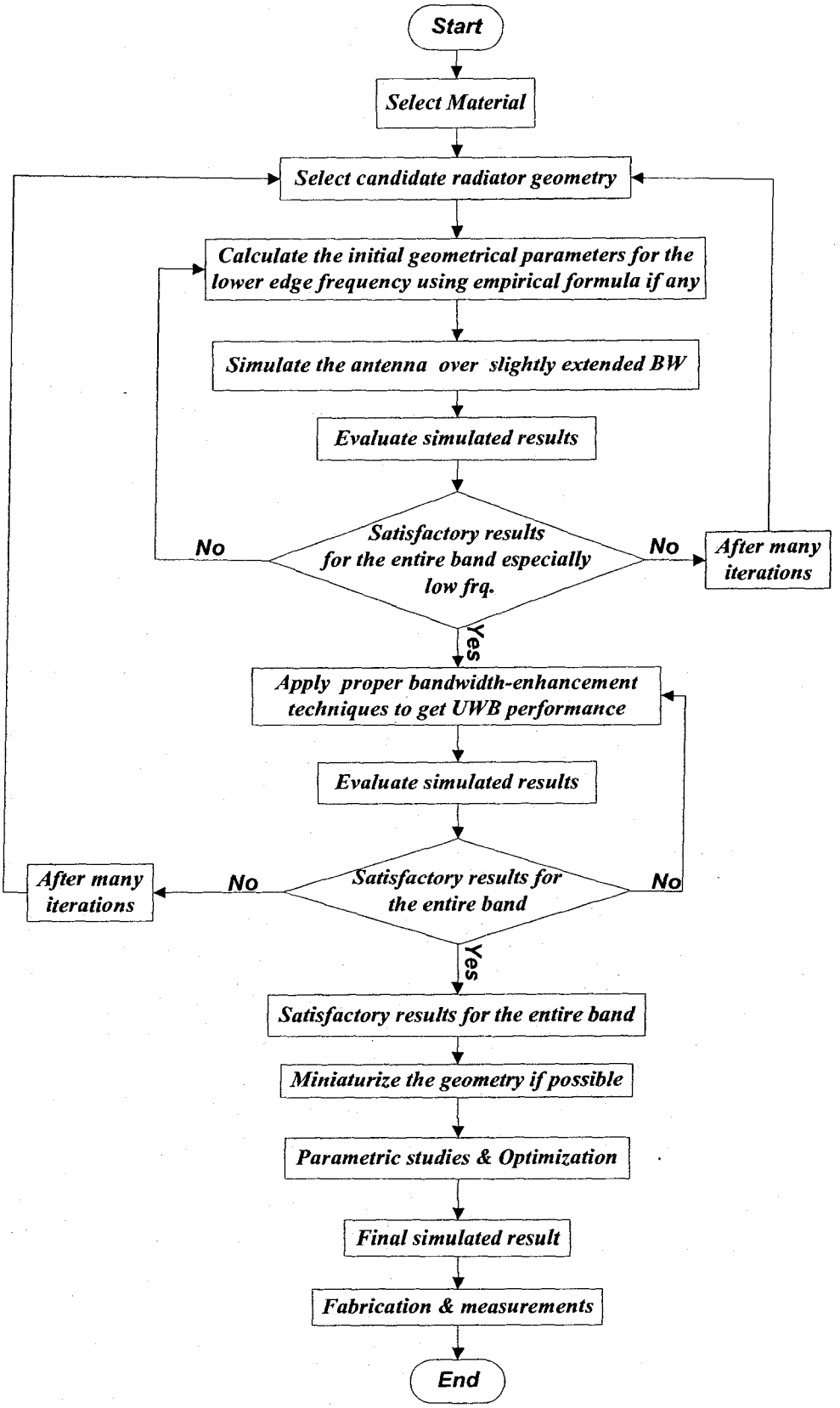

Figure 3.1: Design methodology

3.2 The Stepped-Trapezoidal Patch Antenna

3.2.1 Overview

A novel planar patch antenna with a circular-notch cut fed by a simple microstrip line is proposed and described. It is designed and fabricated for UWB wireless communications and applications over the band 3.1 - 10.6 GHz. This antenna is composed of an isosceles trapezoidal patch with the circular-notch cut and two transition steps as well as a partial ground plane. Because of its structure, we have called it "the stepped-trapezoidal patch antenna" [116]. To obtain the UWB bandwidth, we use many bandwidth enhancement techniques: the use of partial ground plane, adjusting the gap between radiating element and ground plane technique [61], using steps to control the impedance stability [83, 84] and a notch cut technique. The notch cut from the radiator is also used to miniaturize the size of the planar antenna [20]. A parametric study is numerically carried out on the important geometrical parameters to understand their effects on the performance of the proposed antenna in order to then optimize its performance. The measured -10 dB return loss bandwidth for the designed antenna is about 137.2 % (8.7 GHz). The proposed antenna provides an acceptable radiation pattern and a relatively flat gain over the entire frequency band. The measured and simulated results for both return loss and radiation pattern show a very reasonable agreement.

In the following subsections, the design details and related results will be presented and discussed. First, the antenna geometry and design process are explained. Second, the parametric study is carried out to address the effects of the trapezoidal patch height, the notch cut, the feed gap and the two transition steps on the proposed antenna

characteristics and hence optimize the antenna performance based on the optimal value of these parameters. Next, the current distribution is studied in order to miniaturize the size of the antenna by removing parts of the radiator that do not contribute to the radiation. Finally, the simulated and measured return loss, radiation pattern, gain and radiation efficiency are provided and discussed.

3.2.2 Antenna Design

3.2.2.1 Design Process

The antenna is designed based on the developed design methodology mentioned earlier. Figure 3.2 depicts the design steps used to design the proposed antenna. First, the substrate is chosen to be Rogers RT/Duroid 5880 material with a relative permittivity ε_r=2.2 and a thickness of 1.575 mm. Second, the radiator shape is selected to be trapezoidal since it can exhibit a UWB characteristic. Next, the initial parameters are calculated using the following empirical formula reported in [72] after adding the effect of the substrate:

$$f_L(GHz)=\frac{904}{(4\pi h+W+W_1)} \qquad (3.2)$$

Where:

f_L: the frequency corresponding to the lower edge of the bandwidth for the trapezoidal sheet.

W and W_1: the width of the trapezoidal patch bases.

h: the height of the trapezoidal patch.

The dimensions are expressed in mm. This formula is used to predict the lower edge frequency of the bandwidth for the trapezoidal sheet suspended in the space over the ground plane. It is accurate to +/- 9 % for frequencies in the range 500 MHz to 6 GHz.

In our design, the sheet will be a patch printed on substrate, so, the effect of the substrate has to be added to the formula. After adding it, the formula becomes:

$$f_L(GHz) = \frac{904}{(4\pi h + W + W_1)\sqrt{\varepsilon_{reff}}} \qquad (3.3)$$

Where the effective relative permittivity ε_{reff} can be calculated using:

$$\varepsilon_{reff} = \frac{\varepsilon_r + 1}{2} \qquad (3.4)$$

Where

ε_r: the relative permittivity of the substrate

Since the antenna is designed for UWB, it has to operate over 3.1 - 10.6 GHz. Therefore, the lower edge frequency at which the initial parameters will be calculated is 3.1 GHz. Initially, the antenna consists of an isosceles trapezoidal patch and partial ground plane etched on opposite sides of the substrate. The radiator is fed through a microstrip line with 50-Ω characteristic impedance. After setting up the configuration of the antenna, determining the initial parameters and fixing the lower frequency, the simulation is started to confirm the calculated parameters. Then, several bandwidth enhancement techniques are applied to widen the bandwidth and to obtain the UWB performance. These techniques are: adjusting the gap between radiating element and ground plane technique, using steps to control the impedance stability and the notch cut technique used after studying the current distribution as will be discussed later. Therefore,

the notch cut from the radiator is also used to miniaturize the size of the planar antenna.

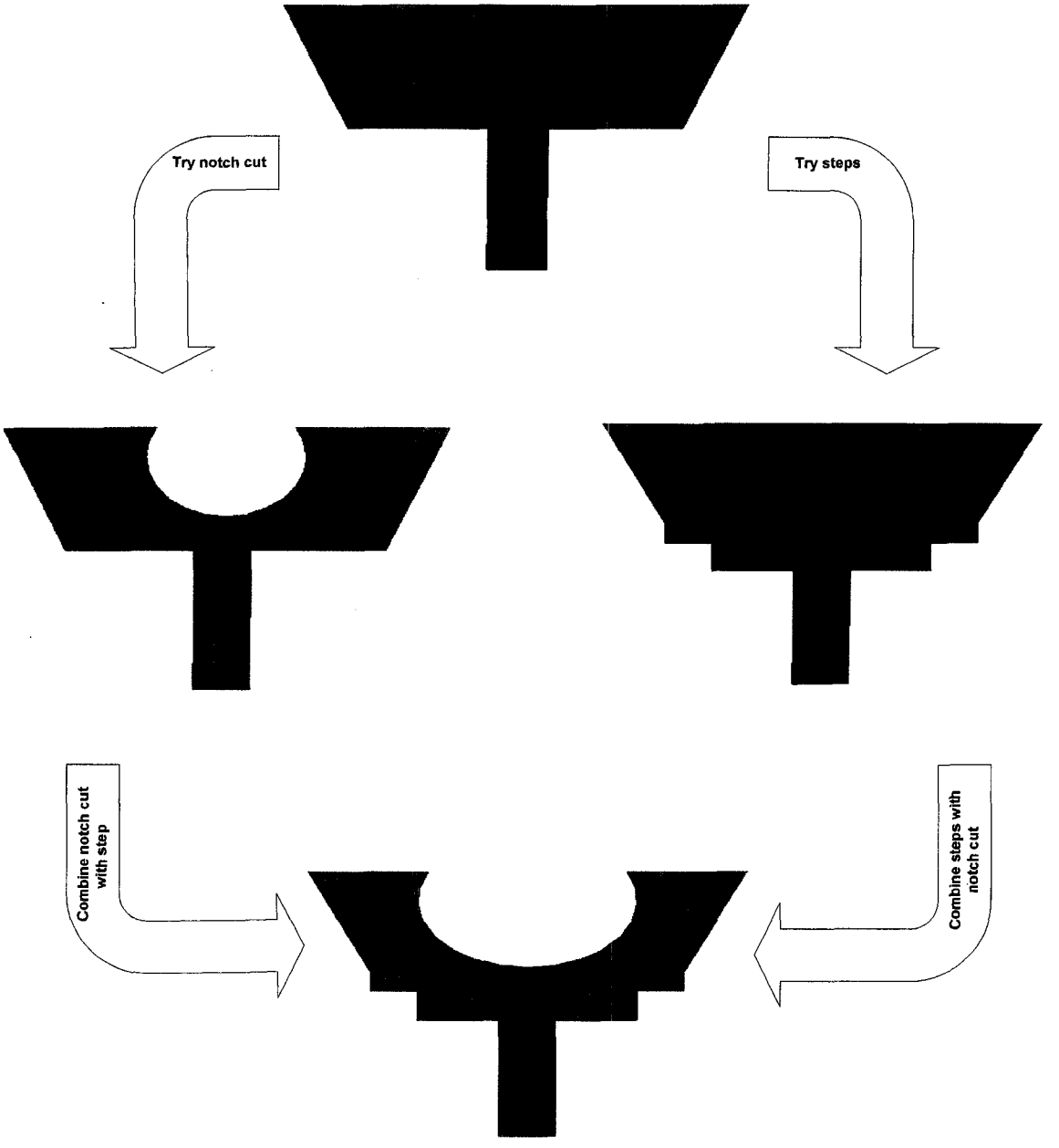

Figure 3.2: Flowchart for the design steps of the stepped-trapezoidal patch antenna

3.2.2.2 Antenna Geometry

Figure 3.3 illustrates the geometry of the printed antenna as well as the Cartesian coordinate system.

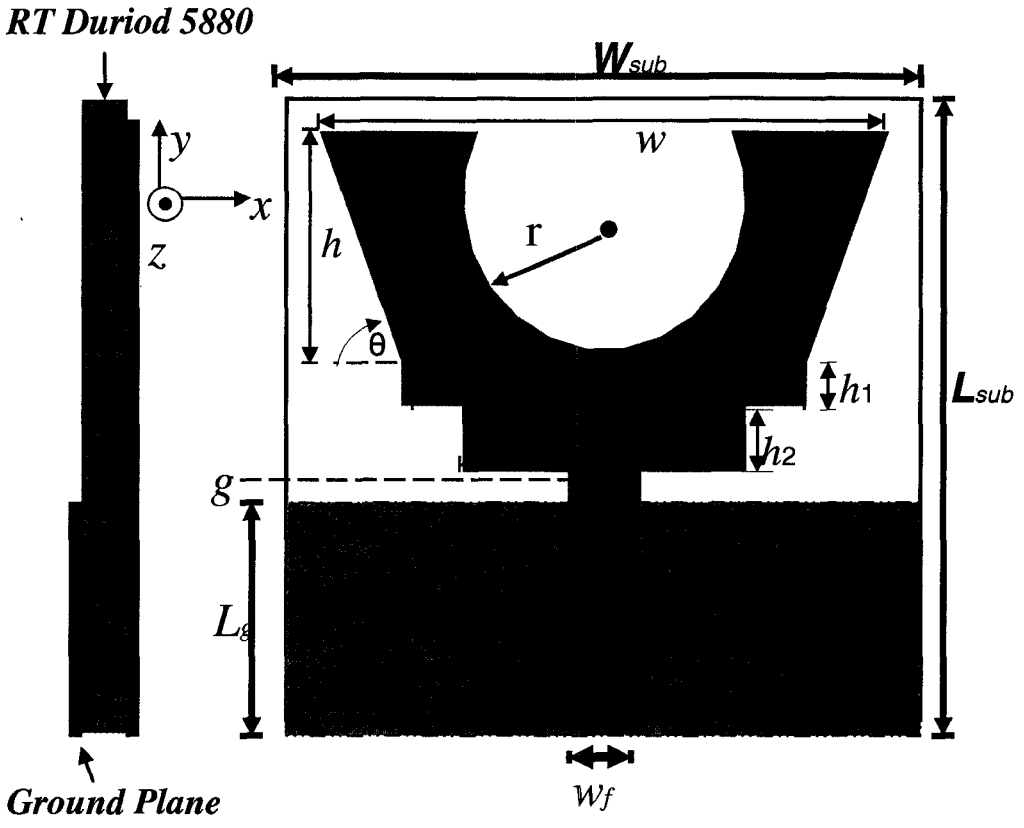

Figure 3.3: The geometry of the stepped-trapezoidal patch antenna

It consists of an isosceles trapezoidal patch with notch cut and two transition steps and a partial finite-size ground plane. The Cartesian coordinate system (x,y,z) is oriented such that the bottom surface of the substrate lies in the x-y plane. All the following parameters are optimal values. The antenna and the partial ground plane are etched on opposite sides of the Rogers RT/Duroid 5880 substrate. The substrate size of the proposed antenna is 30 × 30 mm^2. The dimensions of isosceles trapezoidal patch are w=28 mm, w_1=20 mm and h=10.5 mm. The first transition step of $w_1 \times h_1$ = 20 mm × 2 mm and

second transition step of $w_2 \times h_2 = 14$ mm $\times$ 3 mm are attached to the isosceles trapezoidal patch. To reduce the overall size of the printed antenna and to get a better impedance match, the circular-shaped notch with radius r =7 mm is symmetrically cut in the top middle of the isosceles trapezoidal radiator. The shape of the partial ground plane is selected to be rectangular with dimensions of 11 $\times$ 30 mm^2. The radiator is fed through a microstrip line having a length of 12 mm and width w_f =3.6 mm to ensure 50-Ω characteristic impedance with a feed gap $g = 1$ mm.

3.2.3 Current Distribution

The simulated current distributions of the initial geometry for the proposed antenna before cutting the region of low current density at 3.5 GHz, 6.5 GHz, and 9.5 GHz are shown in Figure 3.4 (a), (b), and (c) respectively. Also, the simulated current distributions of the final geometry for the proposed antenna after cutting the region of low current density at 3.5 GHz, 6.5 GHz, and 9.5 GHz are shown in Figure 3.4 (d), (e), and (f), respectively.

As shown in Figure 3.4 (a), (b), and (c), the current is mainly concentrated on the bottom portion of the patch with very low current density toward and above the center and it is distributed along the edges of the patch, except the top edge, for all frequencies. Also, it is observed that the current distributions are symmetric about the axis of the transmission line and show a coupling between the currents at the bottom outer edge of the patch and the top-edge of the ground plane. From this observation, one can conclude that the region of low current density on the patch is not that important in the antenna performance and could hence be cut out without affecting the antenna performance

especially the radiation characteristics [44,117].

Consequently, a circular section of radius r = 7 mm is symmetrically cut out from the top middle of the isosceles trapezoidal radiator to eliminate a region of low current density as shown in Figure 3.3. After this cut, the current distributions at 3.5 GHz, 6.5 GHz, and 9.5 GHz are depicted in Figure 3.4 (d), (e), and (f), respectively. It is observed that the current distributions in this case are approximately the same as before the cut. In addition, there is also some less intense type of current concentration on the edge of the cutout. This is expected because the cutout edge represents a discontinuity for the surface currents on the patch. As a result of this cut, the size of the antenna is reduced and has lighter weight, which is very desirable from the miniaturization point of view. More degree of freedom in design and possibly less conductor losses are achieved.

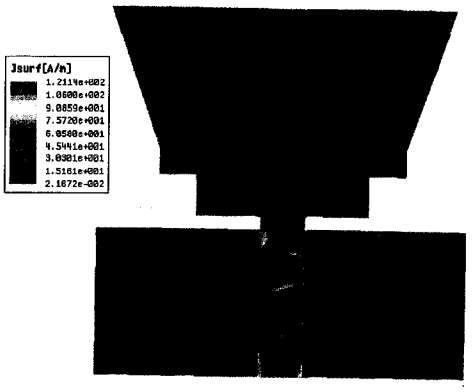

(a) at 3.5 GHz

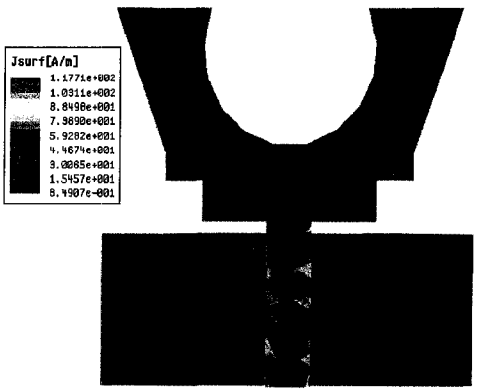

(d) at 3.5 GHz

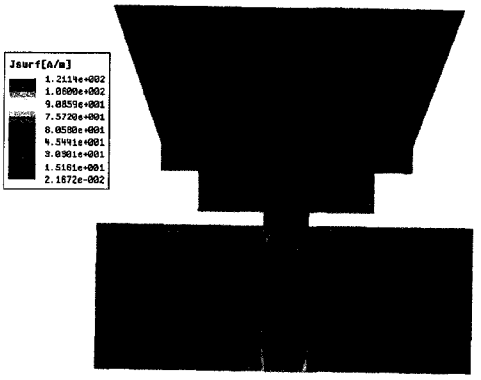

(b) at 6.5 GHz

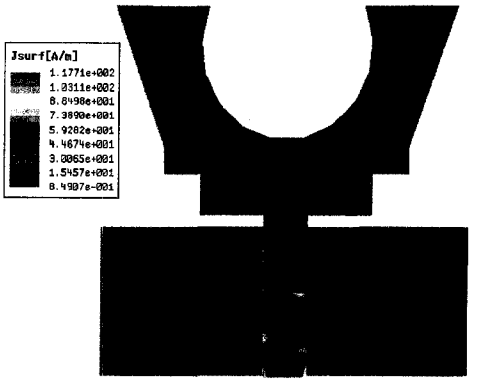

(e) at 6.5 GHz

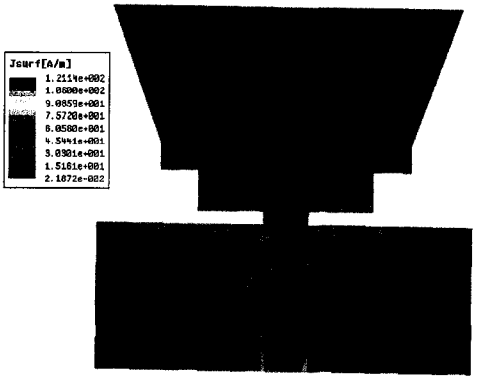

(c) at 9.5 GHz

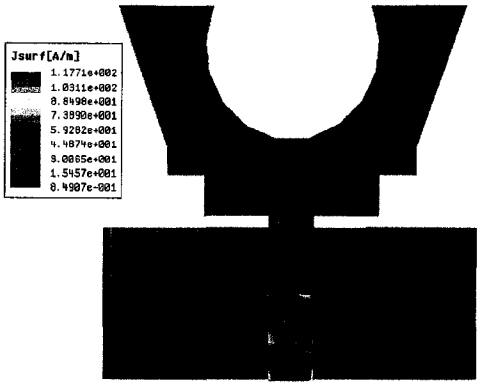

(f) at 9.5 GHz

Figure 3.4: The current distributions of the stepped-trapezoidal patch antenna

3.2.4 Parametric Study

The parametric study is carried out to optimize the antenna and provide more information about the effects of the essential design parameters. The antenna performance is mainly affected by geometrical and electrical parameters, such as the dimensions related to the height of the trapezoidal patch, the notch cut, the two transition steps and the feed gap.

3.2.4.1 Height of the Trapezoidal Patch

Figure 3.5 exhibits the return loss when the trapezoidal patch height changes. The height is represented using the angle (θ) as shown in Figure 3.3. This parameter affects lower edge frequency as well as the middle frequency band. By tuning this parameter, the antenna has better matching impedance over the entire UWB frequency.

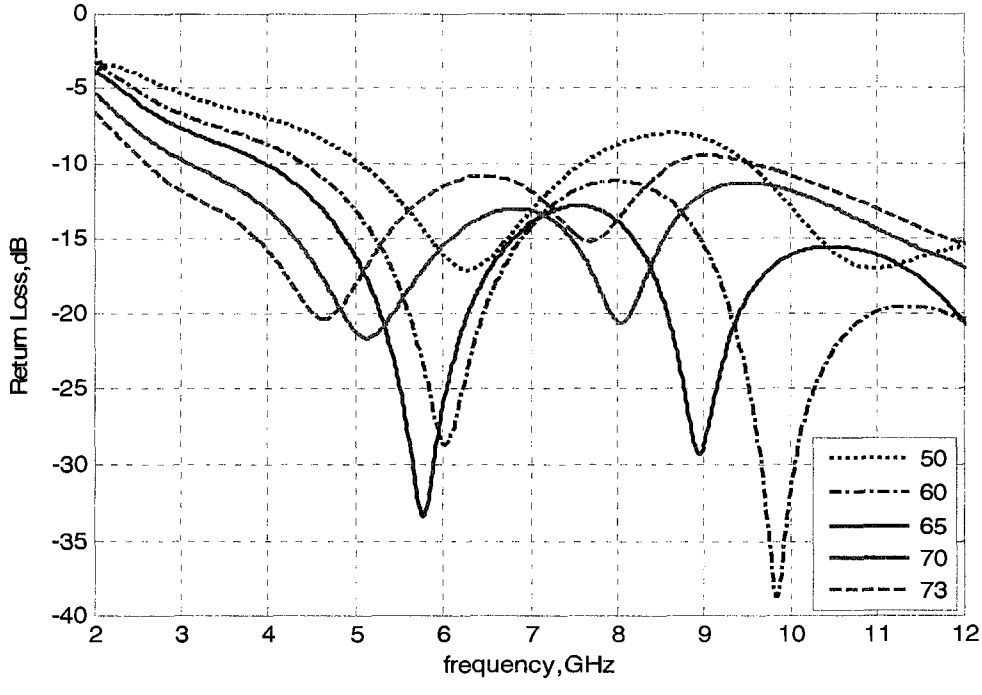

Figure 3.5: Effects of the angle (θ)

3.2.4.2 Notch Cut

The circular-shaped notch cut is described by its radius and the location of its center. Both parameters are studied. The effect of varying the notch radius on the impedance matching is depicted in Figure 3.6. When the radius is increased, the entire band is highly affected, especially the middle and higher frequencies experience higher mismatch levels. It is obviously observed that the notch can be used to reduce the size of the radiator provided that the current distribution has low density in the notch part. On the other hand, when the center of the notch moves in the upper side of the patch, the entire band is slightly influenced. In general, the notch cut parameters affect the impedance matching to a certain extent [20].

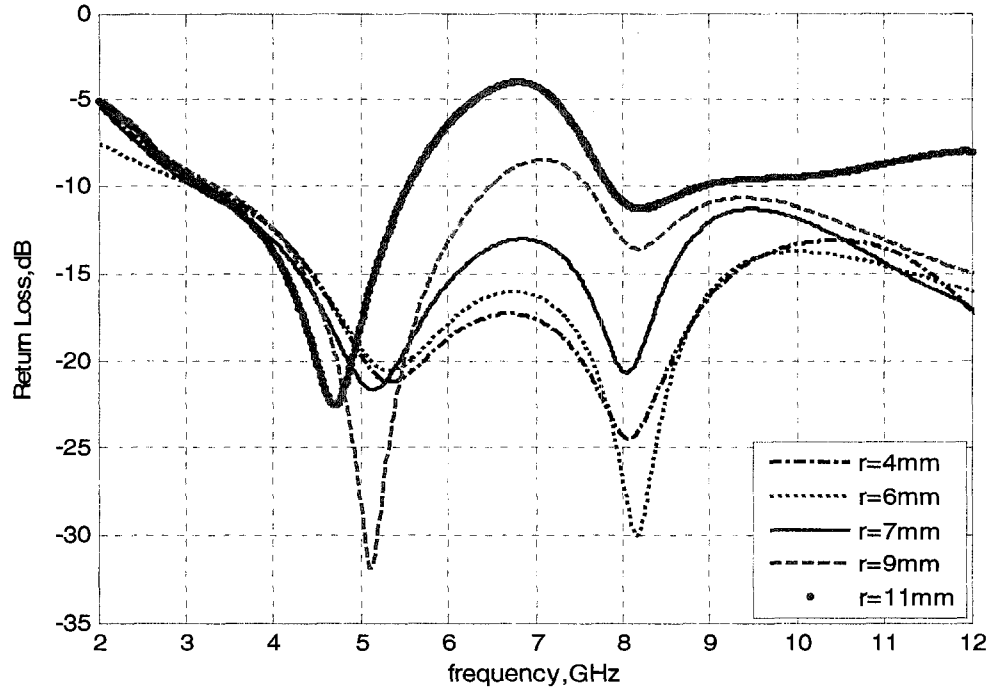

Figure 3.6: Effects of notch cut radius

3.2.4.3 Transition Steps

The effects of the two transition steps are studied. They have great impact on the

matching impedance for the whole band. For example, the effect of the width of the second step is depicted in Figure 3.7. From the plot, the step width greatly affects the entire band, especially at the high frequencies range, because the two steps influence the coupling between the radiator and the ground plane. Thus, by adjusting the steps parameters, the impedance bandwidth can be enhanced [83]. In Figure 3.10, it is clear that a net improvement on the antenna bandwidth is obtained when the two transitions steps are used.

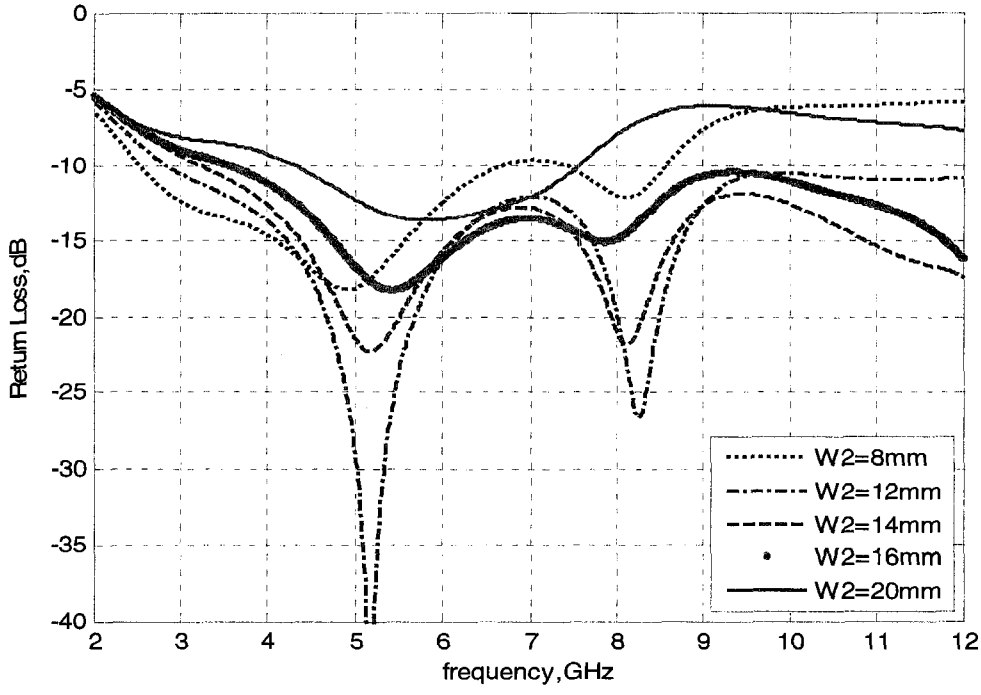

Figure 3.7: Effects of step width

3.2.4.4 Feed Gap

Figure 3.8 shows the effect of the feed gap (g) between the radiator and the upper edge of the system ground plane. The feed gap affects the entire frequency band. By adjusting the feed gap, high impedance matching can be achieved [72].

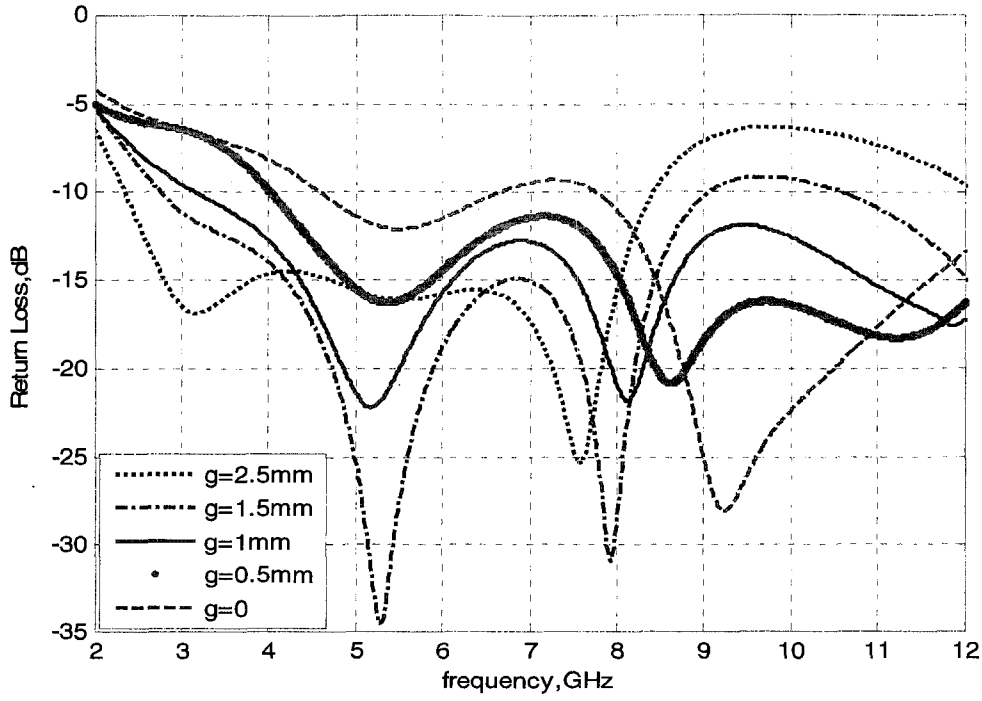

Figure 3.8: Effects of feed gap

3.2.5 Results and Discussion

After taking into account the design considerations described on antenna structure, current distributions and parametric study done to optimize the antenna geometry, the optimized antenna is constructed as shown in Figure 3.9. It is built on Rogers RT/Duroid 5880 material with a relative permittivity ε_r=2.2 and a thickness of 1.575 mm using the following optimized parameters: L_{sub} = 30 mm, W_{sub} =30 mm, w= 28 mm, w_1= 20 mm, h=10.5 mm, h_1= 2 mm, w_2= 14 mm, h_2= 3 mm, r =7 mm, w_f = 3.6, g =1 and L_g= 11 mm. Then, the antenna is experimentally tested to confirm the simulation results. The simulated and measured return loss is presented in addition to the simulated and measured radiation patterns in principle planes. Also, the simulated gain and radiation efficiency are provided.

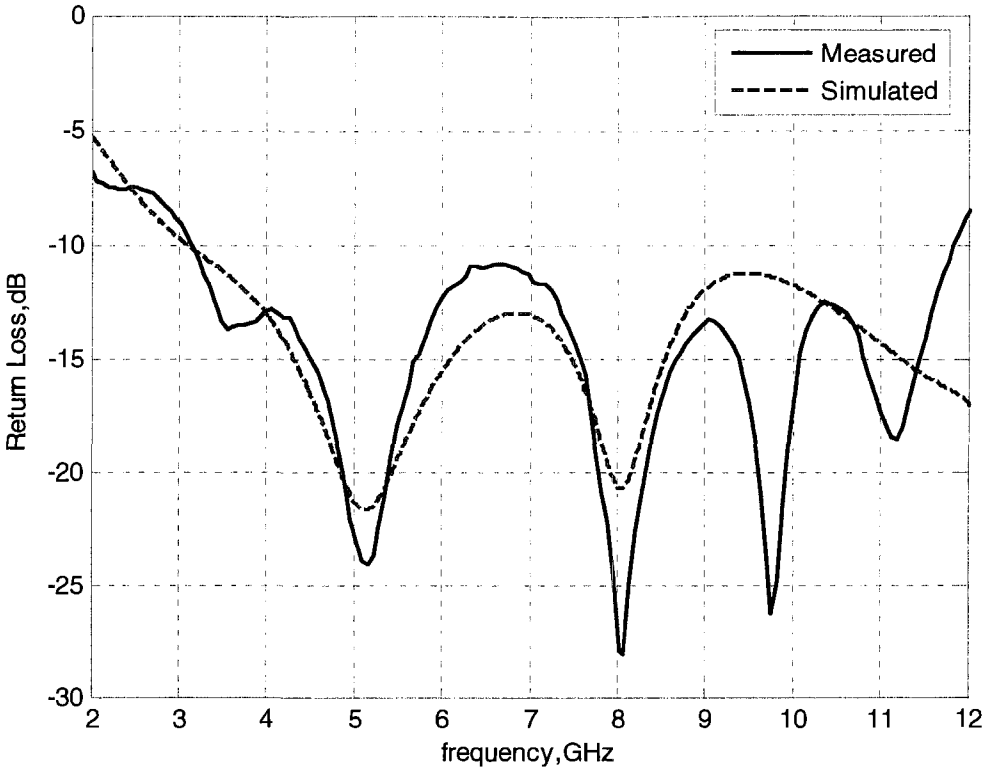

Figure 3.10: The simulated & measured return loss

3.2.5.2 *Antenna Radiation Patterns*

The radiation characteristics of the proposed antenna are also investigated. The two dimensional radiation patterns presented here is taken at two sets of principal cuts, ϕ=0° and ϕ=90°. Referring to the coordinate system attached to the antenna geometry in Figure 3.3, the H-plane is the xz-plane and the E-plane is the yz-plane. Figures 3.11 and 3.12 illustrate the simulated and measured H-plane and E-plane radiation patterns respectively at 3.5, 5.5, 7.5 and 9.5 GHz. The radiation patterns of the antenna are measured inside an anechoic chamber. In general, the simulated and measured results are fairly consistent with each other at most of the frequencies but some discrepancies are noticed at higher frequencies, especially in the E-plane. These discrepancies are most likely a result of the cable leakage current on the coaxial cable that is used to feed the

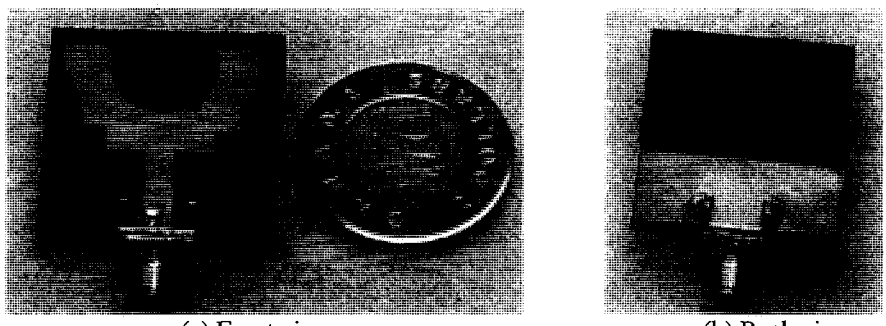

(a) Front view (b) Back view

Figure 3.9: The prototype of the stepped-trapezoidal patch antenna

3.2.5.1 Return Loss

The return loss (S_{11}) of the proposed antenna is measured. As depicted in Figure 3.10, the measured and simulated results are shown for comparison and indicate a reasonable agreement. In fact, the simulated return loss of the antenna is found to remain below -10 dB beyond 12 GHz but that range of frequencies is omitted in Figure 3.10 since it is far out of the allocated bandwidth for UWB communications under consideration. The measured -10 dB return loss bandwidth of the antenna is approximately 8.7 GHz (3.13 - 11.83 GHz) and the antenna shows stable behaviors over the band. Excellent performance is obtained since the measured return loss is very close to the simulated one in most range of the frequency band. Thus, the measurement confirms the UWB characteristic of the stepped-trapezoidal patch antenna as predicted in the simulation.

The measured return loss shows that the antenna is capable of supporting multiple resonance modes, which are closely distributed across the spectrum. Therefore, the overlapping of these resonance modes leads to the UWB characteristic.

antenna prototype in the measurements [118]. This leakage current is known to be frequency sensitive as well. Also, intrinsic noise within the anechoic chamber may contribute to these discrepancies.

Nevertheless, an analysis of the radiation pattern results shows that the proposed antenna is characterized by omni-directional patterns in the H-plane for all in-band frequencies, as in Figure 3.11. The measured *H*-plane patterns follow the shapes of the simulated ones well, except at 9.5 GHz where there is little difference.

For the E-plane patterns, Figure 3.12 shows that they form a figure-of-eight pattern for frequencies up to7.5 GHz but at 9.5 GHz the shape changes. However, the measured *E*-plane patterns generally follow the simulated ones well.

In general, the stepped-trapezoidal patch antenna shows an acceptable radiation pattern variation in its entire operational bandwidth since the degradation happens only for a small part of the entire bandwidth and it is not too severe.

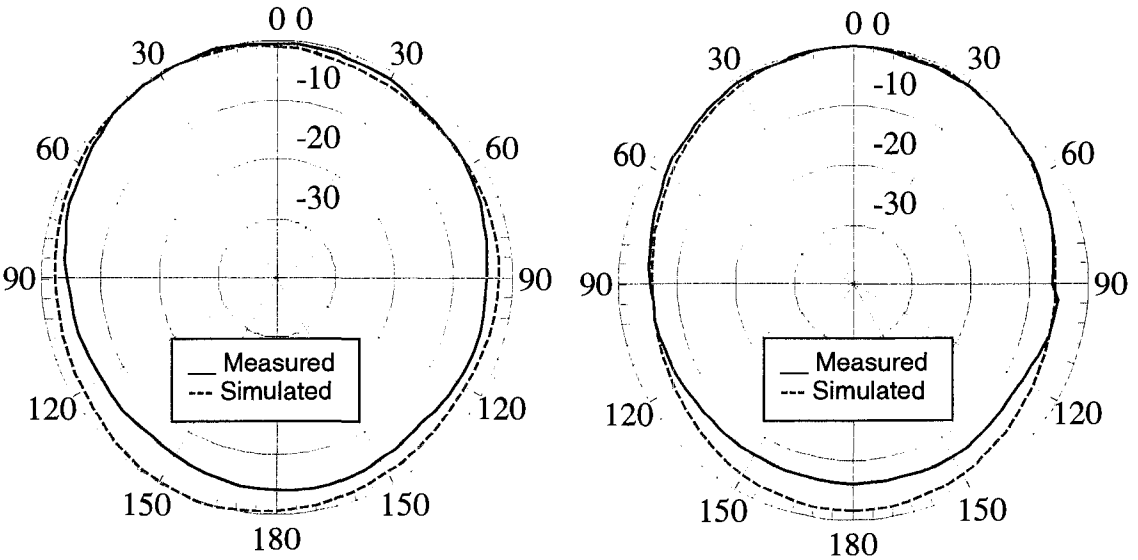

(a) H-plane at 3.5GHz

(b) H-plane at 5.5GHz

(c) H-plane at 7.5GHz

(d) H-plane at 9.5GHz

Figure 3.11: The simulated and measured radiation patterns in the H-plane at 3.5, 5.5, 7.5 and 9.5 GHz

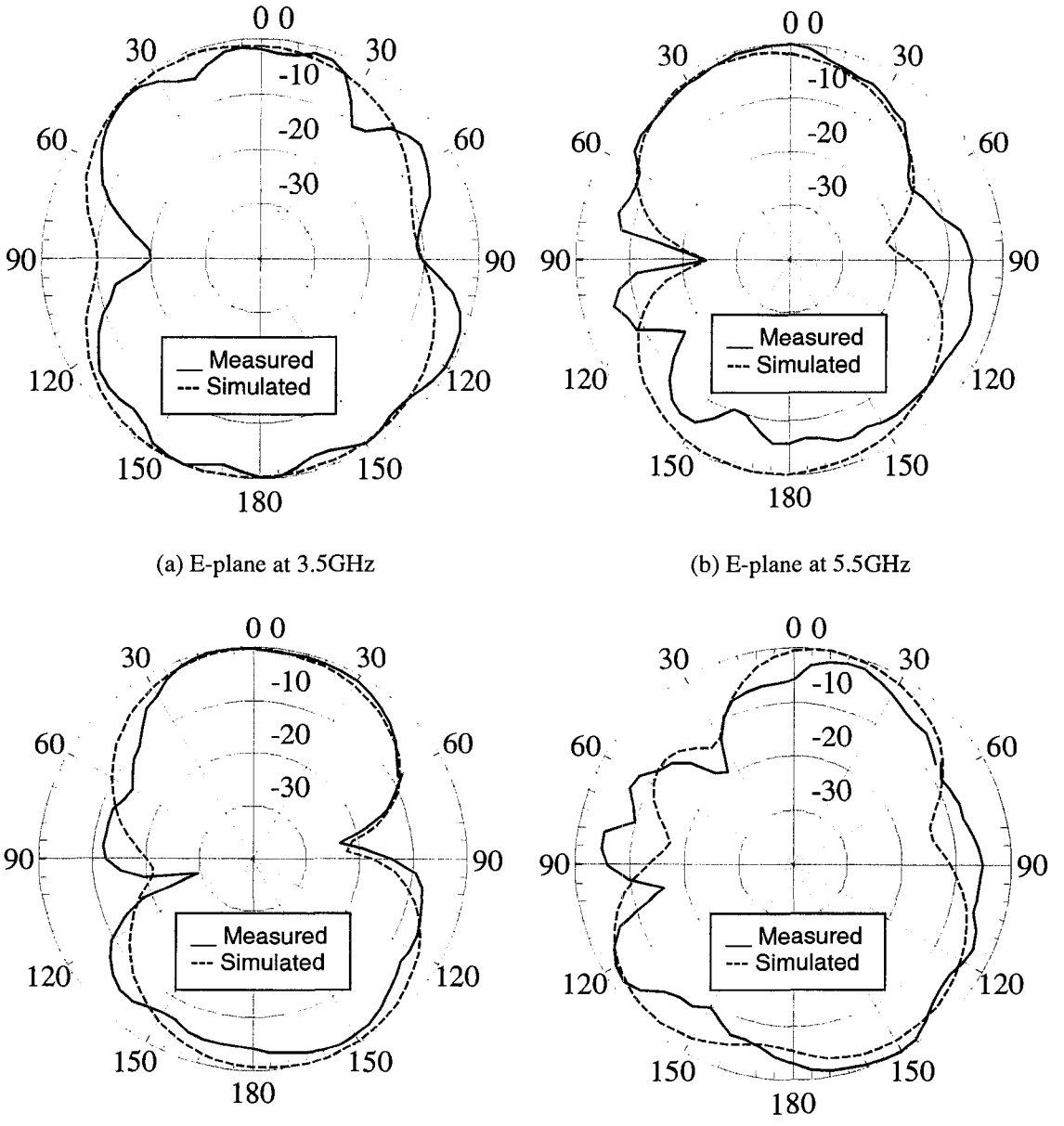

(a) E-plane at 3.5GHz

(b) E-plane at 5.5GHz

(c) E-plane at 7.5GHz

(d) E-plane at 9.5GHz

Figure 3.12: The Simulated and measured radiation patterns in the E-plane at 3.5, 5.5, 7.5 and 9.5 GHz

3.2.5.3 Gain and Radiation Efficiency

The gain and radiation efficiency of the proposed antenna are also found to be suitable for the UWB communications and applications. The simulated antenna gain versus frequency is shown in Figure 3.13. It is greater than 2.9 dBi for all in-band

frequencies and varies from 2.9 dBi to 5.2 dBi over the operating frequency range, resulting in the maximum gain variation of 2.3 dB. The radiation efficiency is substantially high throughout the operational bandwidth of the antenna. Figure 3.14 shows that it is greater than 94 % in most of the operational bandwidth. Ohmic losses are not included in the calculated radiation efficiency.

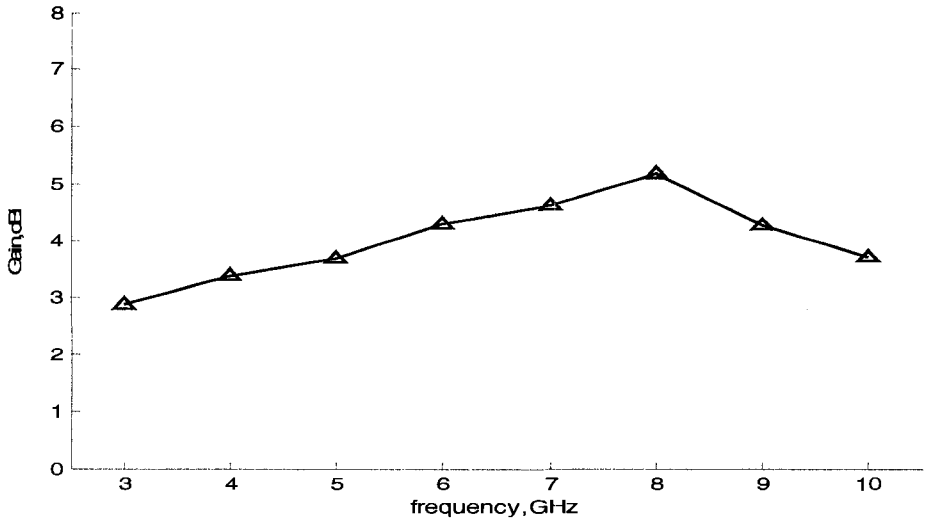

Figure 3.13: Simulated gain

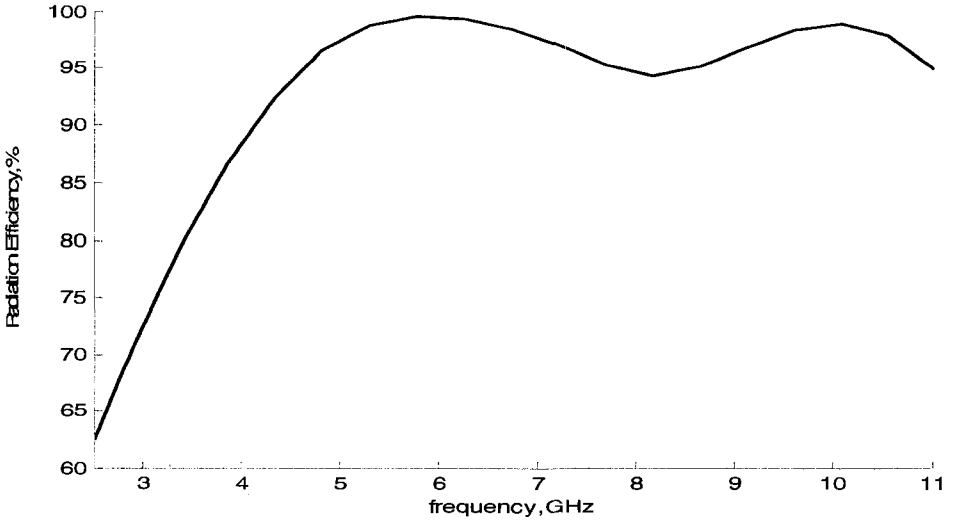

Figure 3.14: Radiation efficiency

3.3 The Trimmed Notch-Cut Patch Antenna

3.3.1 Overview

A novel planar patch antenna with a trimmed notch-cut fed by a simple microstrip line is proposed and described. It is designed and fabricated for UWB wireless communications and applications under the band (3.1-10.6 GHz). This antenna is composed of a planar rectangular patch with notch cut and a transition step fed by a microstrip line with a partial ground plane. Because of its structure, we have called it "the trimmed notch-cut patch antenna" [119]. To obtain UWB bandwidth, we use several bandwidth-enhancement techniques: the use of partial ground plane, adjusting the gap between radiating element and a ground plane technique [61], using steps to control the impedance stability [84] and a notch cut technique which is also used to reduce the size of the planar antenna [20]. A parametric study is numerically carried out on the important geometrical parameters to understand their effects on the proposed antenna and therefore optimize its performance. The measured -10 dB return loss bandwidth for the designed antenna is about 132.1 % (7.5 GHz). The proposed antenna provides an acceptable radiation pattern and a relatively flat gain over the entire frequency band. The measured and simulated results for both bandwidth and radiation pattern shows a very reasonable agreement.

In the following subsections, the design details and related results will be presented and discussed. First, the antenna geometry and design process are explained. Second, the parametric study is carried out to address the effects of the notch cut, the transition step and the feed gap on the proposed antenna characteristics and hence

optimize the antenna performance accordingly. Next, the current distribution is studied in order to miniaturize the size of the antenna by removing parts of the radiator that do not contribute to the radiation. Finally, the simulated and measured results, such as return loss, radiation pattern, gain and radiation efficiency are provided and discussed.

3.3.2 Antenna Design

3.3.2.1 Design Process

The antenna is designed based on the developed design methodology mentioned earlier. Figure 3.15 depicts the design steps used to design the proposed antenna. First, the substrate is chosen to be Rogers RT/Duroid 5880 material with a relative permittivity ε_r=2.2 and a thickness of 1.575 mm. Second, the radiator shape is selected to be rectangular. Next, the initial parameters are calculated using the empirical formula reported in [61] after adding the effect of the substrate:

It is found that the frequency corresponding to the lower edge of the bandwidth of the monopole antenna can be predicted approximately by equating the area of the planar configuration to that of a cylindrical wire and given by:

$$2\pi rl=hW \qquad (3.5)$$

So, the resonant frequency is given by:

$$f_L(GHz)=\frac{c}{\lambda}=\frac{30\times 0.24}{l+r} \qquad (3.6)$$

Where:

f_L: the frequency corresponding to the lower edge of the bandwidth.

C: the light speed.

λ : the wavelength

l: the height of the cylindrical wire which is same as that of planar configuration height

r: the equivalent radius of the cylindrical wire

W: the width of the rectangular patch.

h: the height of the rectangular patch.

The dimensions are expressed in centimeters. This simple formula is used to predict the lower edge frequency of the bandwidth for the monopole suspended in the space over the ground plane. It is accurate to +/- 8 %.

In our design, the sheet will be a patch printed on the substrate, so, the effect of the substrate has to be added to the formula. After adding it, the formula becomes:

$$f_L(GHz)=\frac{30\times 0.24}{(l+r)\sqrt{\varepsilon_{reff}}} \qquad (3.7)$$

Where the effective relative permittivity ε_{reff} can be calculated using Equation 3.4:

Since the antenna is designed for UWB, it has to operate over 3.1 - 10.6 GHz. Therefore, the lower edge frequency at which the initial parameters will be calculated is 3.1 GHz. Initially, the antenna consists of a rectangular patch and partial ground plane etched on opposite sides of the substrate. The radiator is fed through a microstrip line with 50-Ω characteristic impedance. After setting up the configuration of the antenna, determining the initial parameters and fixing the lower frequency, the simulation is performed to confirm the calculated parameters. Then, several bandwidth enhancement techniques are applied to widen the bandwidth and obtain UWB performance. These techniques are: adjusting the gap between radiating element and ground plane technique, using a step to control the impedance stability and notch cut technique, which is used after

studying the current distribution as will be discussed later. Therefore, the notch cut from the radiator is also used to miniaturize the size of the planar antenna.

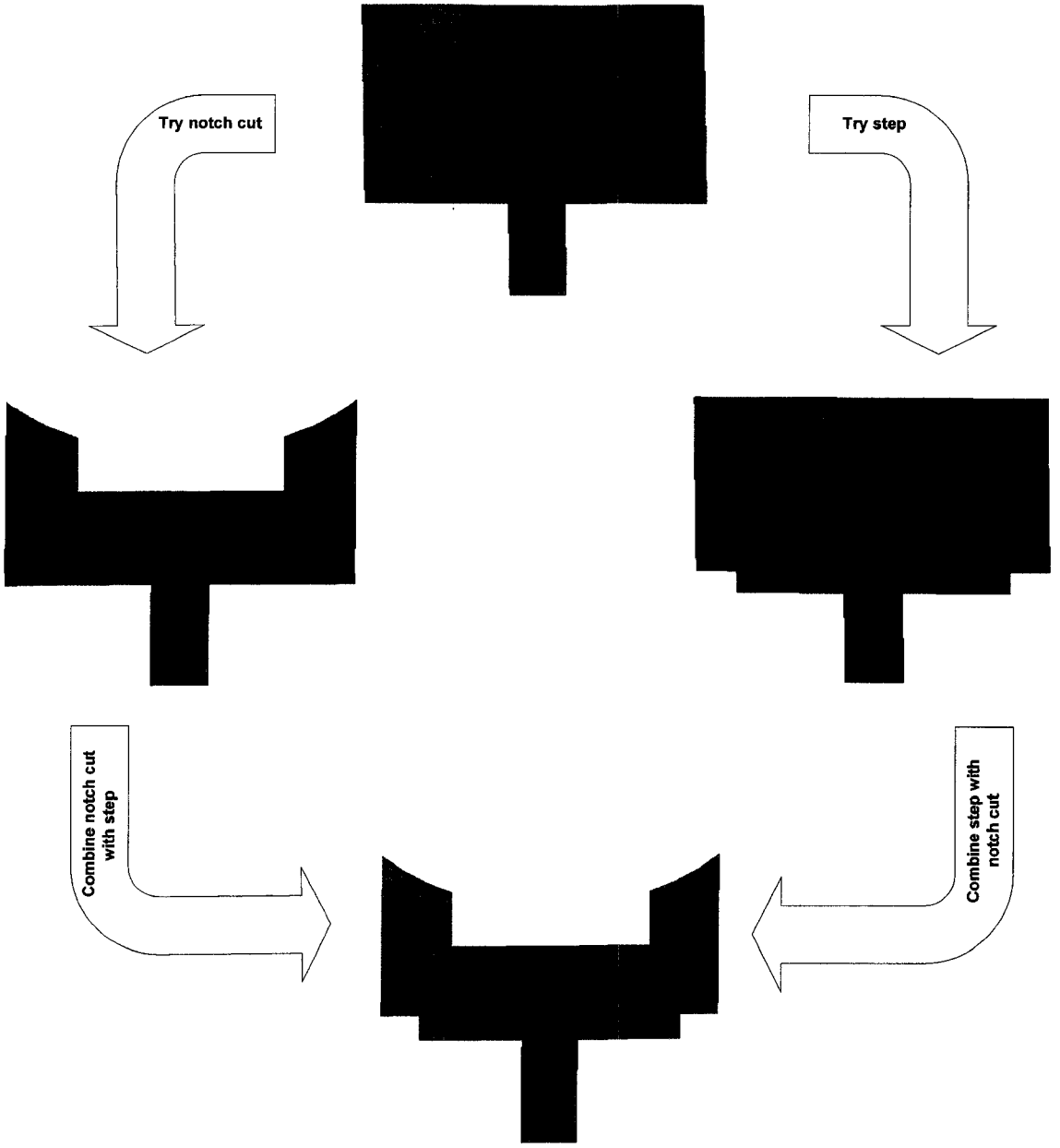

Figure 3.15: Flowchart for the design steps of the trimmed notch-cut patch antenna

3.3.2.2 Antenna Geometry

Figure 3.16 illustrates the geometry of the printed antenna as well as the Cartesian coordinate system.

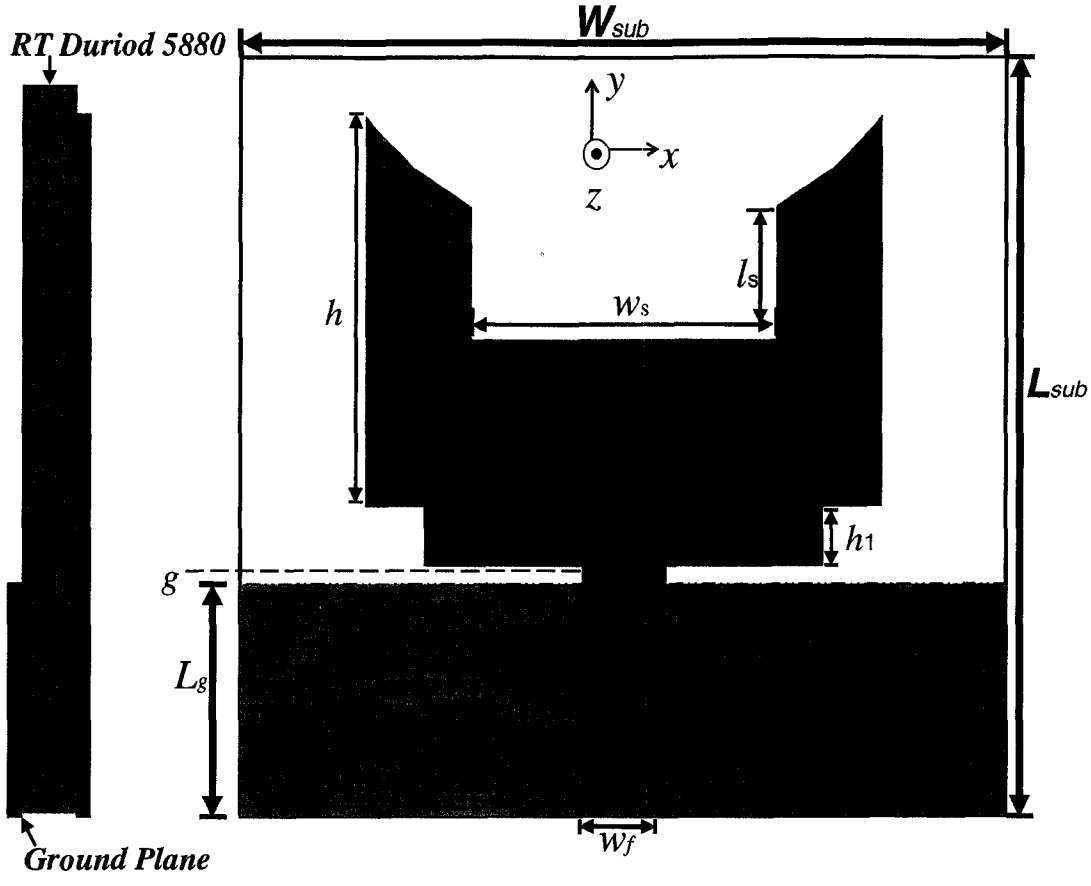

Figure 3.16 : The geometry of the trimmed notch-cut patch antenna

It consists of a rectangular patch with notch cut and the transition step as well as the partial ground plane. The Cartesian coordinate system (x,y,z) is oriented such that the bottom surface of the substrate lies in the x-y plane. All the following parameters are the optimal dimensions. The antenna and the partial ground plane are oppositely etched on the Rogers RT/Duroid 5880 substrate. The substrate size of the proposed antenna is 40 × 32 mm^2. The dimensions of the rectangular patch are w=22 mm and h=16.33 mm. The transition step of $w_1 \times h_1$ = 17 mm × 2.5 mm is attached to the rectangular patch. To reduce the overall size of the printed antenna and to get better impedance matching, a rectangular-shaped notch with dimensions of $l_s \times w_s$ = 5.6 mm × 13 mm is symmetrically cut in the top middle of the radiator and both top edges of the patch are trimmed. The shape

of the partial ground plane is rectangular with dimensions of 9.5 × 40 mm^2. The radiator is fed through a microstrip line having a length of 10.5 mm and width of w_f =3.6 mm to ensure 50-Ω input impedance with a feed gap g = 1.0 mm. The 50 Ω-microstrip line is printed on the same side of the substrate as the radiator.

3.3.3 Current Distribution

The simulated current distributions of the initial geometry for the proposed antenna before cutting the region of low current density at 3.5 GHz, 6.5 GHz, and 9.5 GHz are shown in Figure 3.17 (a), (b), and (c) respectively. Also, the simulated current distributions of the final geometry for the proposed antenna after cutting the region of low current density at 3.5 GHz, 6.5 GHz, and 9.5 GHz are shown in Figure 3.17 (d), (e), and (f), respectively.

As shown in Figure 3.17 (a), (b), and (c), the current is mainly concentrated on the bottom portion of the patch with very low current density toward and above the center and it is distributed along the edges of the patch, except the top edge, for all frequencies. Also, it is observed that the current distributions are symmetric about the axis of the transmission line. Therefore, one can conclude that the region of low current density on the patch is not that important for the overall antenna performance and could hence be cut out.

Consequently, a rectangular section with dimensions of $l_s \times w_s$ = 5.6 mm × 13 mm is symmetrically cut out from the top middle of the rectangular radiator. Both top edges of the patch are also trimmed to eliminate a region of low current density as shown in Figure 3.16. After this cut, the current distributions at 3.5 GHz, 6.5 GHz, and 9.5 GHz are

depicted in Figure 3.17 (d), (e), and (f), respectively. It is observed that the current distributions in this case are approximately the same as before the cut. As a result of this cut, the size of the antenna is reduced and has lighter weight, which is very desirable for more degrees of freedom in design and possibly less conductor losses.

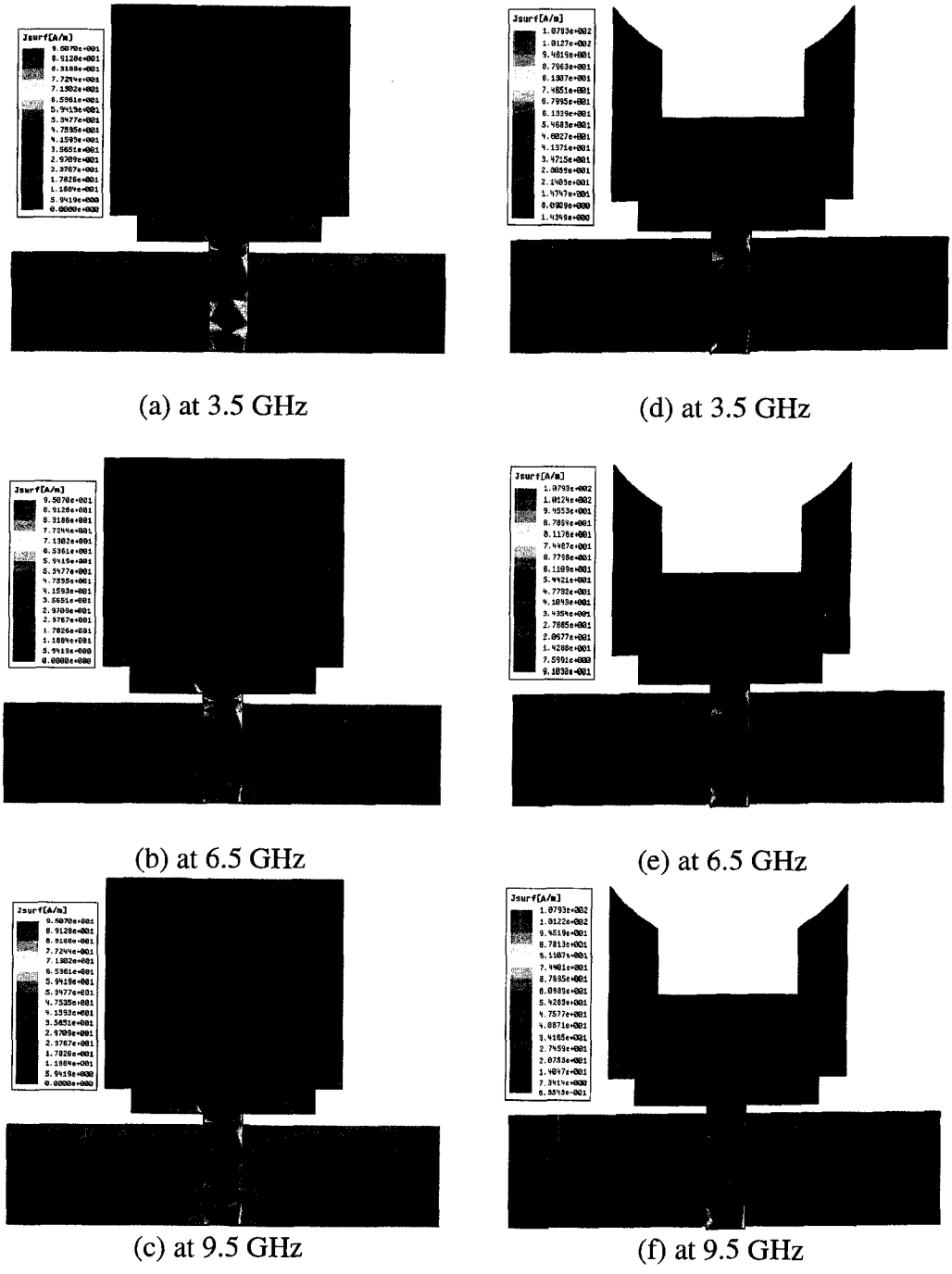

(a) at 3.5 GHz

(d) at 3.5 GHz

(b) at 6.5 GHz

(e) at 6.5 GHz

(c) at 9.5 GHz

(f) at 9.5 GHz

Figure 3.17: The current distributions of the trimmed notch-cut patch antenna

3.3.4 Parametric Study

The parametric study is carried out to optimize the antenna and provide more information about the effects of the essential design parameters. The antenna performance is mainly affected by geometrical parameters, such as the dimensions related to the notch cut, the transition step and the feed gap.

3.3.4.1 Notch Cut

The effect of the rectangular-shaped notch dimensions (l_s, w_s) on the return loss is studied. It is observed that the width of the notch affects the impedance matching, especially at the middle frequencies as shown in Figure 3.18. It experiences mismatch when the width increases. Also, the lower edge frequency of the bandwidth is slightly shifted to higher frequencies and the higher frequencies are slightly shifted to lower frequencies once the width increases. On the other hand, the length of the notch slightly influences the impedance matching. Therefore, the effects of the notch cut parameters are very limited. It is also noted that the notch can be used to reduce the size of the radiator as explained earlier.

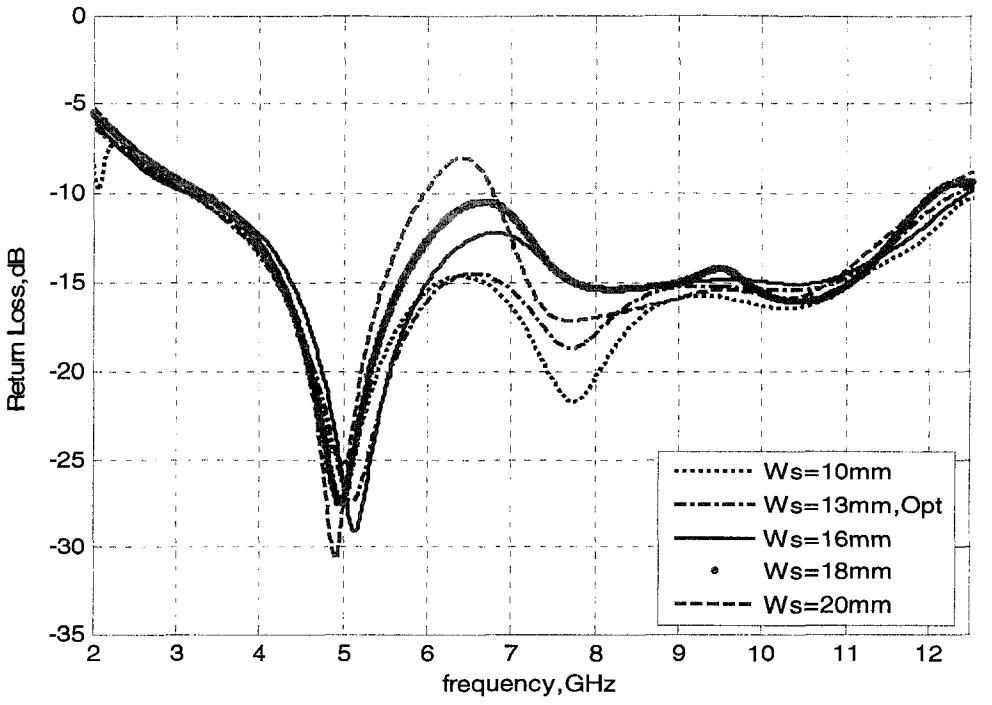

Figure 3.18: Effects of notch width

3.3.4.2 *Transition Step*

The effects of the transition step in terms of width and height are studied. It greatly impacts the matching impedance for the entire band. The effect of transition step width is plotted in Figure 3.19. The step width highly affects the whole band. When the width decreases, the middle and higher frequencies are greatly affected and exhibit mismatch. In contrast, when the width increases to be the same as the radiator width, the lower and higher frequencies are greatly affected and exhibit mismatch. In addition, the transition step height affects the entire band drastically as depicted in Figure 3.20. It is observed that when the height is getting smaller, the whole band is affected. Consequently, the transition step is very important technique since it influences the coupling between the radiator and the ground plane, provides a well-matched traveling mode and smooth impedance transition between the feed line and the radiator.

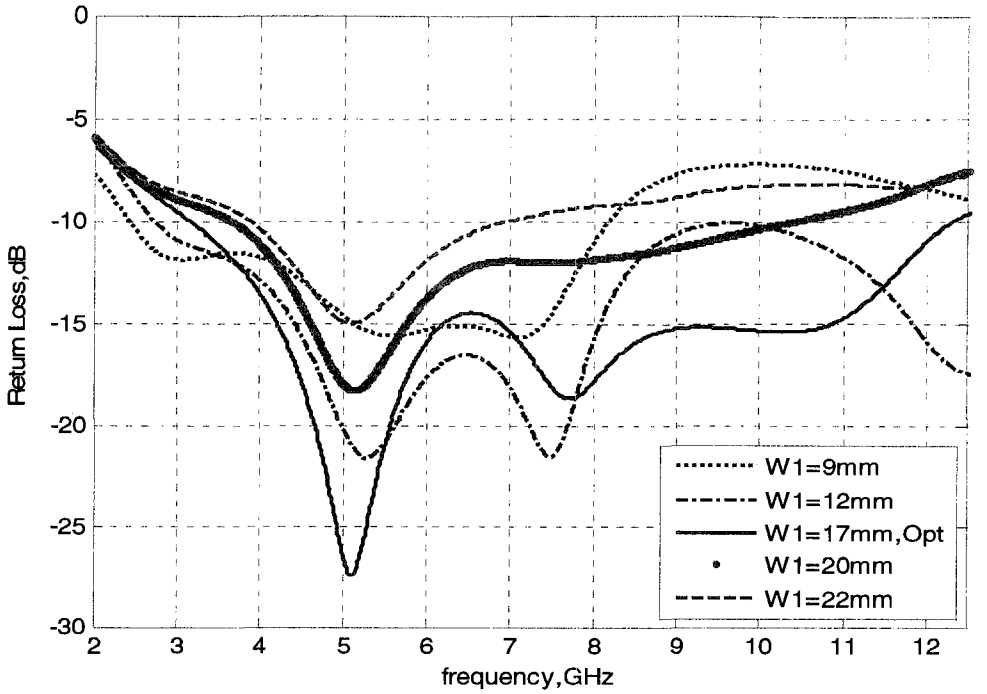

Figure 3.19: Effects of step width

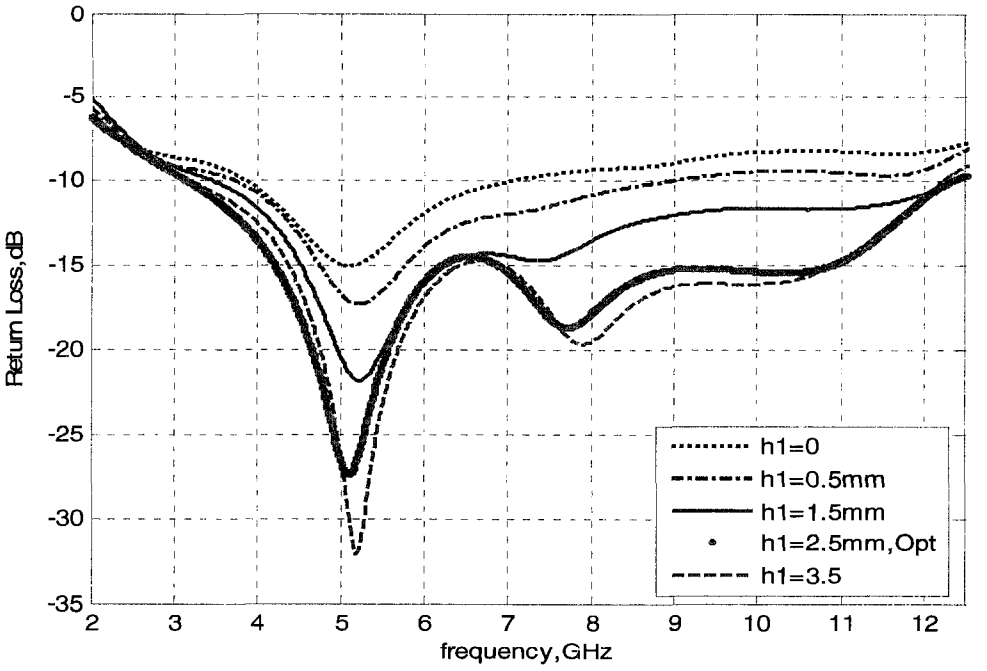

Figure 3.20: Effects of step height

3.3.4.3 Feed Gap

Figure 3.21 shows the effect of the feed gap (g) between the radiator and the upper

edge of the ground plane. The feed gap drastically affects the entire frequency band. It is noticed that when the feed gap is getting smaller, it affects the first half of the operational bandwidth (low and middle frequencies). On the other hand, when it is getting larger, it affects the second half of the operational bandwidth (middle and high frequencies). Therefore, the feed gap is very crucial for the impedance matching since it can reduce the coupling between the currents at the bottom outer edge of the patch and the top-edge of the ground plane. The feed gap thus has to be precisely tuned to achieve the desirable impedance matching.

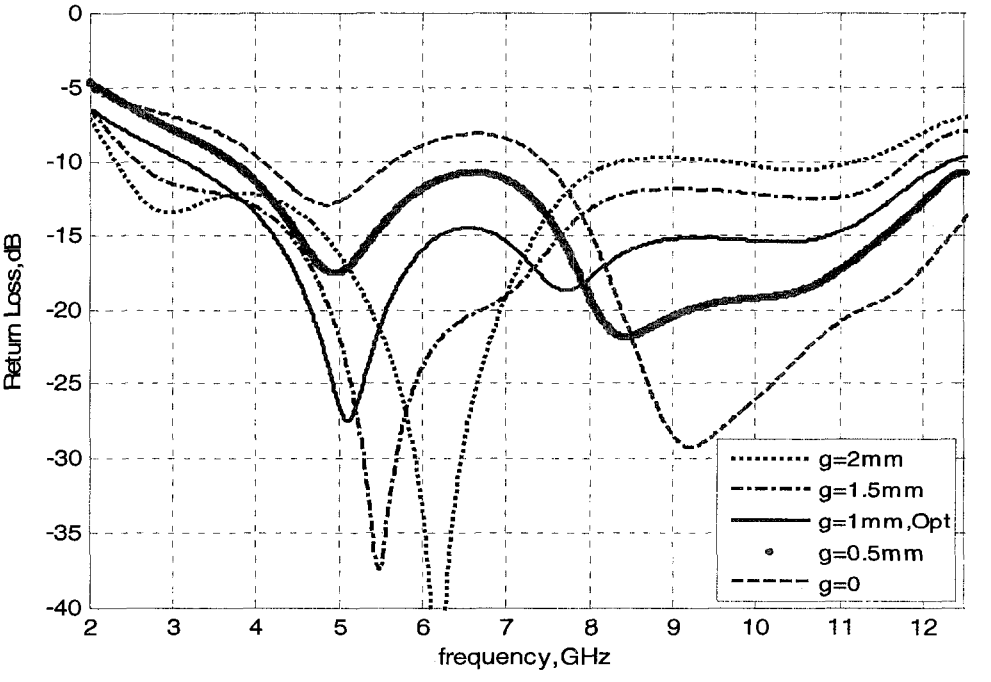

Figure 3.21: Effects of feed gap

3.3.5 Results and Discussion

After taking into account the design considerations described on antenna structure, current distributions and parametric study done to optimize the antenna geometry, the optimized antenna is constructed as shown in Figure 3.22. It is built on Rogers RT/Duroid

5880 material with a relative permittivity ε_r=2.2 and a thickness of 1.575 mm using the following optimal parameters: L_{sub} =40 mm, W_{sub} =30 mm, w=22 mm, h=16.33 mm, w_1=17 mm, h_1=2.5 mm, l_s =5.6 mm, w_s =13 mm, w_f =3.6, g=1 and L_g=9.5 mm. Then, the antenna is experimentally tested to confirm the simulation results. The simulated and measured return loss is presented as well as the simulated and measured radiation patterns in principle planes. Also, the simulated gain and radiation efficiency are provided.

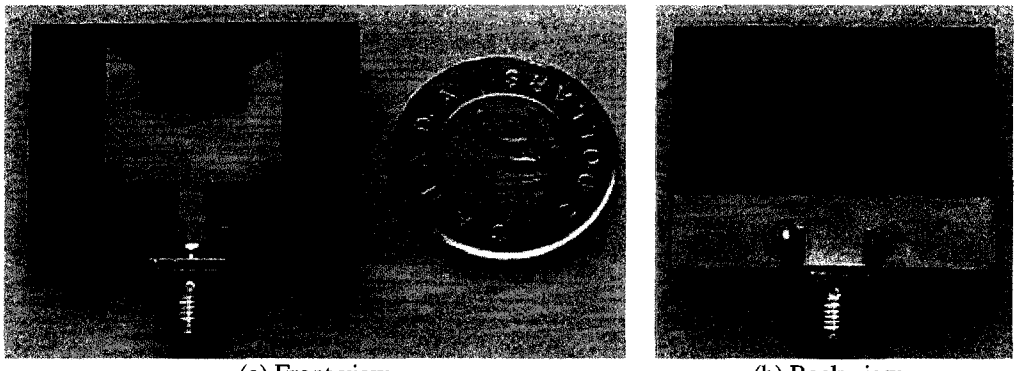

(a) Front view (b) Back view

Figure 3.22: The prototype of the trimmed notch-cut patch antenna

3.3.5.1 Return Loss

The return loss (S_{11}) of the proposed antenna is measured. As depicted in Figure 3.23, the measured and simulated results are shown for comparison and indicate a reasonable agreement. The measured -10 dB return loss bandwidth of the antenna is approximately 7.5 GHz (3.1 - 10.6 GHz) and the antenna shows stable behaviors over the band. Thus, the measurement confirms the UWB characteristic of the trimmed notch-cut patch antenna as predicted in the simulation.

The measured return loss shows that the antenna is capable of supporting multiple resonance modes which are closely distributed across the spectrum. There are two

resonance modes formed by the antenna. Therefore, the overlapping of these resonance modes leads to the UWB characteristic.

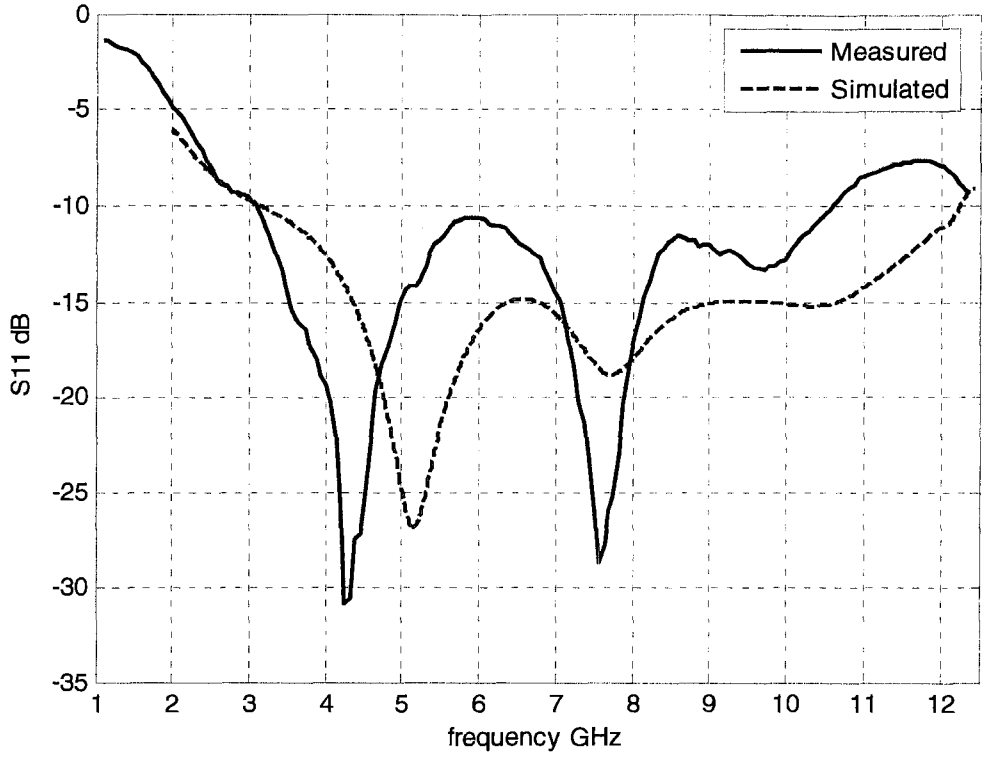

Figure 3.23: The simulated & measured return loss

3.3.5.2 *Antenna Radiation Patterns*

The radiation characteristics of the proposed antenna are also investigated. The two dimensional radiation patterns presented here are taken at two sets of principal cuts, ϕ=0° and ϕ=90°. Referring to the coordinate system attached to the antenna geometry in Figure 3.16, the H-plane is the xz-plane and the E-plane is the yz-plane. Figures 3.24 and 3.25 illustrate the simulated and measured H-plane and E-plane radiation patterns respectively at 3.5, 5.5, 7.5 and 9.5 GHz. In general, the simulated and measured results are fairly consistent with each other at most of the frequencies but some discrepancies are noticed between them at higher frequencies, especially in the E-plane due to the cable

leakage current during the measurements and the intrinsic noise within the anechoic chamber [118].

However, an analysis of the radiation pattern results shows that the proposed antenna is characterized by omni-directional patterns in the H-plane for all in-band frequencies as in Figure 3.24. The measured *H*-plane patterns follow the shapes of the simulated ones well except at 9.5 GHz where there is little difference.

For the E-plane patterns, Figure 3.25 shows that the simulated patterns form figure-of-eight patterns and the measured patterns generally follow the simulated ones with some discrepancies.

In general, the trimmed notch-cut patch antenna shows an acceptable radiation pattern variation in its entire operational bandwidth since the degradation happens only for a small part of the entire bandwidth and it is not too severe.

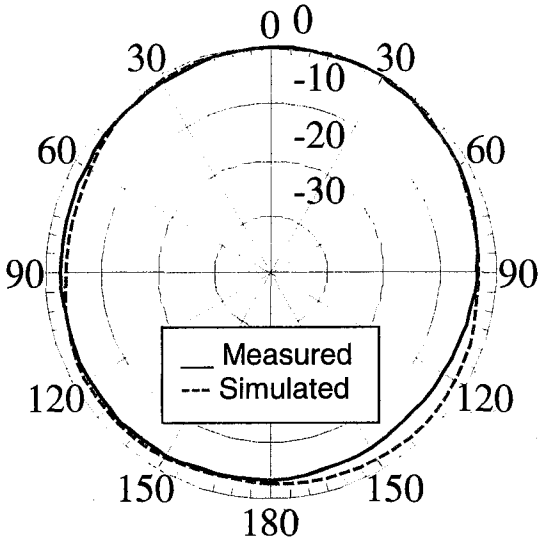

(a) H-plane at 3.5GHz

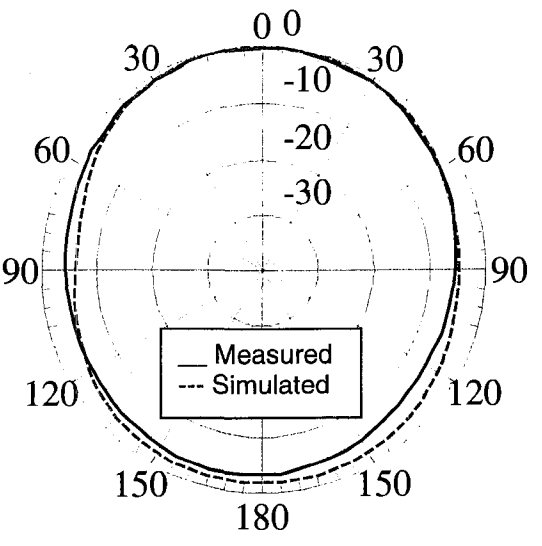

(b) H-plane at 5.5GHz

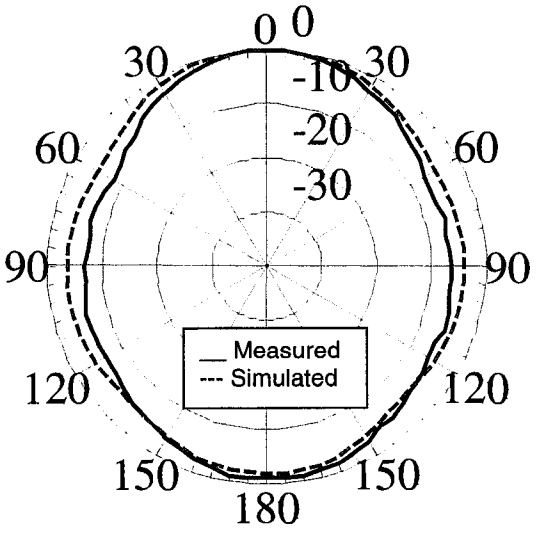

(c) H-plane at 7.5GHz

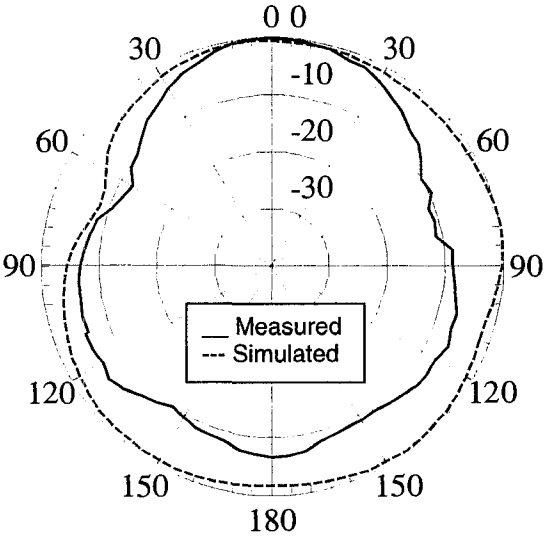

(d) H-plane at 9.5GHz

Figure 3.24: The simulated and measured radiation patterns in the H-plane at 3.5, 5.5, 7.5 and 9.5 GHz

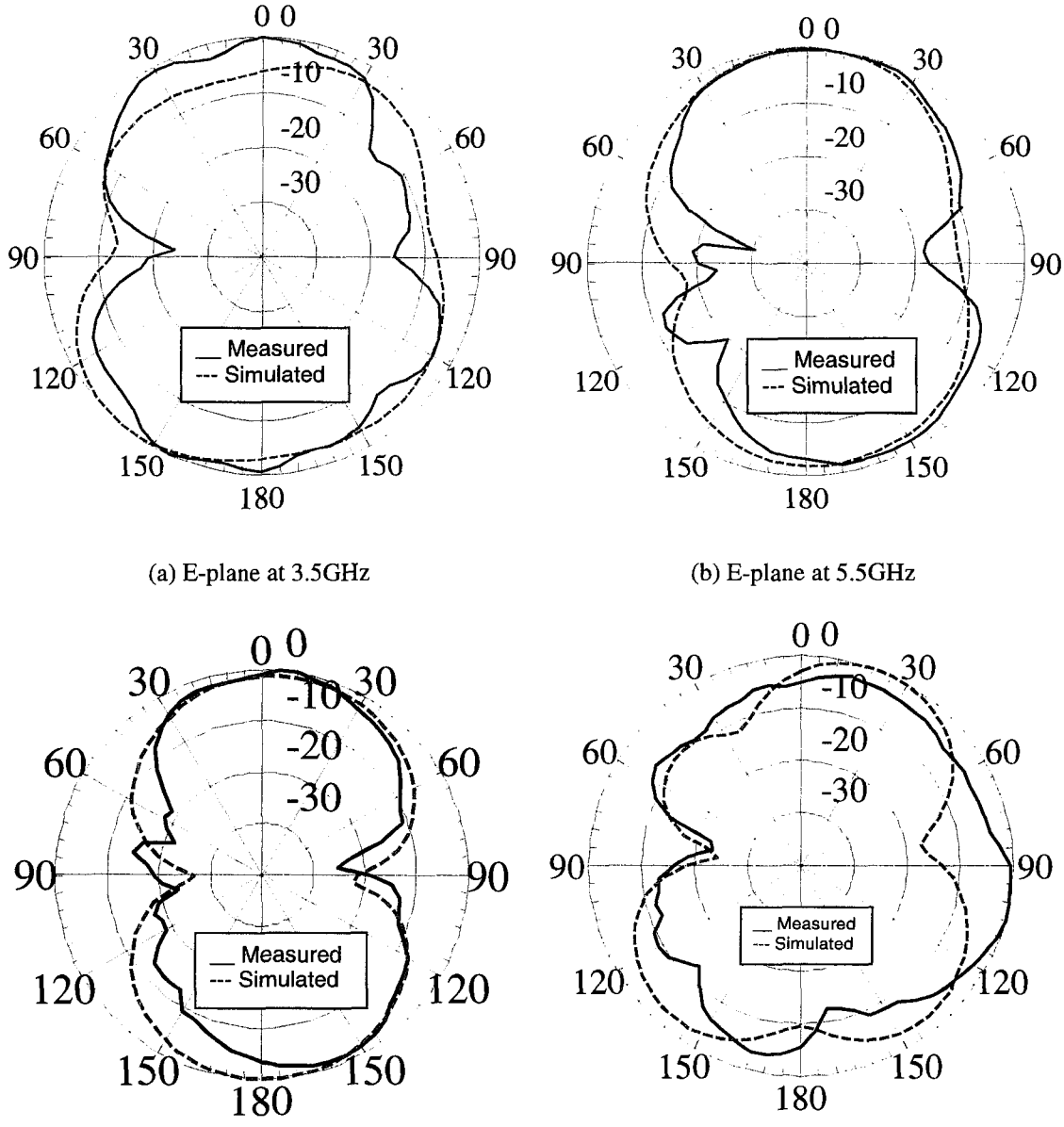

(a) E-plane at 3.5GHz

(b) E-plane at 5.5GHz

(c) E-plane at 7.5GHz

(d) E-plane at 9.5GHz

Figure 3.25: The simulated and measured radiation patterns in the E-plane at 3.5, 5.5, 7.5 and 9.5 GHz

3.3.5.3 Gain and Radiation Efficiency

The gain and radiation efficiency versus frequency of the proposed antenna are also found to be suitable for the UWB communications and applications. The simulated antenna gain versus frequency is shown in Figure 3.26. It is greater than 3.5 dBi for all in-

band frequencies and varies from 3.5 dBi to 4.7 dBi over the operating frequency range, resulting in the maximum gain variation of 1.2 dB. The radiation efficiency is substantially high throughout the operational bandwidth of the antenna. Figure 3.27 shows that it is greater than 80 % in the entire operational bandwidth.

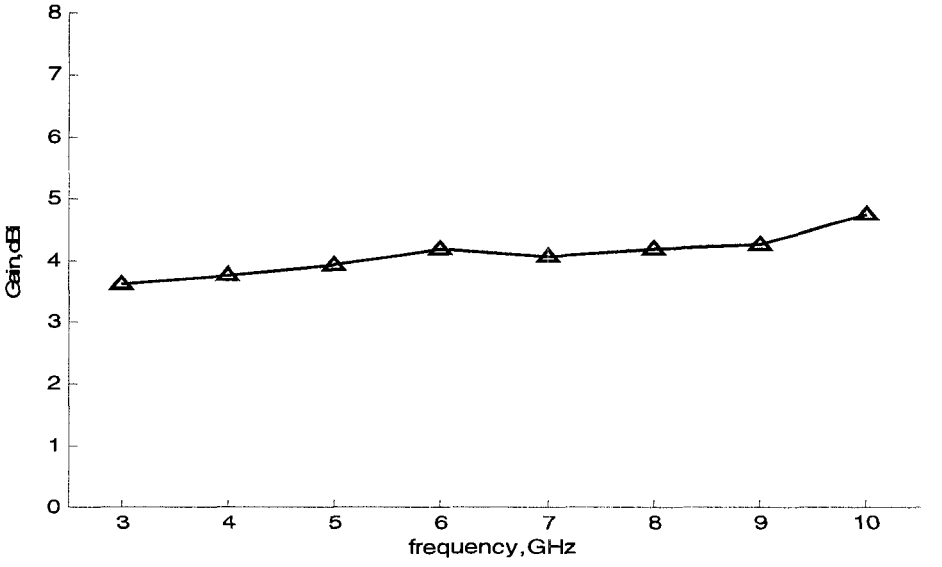

Figure 3.26: Simulated gain

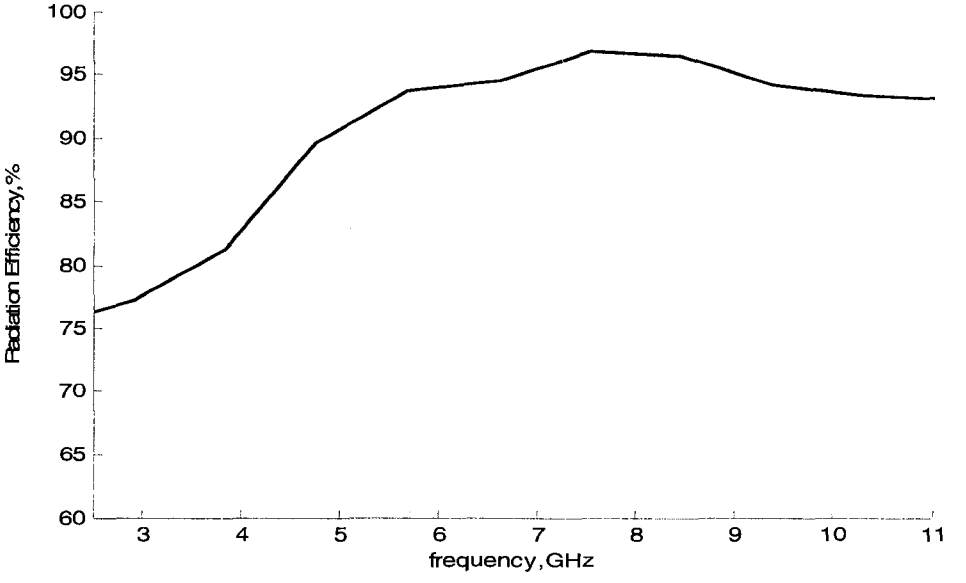

Figure 3.27: Radiation efficiency

3.4 Conclusion

In this chapter, two novel, small, low-cost and efficient UWB printed microstrip antennas are proposed for UWB wireless communications and applications. They are designed to satisfied frequency domain UWB requirements. The antennas are namely: the stepped-trapezoidal patch antenna and the trimmed notch-cut patch antenna.

The stepped-trapezoidal patch antenna operates over a bandwidth of 137.2 % (3.13-11.83 GHz) with a flat gain of 2.3 dB variations and a minimum radiation efficiency of 94 %. The trimmed notch-cut patch antenna operates over a bandwidth of 132.1 % (3.1-10.6 GHz) with a flat gain of 1.2 dBi variations and a minimum radiation efficiency of 90 %. Both antennas provide nearly omni-directional radiation patterns in H-plane and an acceptable radiation pattern in E-plane over the entire frequency band. The measured and simulated results for both bandwidth and radiation pattern show a very reasonable agreement. The table below shows a comparison of the two designed antennas.

Antennas	Bandwidth (GHz)	Radiation Patterns	Gain variations (dB)	Radiation efficiency (%)
Stepped-trapezoidal	8.70	Nearly omni-directional	2.3	94
Trimmed notch-cut	7.50	Nearly omni-directional	1.2	80

Table 3.1: Comparison of antenna characteristics

CHAPTER FOUR

Beveled Ultra-Wideband Antennas

4.1 Introduction

In this chapter, three novel, small, low-cost and efficient UWB printed microstrip antennas are proposed for UWB wireless communications and applications. They are designed to satisfy frequency domain UWB requirements. The antennas are namely: the elliptical patch antenna, the double-beveled patch antenna and the band-rejected elliptical patch antenna. After designing the elliptical antenna, the double-beveled patch antenna is designed to have extra freedom in controlling the impedance bandwidth matching since it has two bevels angles that can be adjusted to achieve UWB characteristic without increasing the size of the antennas. In contrast, the elliptical antenna can be mainly adjusted to achieve UWB characteristic by increasing the size of antenna. Both antennas are designed, simulated and then fabricated. The structural properties and performance characteristics of the two antennas are investigated by numerical simulations and verified by measurements. The design process, parametric study, optimization as well as simulated and measured results, such as VSWR, radiation characteristics, gain and radiation

efficiency are provided. For the band-rejected elliptical patch antenna, the structural properties and performance characteristics are numerically and experimentally investigated. The design process, optimization as well as simulated and measured results, such as VSWR, radiation characteristics, gain and radiation efficiency are provided.

4.2 The Elliptical Patch Antenna

4.2.1 Overview

A new planar elliptical antenna with a notch-cut fed by a simple microstrip line is proposed and described. It is designed and fabricated for UWB wireless communications and applications under the band (3.1-10.6 GHz). This antenna is composed of a planar elliptical patch with notch cut fed by a microstrip line flushed on a partial ground plane. Because of its structure, we have called it "the elliptical patch antenna" [120]. To obtain UWB bandwidth, we use several bandwidth-enhancement techniques: the use of partial ground plane, adjusting the gap between radiating element and a ground plane technique [61] and a notch cut technique which also contributes in miniaturizing the size of the planar antenna [20]. A parametric study is numerically carried out on the important geometrical parameters to understand their effects on the proposed antenna and therefore optimize its performance. The measured -10 dB return loss (VSWR<2) bandwidth for the designed antenna is about 140.9 % (8.15 GHz). The proposed antenna provides an acceptable radiation pattern and a relatively flat gain over the entire frequency band. The measured and simulated results for both bandwidth and radiation pattern show a very

reasonable agreement.

In the following subsections, the design details and related results will be presented and discussed. First, the antenna geometry and design process are explained. Second, the parametric study is carried out to address the effects of the dimensions related to the radii, the notch cut and the feed gap on the proposed antenna characteristics and hence optimize the antenna performance accordingly. Next, the current distribution is studied in order to miniaturize the size of the antenna by removing parts of the radiator that do not contribute to the radiation. Finally, the simulated and measured results, such as VSWR, radiation pattern, gain and radiation efficiency are provided and discussed.

4.2.2 Antenna Design

4.2.2.1 Design Process

The antenna is designed according to the developed design methodology mentioned earlier. Figure 4.1 depicts the design steps used to design the proposed antenna. First, the substrate is chosen to be Rogers RT/Duroid 5880 material with a relative permittivity ε_r=2.2 and a thickness of 1.575 mm. Second, the radiator shape is selected to be elliptical. Next, the initial parameters are calculated using the empirical formula (Equation 3.6) mentioned in the previous chapter. The only difference is the ellipse area which is лab. Thus, Equation 3.5 will be:

$$2\pi rl = \pi ab \qquad (4.1)$$

Where a and b are the semi-major and minor axes of the ellipse.

Since the antenna is designed for UWB, it has to operate over 3.1 - 10.6 GHz. Therefore, the lower edge frequency at which the initial parameters will be calculated is

3.1 GHz. Initially, the antenna consists of an elliptical patch and partial ground plane etched on opposite sides of the substrate. The radiator is fed through a microstrip line with 50-Ω characteristic impedance. After setting up the configuration of the antenna, determining the initial parameters and fixing the lower frequency, the simulation is performed to confirm the calculated parameters. Then, several bandwidth-enhancement techniques are applied to widen the bandwidth and obtain UWB performance. These techniques are: adjusting the gap between the radiating element and ground plane technique, and use of a notch cut technique used after studying the current distribution, as will be discussed later. Therefore, the notch cut from the radiator is also used to miniaturize the size of the planar antenna.

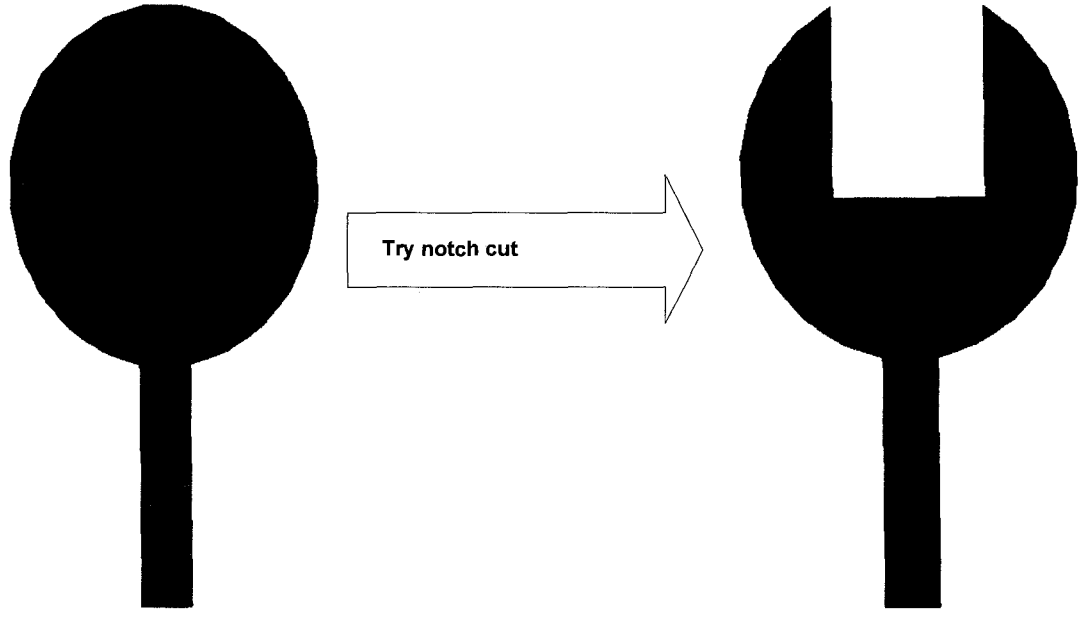

Figure 4.1: Flowchart for the design steps of the elliptical patch antenna

4.2.2.2 Antenna Geometry

Figure 4.2 illustrates the geometry of the printed antenna as well as the Cartesian coordinate system.

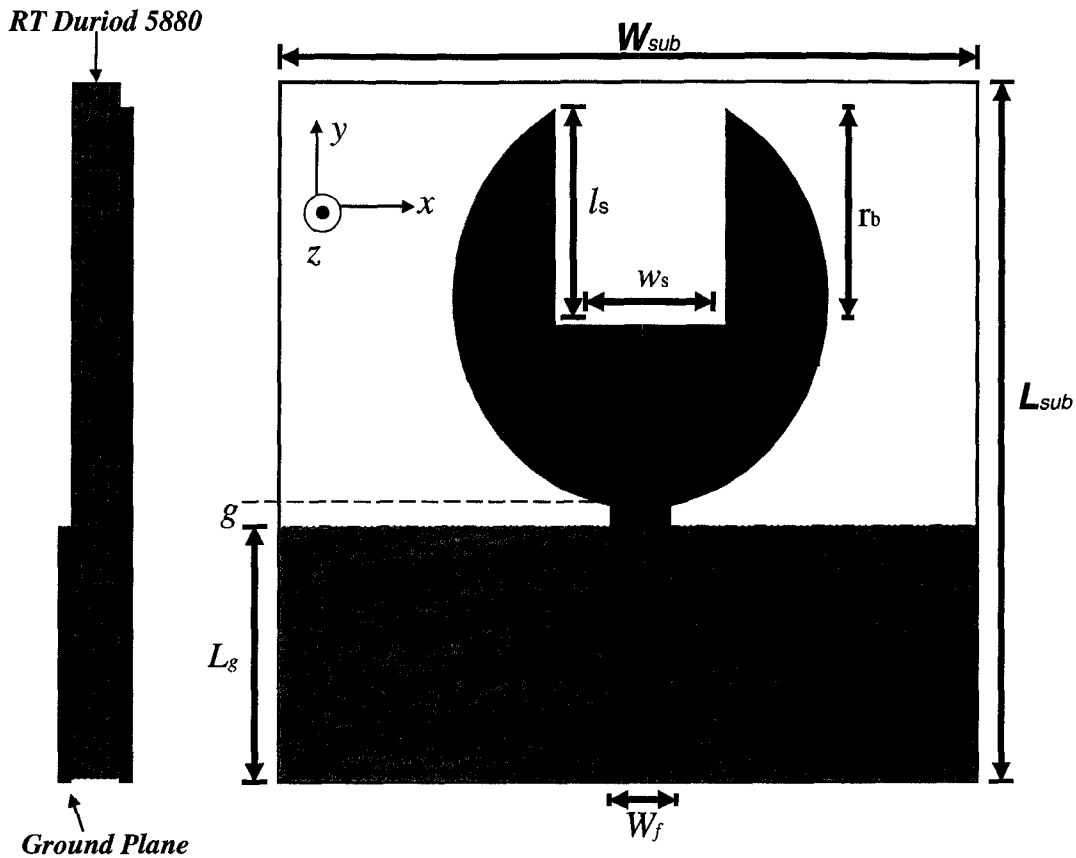

Figure 4.2 : The geometry of the elliptical patch antenna

It consists of an elliptical patch with notch cut and the partial ground plane. The Cartesian coordinate system (x,y,z) is oriented such that the bottom surface of the substrate lies in the x-y plane. All the following parameters are in the optimal dimensions. The antenna and the partial ground plane are oppositely etched on the Rogers RT/Duroid 5880 substrate. The substrate size of the proposed antenna is 38 × 35 mm^2. The semi-minor and semi-major axes of the elliptical patch are chosen to be r_a = 11 mm and r_b = 11.5 mm. To reduce the overall size of the printed antenna and to get better impedance matching, a rectangular-shaped notch with dimensions of $l_s \times w_s$ = 13 mm × 10 mm is symmetrically cut in the top middle of the radiator. The shape of the partial ground plane is rectangular with dimensions of 14.7 × 35 mm^2. The radiator is fed through a microstrip

line having a length of 15 mm and width of w_f=3.6 mm to ensure 50-Ω input impedance with a feed gap g = 0.3 mm. The 50 Ω-microstrip line is printed on the same side of the substrate as the radiator.

4.2.3 Current Distribution

The simulated current distributions of the initial geometry for the proposed antenna, before cutting the region of low current density at 3.5 GHz, 6.5 GHz, and 9.5 GHz, are shown in Figure 4.3 (a), (b), and (c) respectively. Also, the simulated current distributions of the final geometry for the proposed antenna, after cutting the region of low current density at 3.5 GHz, 6.5 GHz, and 9.5 GHz, are shown in Figure 3.17 (d), (e), and (f), respectively.

As shown in Figure 4.3 (a), (b), and (c), the current is mainly concentrated on the bottom portion of the patch with very low current density toward and above the center and is distributed along the edges of the patch, except the top edge, for all frequencies. Also, it is observed that the current distributions are symmetric about the axis of the transmission line. Thus, the region of low current density on the patch is not that important in the antenna performance and could hence be cut out.

Consequently, a rectangular section with dimensions of $l_s \times w_s$ = 13 mm × 10 mm is symmetrically cut out from the top middle of the rectangular radiator to eliminate a region of low current density as shown in Figure 4.2. After this cut, the current distributions at 3.5 GHz, 6.5 GHz, and 9.5 GHz are depicted in figure 4.3 (d), (e), and (f), respectively. It is observed that the current distributions in this case are approximately the same as before the cut. As a result of this cut, the size of the antenna is reduced and has

lighter weight, which is very desirable for more degree of freedom in design and possibly less conductor losses.

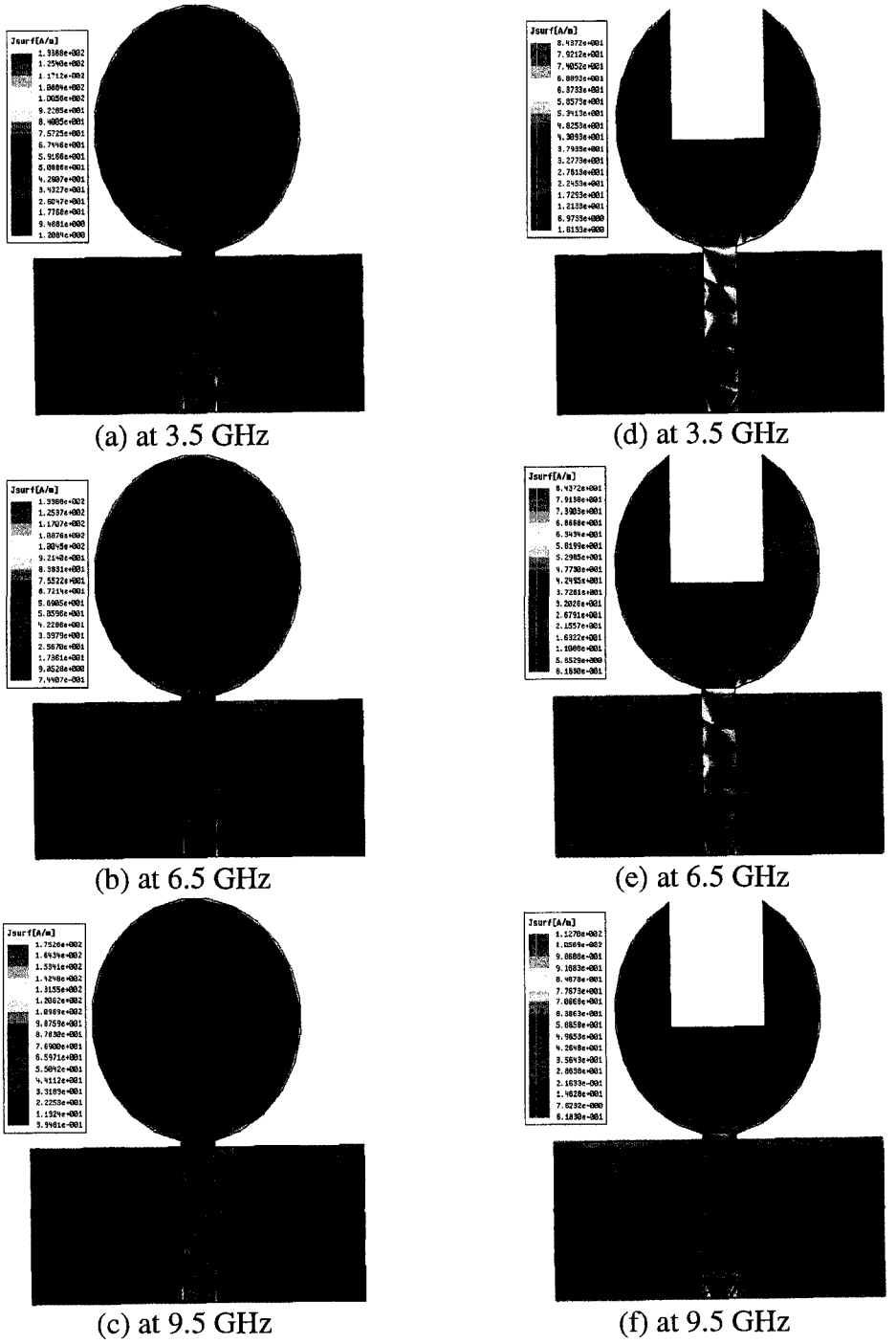

Figure 4.3: The current distributions of the elliptical patch antenna

4.2.4 Parametric Study

The parametric study is carried out to optimize the antenna and provide more information about the effects of the essential design parameters. The antenna performance is mainly affected by geometrical parameters, such as the dimensions related to the radii, the notch cut and the feed gap.

4.2.4.1 Elliptical Patch Radius

Figure 4.4 exhibits the return loss when the elliptical patch semi-axis (r_b) changes. This parameter affects lower edge frequency as well as the middle frequency band. Thus, the elliptic patch has better impedance match over a wider frequency range, which has similar effect of beveling the radiating element and trimming the square edge near the ground plane [17, 22]. It is obvious that the return loss over the UWB is better when the radius increases but at the cost of increasing antenna sizes.

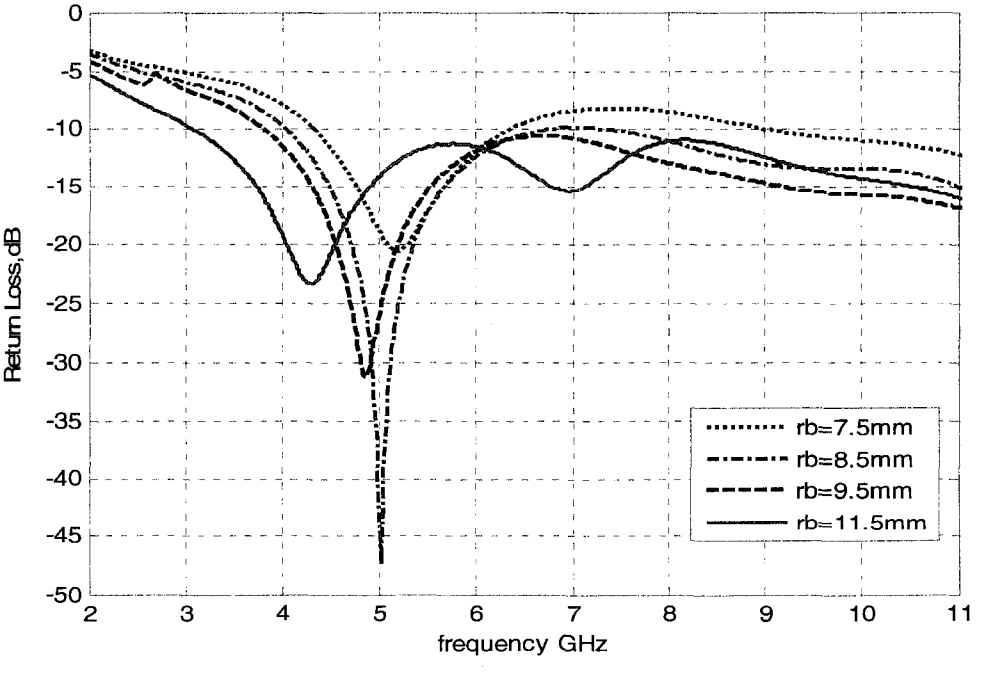

Figure 4.4: Effects of elliptical radius

4.2.4.2 Notch Cut

The dimensions of the notch (l_s, w_s) are studied. The effect of varying the parameters on the impedance matching is depicted in Figure 4.5. It is obviously observed that the width of the notch has a major effect on the impedance matching over the entire band but especially at lower operating frequencies. When the width is increased, the lower edge frequency of the bandwidth is greatly affected and shifted to higher frequencies. In addition, the middle and higher frequencies are affected with higher mismatch levels. On the other hand, the length of the notch slightly influences the lower edge frequency and causes mismatch in the middle. In general, all the notch cut parameters affect the impedance matching to a certain extent.

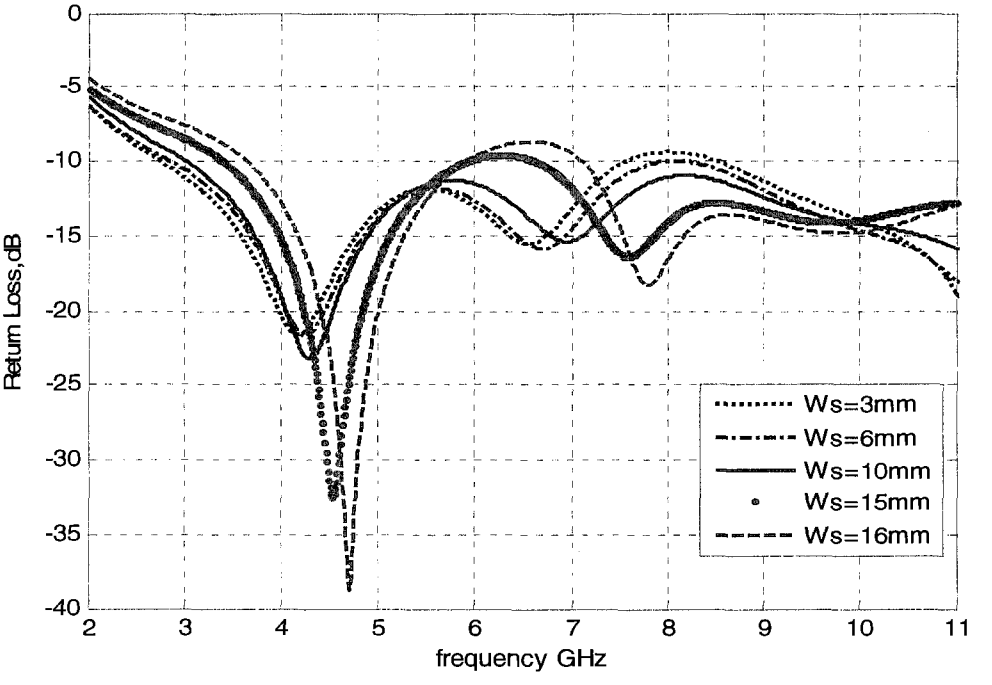

Figure 4.5: Effects of notch width

4.2.4.3 Feed Gap

Figure 4.6 shows the effect of the feed gap (g) between the radiator and the upper

edge of the system ground plane. The feed gap affects lower and higher frequency band. By varying the feed gap, impedance matching can be improved.

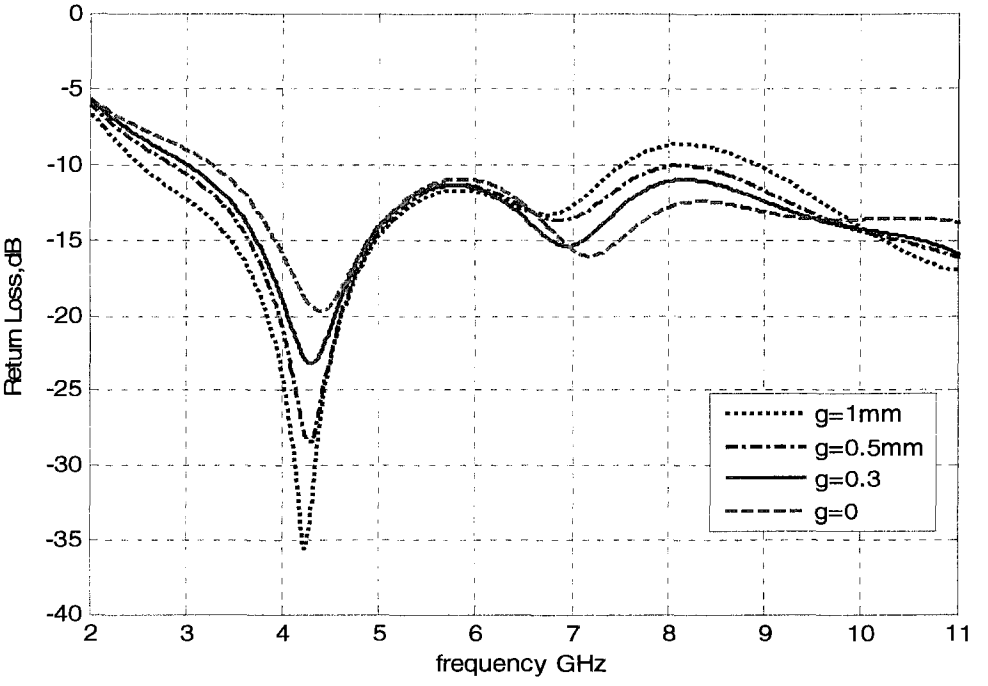

Figure 4.6: Effects of feed gap

4.2.5 Results and Discussion

After taking into account the design considerations described on antenna structure, current distributions and parametric study done to optimize the antenna geometry, the optimized antenna is constructed as shown in Figure 4.7. It is built on Rogers RT/Duroid 5880 material with a relative permittivity ε_r=2.2 and a thickness of 1.575 mm using the following optimal parameters: L_{sub} =38 mm, W_{sub} =35 mm, r_a=11 mm, r_b =11.5, l_s =5.6 mm, w_s =13 mm, w_f =3.6, g=0.3 and L_g=14.7 mm. Then, the antenna is experimentally tested to confirm the simulation results. The simulated and measured VSWR is presented as well as the simulated and measured radiation patterns in principle planes. Also,

simulated gain and radiation efficiency are provided.

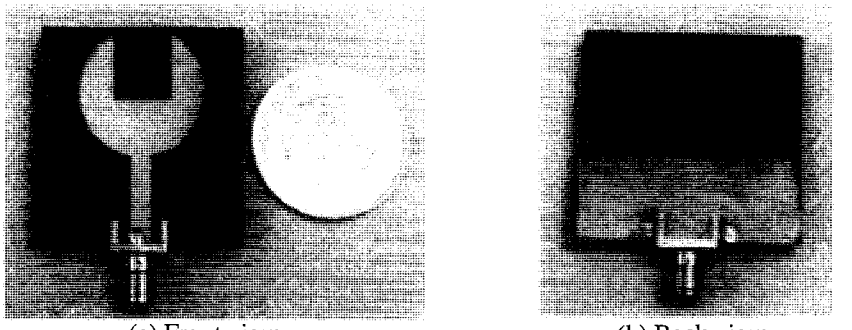

(a) Front view (b) Back view

Figure 4.7: The prototype of the elliptical patch antenna

4.2.5.1 VSWR

The VSWR of the proposed antenna is measured. As depicted in Figure 4.8, the measured and simulated results indicate a reasonable agreement. The measured -10 dB return loss (VSWR<2) bandwidth of the antenna is approximately 8.15 GHz (2.65 - 10.80 GHz) and the antenna shows stable behaviors over the band. Thus, the measurement confirms the UWB characteristic of the elliptical patch antenna as predicted in the simulation.

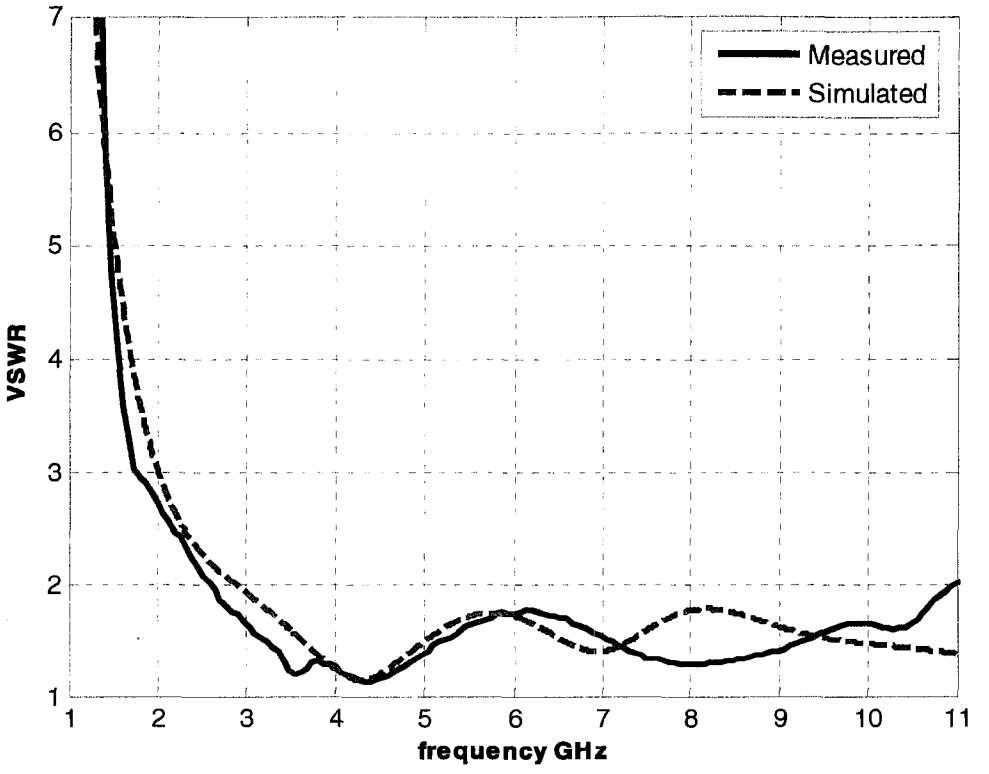

Figure 4.8: The simulated & measured VSWR

4.2.5.2 *Antenna Radiation Patterns*

The radiation characteristics of the proposed antenna are also investigated. The two dimensional radiation patterns presented here are taken at two sets of principle cuts, ϕ=0° and ϕ=90°. Referring to the coordinate system attached to the antenna geometry in figure 4.2, the H-plane is the xz-plane and the E-plane is the yz-plane. Figures 4.9 and 4.10 illustrate the simulated and measured H-plane and E-plane radiation patterns respectively at 3.5, 5.5, 7.5 and 9.5 GHz. In general, the simulated and measured results are fairly consistent with each other at most of the frequencies but some discrepancies are noticed between them at higher frequencies, especially in the E-plane due to the cable leakage current during the measurements and the intrinsic noise in the anechoic chamber.

However, an analysis of the radiation pattern results shows that the proposed

antenna is characterized by omni-directional patterns in the H-plane for all in-band frequencies, as in Figure 4.9. The measured *H*-plane patterns follow the shapes of the simulated ones well, except at 9.5 GHz where there is very little difference.

For the E-plane patterns, Figure 4.10 shows that the measured patterns generally follow the simulated ones with some discrepancies.

In general, the elliptical patch antenna shows an acceptable radiation pattern variation in its entire operational bandwidth since the degradation happens only for a small portion of the entire bandwidth and it is not too severe.

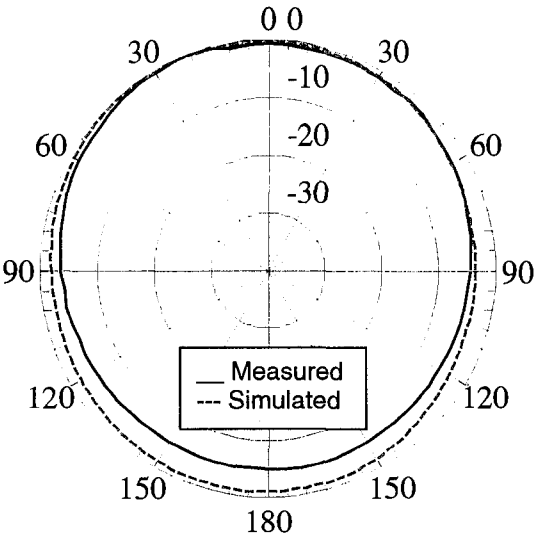

(a) H-plane at 3.5GHz

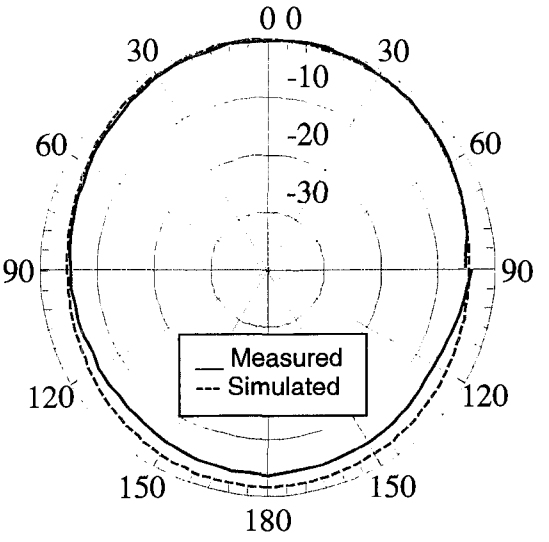

(b) H-plane at 5.5GHz

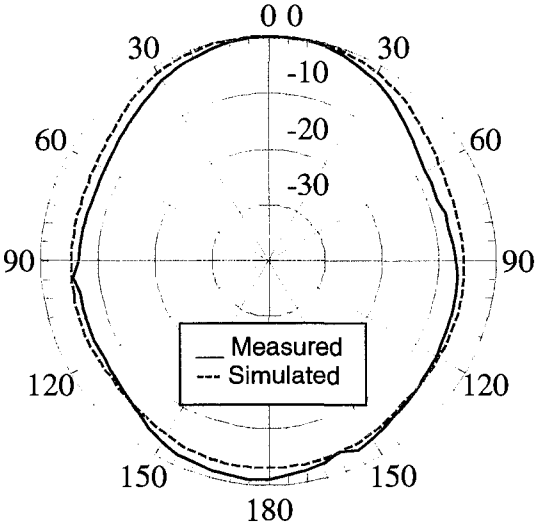

(c) H-plane at 7.5GHz

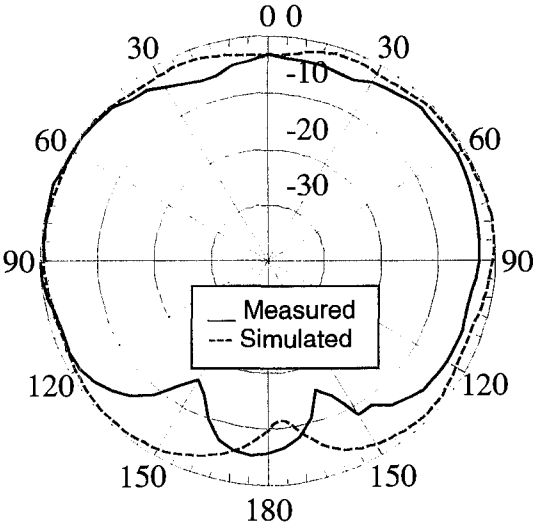

(d) H-plane at 9.5GHz

Figure 4.9: The simulated and measured radiation patterns in the H-plane at 3.5, 5.5, 7.5 and 9.5 GHz

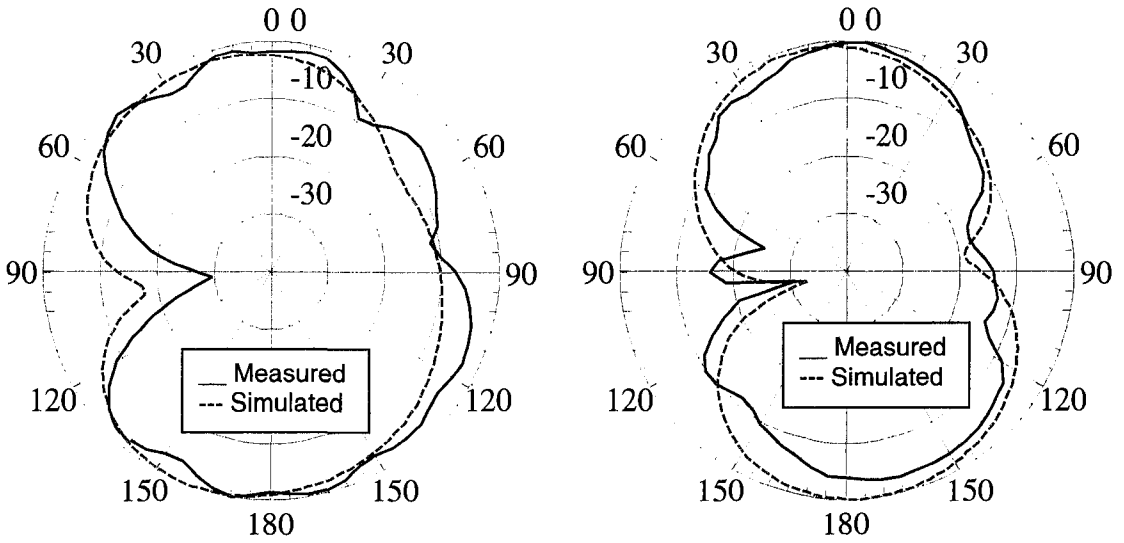

(a) E-plane at 3.5GHz

(b) E-plane at 5.5GHz

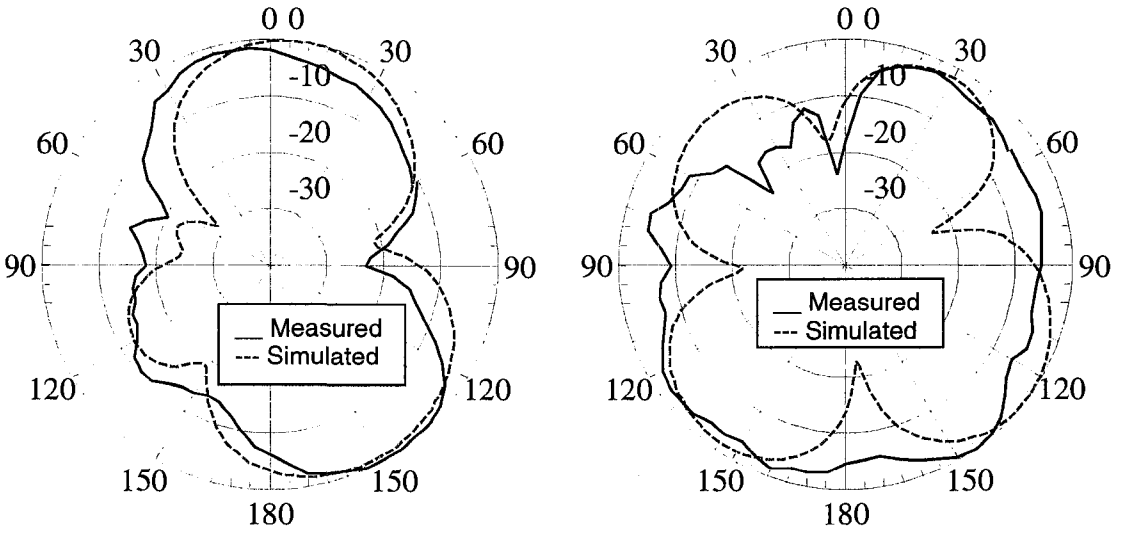

(c) E-plane at 7.5GHz

(d) E-plane at 9.5GHz

Figure 4.10: The simulated and measured radiation patterns in the E-plane at 3.5, 5.5, 7.5 and 9.5 GHz

4.2.5.3 *Gain and Radiation Efficiency*

The gain and radiation efficiency versus frequency of the proposed antenna are also found to be suitable for the UWB communications and applications. The simulated antenna gain versus frequency is shown in Figure 4.11. It is greater than 3.6 dBi for all in-band frequencies and varies from 3.6 dBi to 6.1 dBi over the operating frequency range,

resulting in the maximum gain variation of 2.5 dB. The radiation efficiency is substantially high throughout the operational bandwidth of the antenna. Figure 4.12 shows that it is greater than 85 % in most of the operational bandwidth.

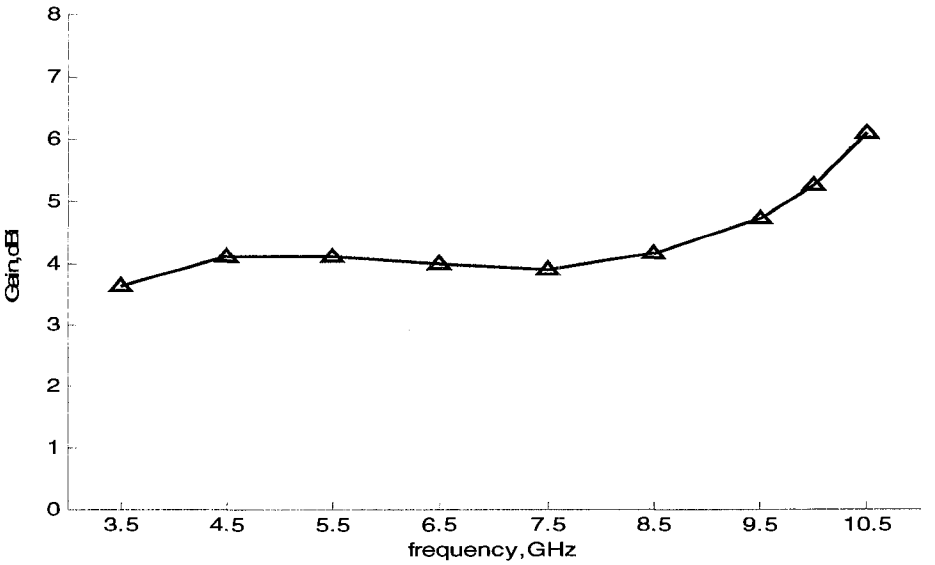

Figure 4.11: Simulated gain

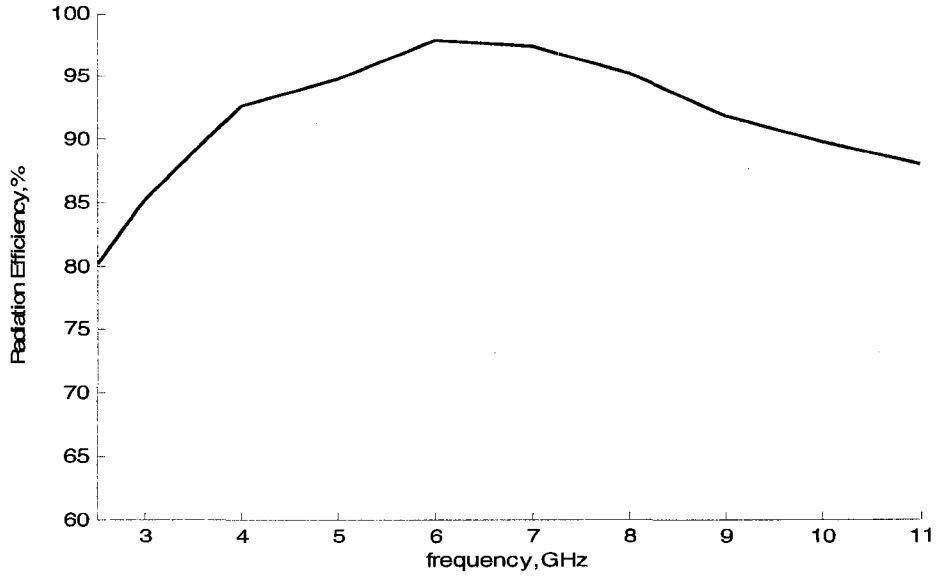

Figure 4.12: Radiation efficiency

4.3 The Double-Beveled Patch Antenna

4.3.1 Overview

A novel planar patch antenna with a notch-cut fed by a simple microstrip line is proposed and described. It is designed and fabricated for UWB wireless communications and applications under the band (3.1-10.6 GHz). This antenna is composed of a symmetrical double-beveled planar patch antenna with notch cut fed by a microstrip line folded on a partial ground plane. Because of its structure, we have called it "the Double-Beveled Patch Antenna" [121]. To obtain UWB bandwidth, we use several bandwidth enhancement techniques: the use of partial ground plane, adjusting the gap between radiating element and a ground plane technique [61], the use of bevels technique [77,78] and a notch cut technique used also to reduce the size of the planar antenna [20]. A parametric study is numerically carried out on the important geometrical parameters to understand their effects on the proposed antenna and therefore optimize its performance. The measured -10 dB return loss (VSWR<2) bandwidth for the designed antenna is about 142.8 % (9.74 GHz). The proposed antenna provides an acceptable radiation pattern and a relatively flat gain over the entire frequency band. The measured and simulated results for both bandwidth and radiation pattern show a very reasonable agreement.

In the following subsections, the design details and the related results will be presented and discussed. First, the antenna geometry and design process are explained. Second, the parametric study is carried out to address the effects of the bevels, the notch cut and the feed gap on the proposed antenna characteristics and hence optimize the antenna performance accordingly. Next, the current distribution is studied in order to

miniaturize the size of the antenna by removing parts of the radiator that do not radiate. Finally, the simulated and measured results, such as VSWR, radiation pattern, gain and radiation efficiency are provided and discussed.

4.3.2 Antenna Design

4.3.2.1 Design Process

The antenna is designed based on the developed design methodology mentioned earlier. Figure 4.13 depicts the design steps used to design the proposed antenna. First, the substrate is chosen to be Rogers RT/Duroid 5880 material with a relative permittivity ε_r = 2.2 and a thickness of 1.575 mm. Second, the radiator shape is selected to be rectangular. Next, the initial parameters are calculated using the empirical formula (Equation 3.7) mentioned in the previous chapter.

Since the antenna is designed for UWB, it has to operate over 3.1 - 10.6 GHz. Therefore, the lower edge frequency at which the initial parameters will be calculated is 3.1 GHz. Initially, the antenna consists of a rectangular patch and partial ground plane etched on opposite sides of the substrate. The radiator is fed through a microstrip line with 50-Ω characteristic impedance. After setting up the configuration of the antenna, determining the initial parameters and fixing the lower frequency, the simulation is performed to confirm the calculated parameters. Then, several bandwidth-enhancement techniques are applied to widen the bandwidth and obtain UWB performance. These techniques are: adjusting the gap between radiating element and ground plane technique, the bevels technique and notch cut technique used after studying the current distribution as will be discussed later. Therefore, the notch cut from the radiator is also used to

miniaturize the size of the planar antenna.

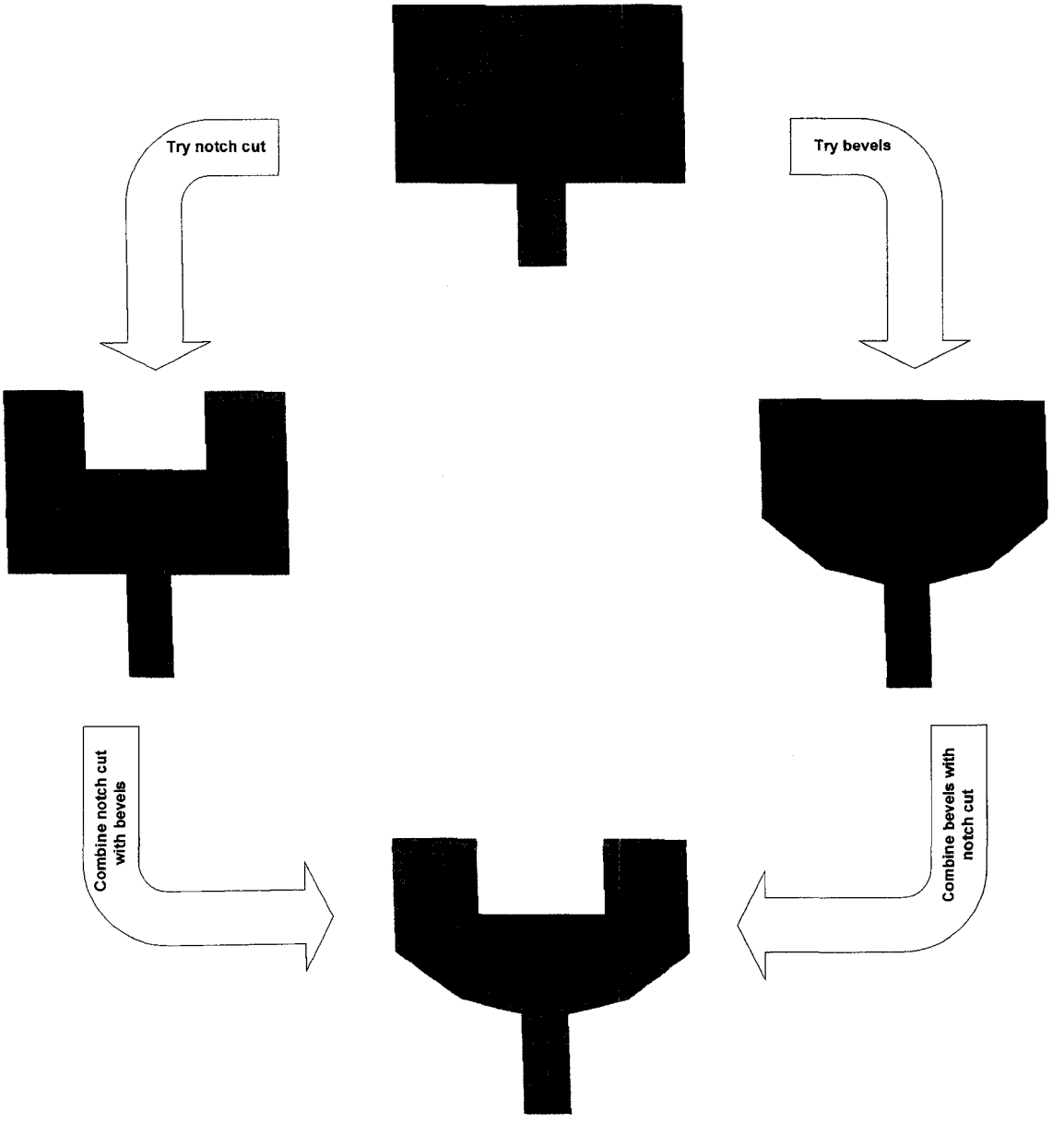

Figure 4.13: Flowchart for the design steps of the double-beveled patch antenna

4.3.2.2 *Antenna Geometry*

Figure 4.14 illustrates the geometry of the printed antenna as well as the Cartesian coordinate system.

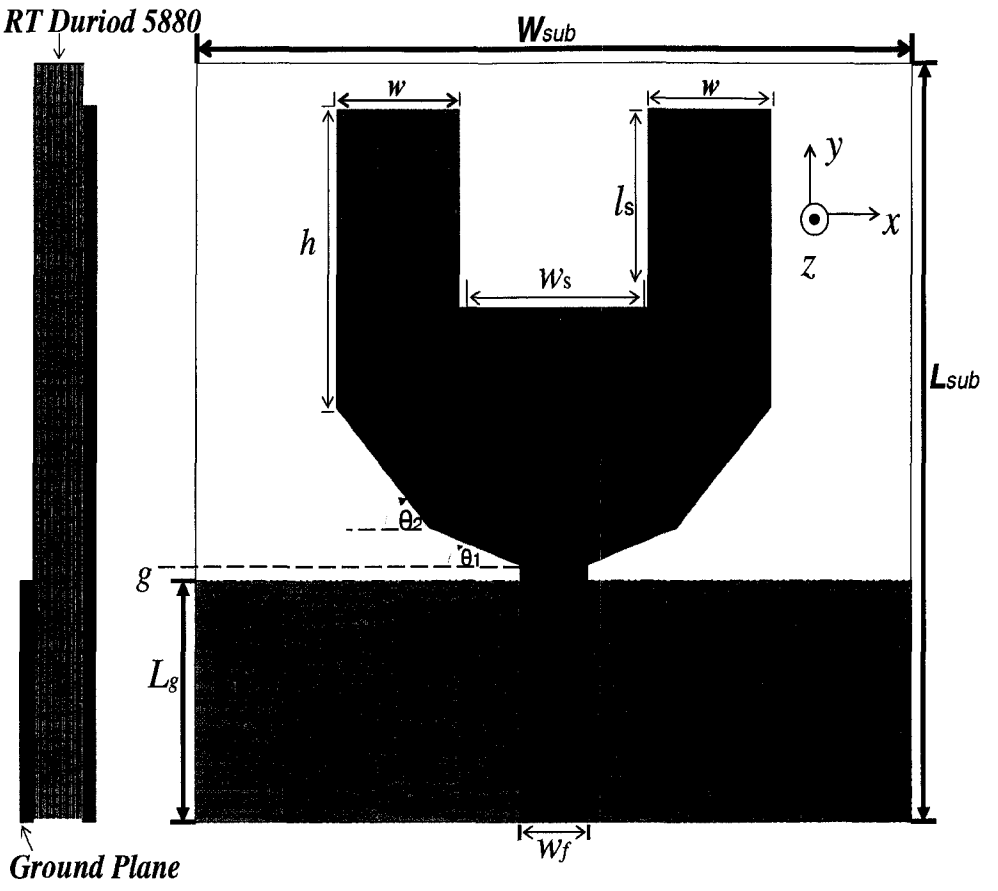

Figure 4.14 : The geometry of the double-beveled patch antenna

It consists of a symmetrical double-beveled patch with notch cut and a partial ground plane. The Cartesian coordinate system (x,y,z) is oriented such that the bottom surface of the substrate lies in the x-y plane. All the following parameters are in the optimal dimensions. The antenna and the partial ground plane are oppositely etched on the Rogers RT/Duroid 5880 substrate. The substrate size of the proposed antenna is 40×31 mm^2. The parameters of the symmetrical double-beveled patch are w=6.5 mm, h=12 mm, θ_1 =17.5° (the angle of the first bevel) and θ_2 =45° (the angle of the second bevel). To reduce the overall size of the printed antenna and to get better impedance matching, a rectangular-shaped notch with dimensions of $l_s \times w_s$ = 8 mm × 10 mm is symmetrically cut in the top middle of the radiator. The shape of the partial ground plane is rectangular

with dimensions of 10 × 40 mm^2. The radiator is fed through a microstrip line having a length of 10.5 mm and width w_f=3.6 mm to ensure 50-Ω input impedance with a feed gap g = 0.5 mm. The 50 Ω-microstrip line is printed on the same side of the substrate as the radiator.

4.3.3 Current Distribution

The simulated current distributions of the initial geometry for the proposed antenna, before cutting the region of low current density at 3.5 GHz, 6.5 GHz, and 9.5 GHz, are shown in Figure 4.15 (a), (b), and (c) respectively. Also, the simulated current distributions of the final geometry for the proposed antenna, after cutting the region of low current density at 3.5 GHz, 6.5 GHz, and 9.5 GHz, are shown in Figure 4.15 (d), (e), and (f), respectively.

As shown in Figure 4.15 (a), (b), and (c), the current is mainly concentrated on the bottom portion of the patch with very low current density toward and above the center and it is distributed along the edges of the patch, except the top edge, for all frequencies. Also, it is observed that the current distributions are symmetric about the axis of the transmission line. Thus, one can conclude that the region of low current density on the patch is not vital in the antenna performance and could therefore be cut out.

Consequently, a rectangular section with dimensions of $l_s \times w_s$ = 8 mm × 10 mm is symmetrically cut out from the top middle of the rectangular radiator to eliminate a region of low current density as shown in Figure 4.14. After this cut, the current distributions at 3.5 GHz, 6.5 GHz, and 9.5 GHz are depicted in Figure 4.15 (d), (e), and (f), respectively. It is observed that the current distributions in this case are approximately the same as

before the cut. As a result of this cut, the size of the antenna is reduced and has lighter weight, which is very desirable for more degree of freedom in design and possibly less conductor losses.

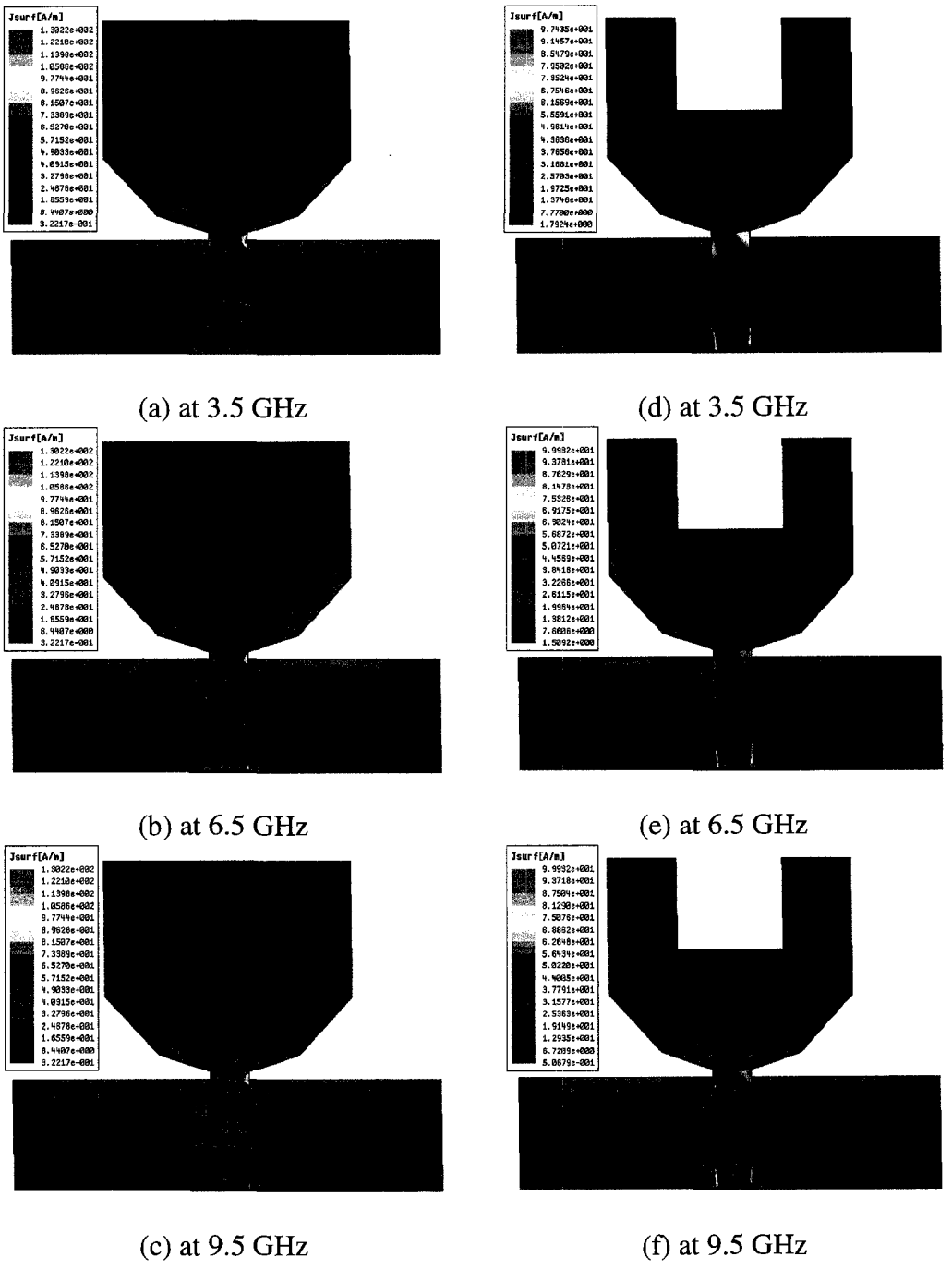

(a) at 3.5 GHz (d) at 3.5 GHz

(b) at 6.5 GHz (e) at 6.5 GHz

(c) at 9.5 GHz (f) at 9.5 GHz

Figure 4.15: The current distributions of the double-beveled patch antenna

4.3.4 Parametric Study

The parametric study is carried out to optimize the antenna and provide more information about the effects of the essential design parameters. The antenna performance is mainly affected by geometrical parameters, such as the dimensions related to the notch cut, the bevels and feed gap.

4.3.4.1 Notch Cut

The effect of the rectangular-shaped notch dimensions (l_s, w_s) on the return loss is studied. It is observed that the width of the notch has a major effect on the impedance matching over the entire frequency range, as shown in Figure 4.16. The lower edge frequency of the bandwidth is shifted to higher frequencies once the width increases. Also, the middle and higher frequencies are affected with higher mismatch levels. On the other hand, the length of the notch slightly influences the lower edge frequency. It is also observed that the notch can be used to reduce the size of the radiator, as explained earlier using the current distribution.

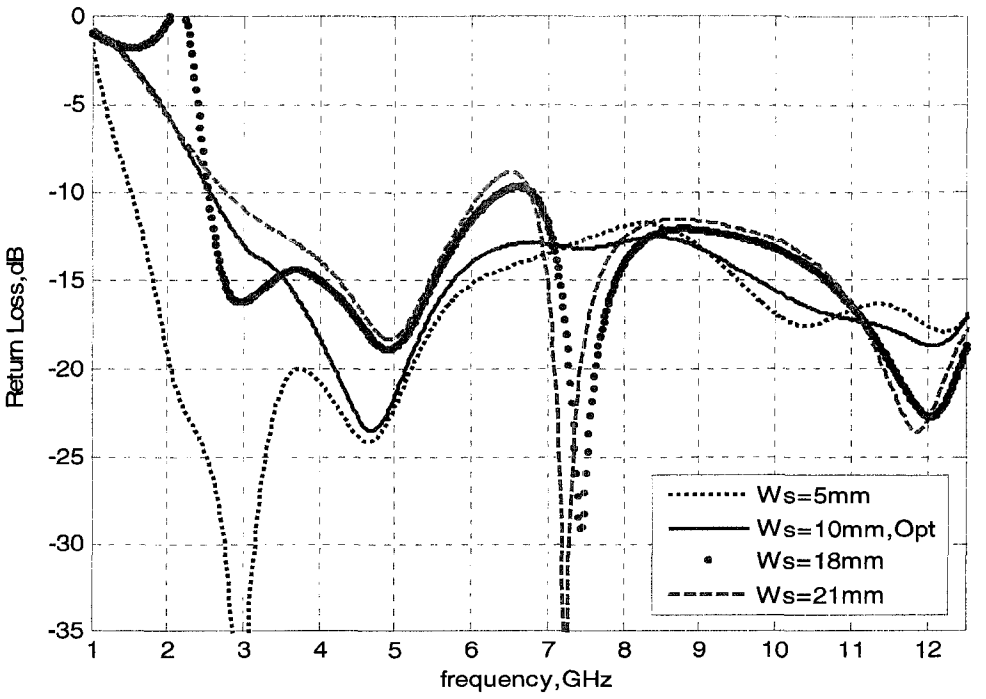

Figure 4.16: Effects of the width of notch cut

4.3.4.2 *Bevels*

The double bevels dimensions influence the matching impedance for the whole band, especially at high frequencies, as shown in Figure 4.17 and 4.18. The high frequencies can be controlled and the entire band can be enhanced by adjusting the bevel angles [77, 78]. As depicted in Figure 4.17, by varying the angle of the first bevel (θ_1), the low and middle frequencies are highly influenced. Also, the second bevel plays a great role in the impedance matching. As shown in Figure 4.18, by varying the angle of the second bevel (θ_2), the whole band is affected especially at middle and high frequencies. Thus, using two progressive bevels provides more degree of freedom and by adjusting them, the bandwidth will be widened as well as excellent level of matching can be achieved.

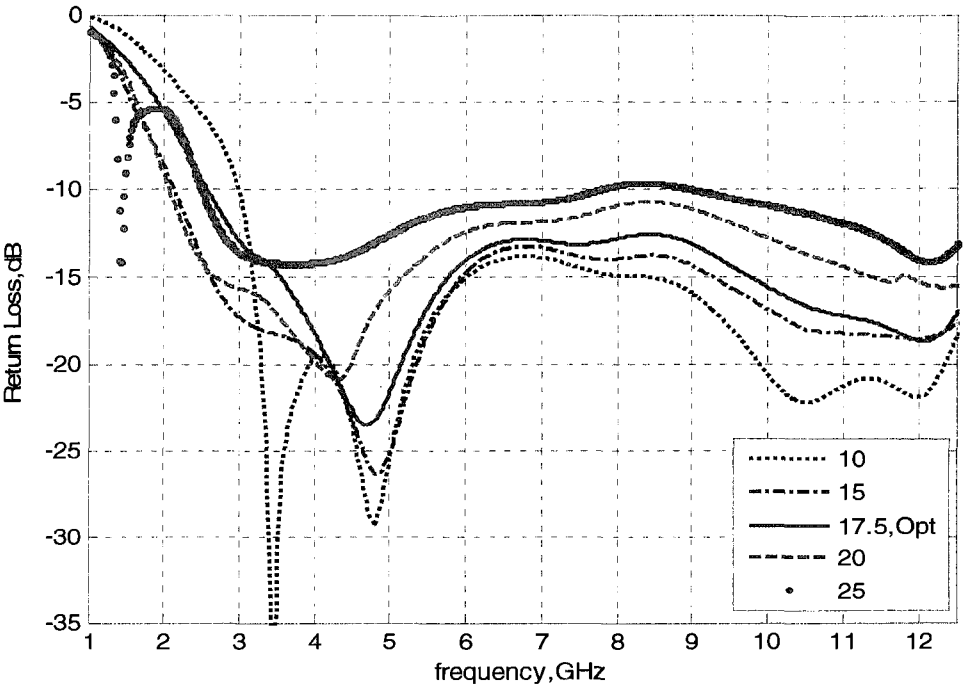

Figure 4.17: Effects of first bevel angle

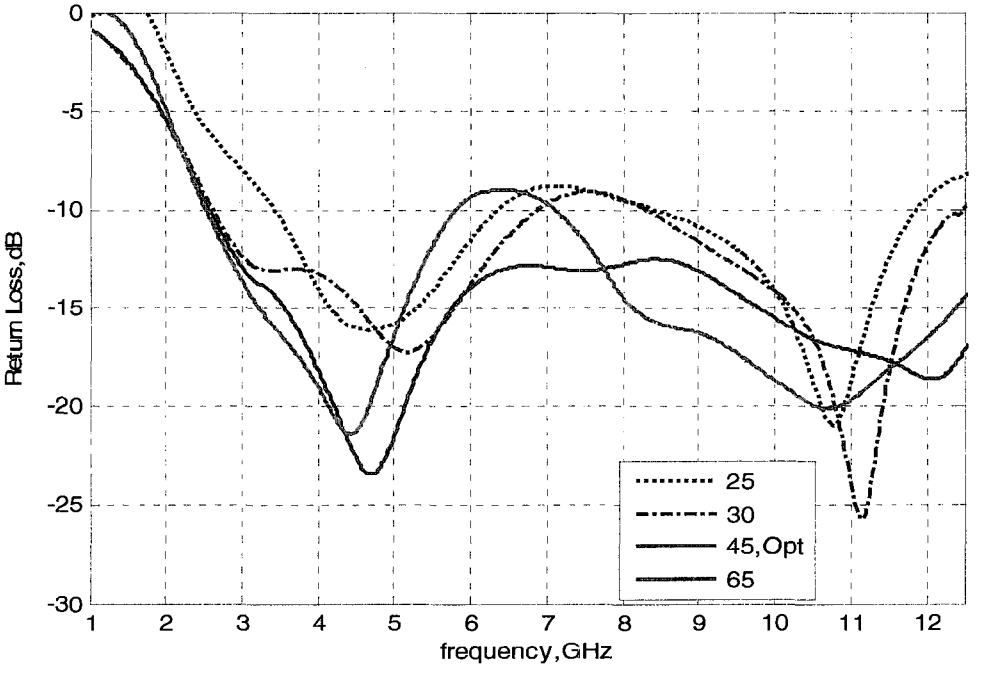

Figure 4.18: Effects of second bevel angle

4.3.4.3 Feed Gap

Figure 4.19 shows the effect of the feed gap (g) between the radiator and the upper

edge of the partial ground plane. The feed gap affects the entire frequency band but with higher sensitivity at low frequencies. By adjusting the feed gap, high impedance matching can be achieved.

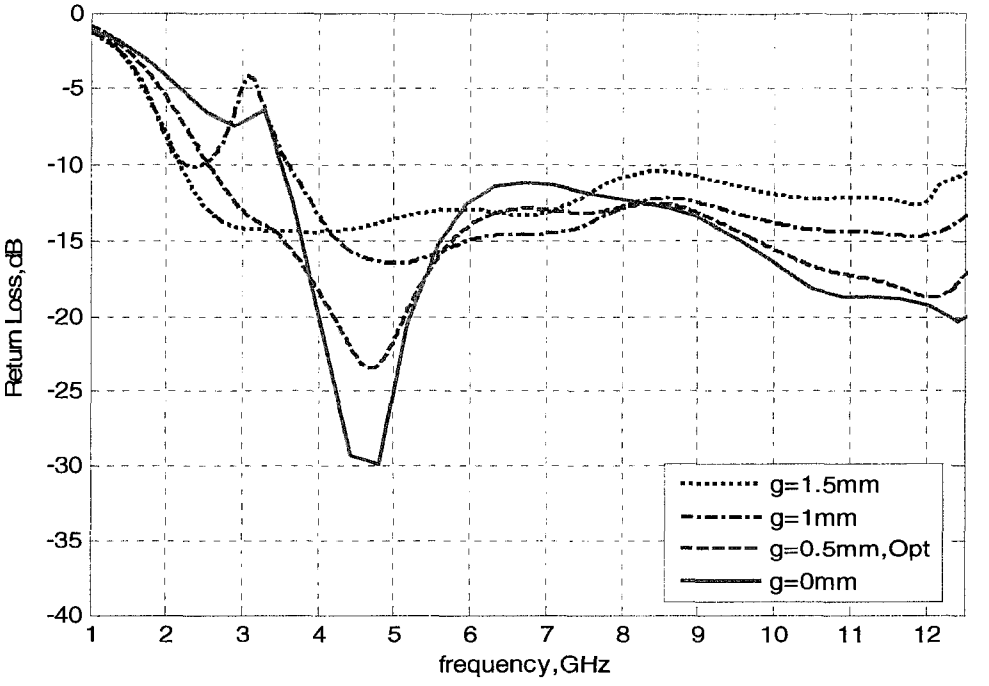

Figure 4.19: Effects of feed gap

4.3.5 Results and Discussion

After taking into account the design considerations described on antenna structure, current distributions and parametric study done to optimize the antenna geometry, the optimized antenna is constructed as shown in Figure 4.20. It is built on Rogers RT/Duroid 5880 material with a relative permittivity ε_r=2.2 and a thickness of 1.575 mm using the following optimal parameters: L_{sub} =31 mm, W_{sub} =40 mm, h=12, w=6.5 mm, θ_1 =17.5°, θ_2 =45°, mm, l_s =8 mm, w_s =10 mm, w_f =3.6, g=0.5 and L_g=10 mm. Then, the antenna is experimentally tested to confirm the simulation results. The simulated and measured VSWR is presented as well as the simulated and measured radiation patterns in principle

planes. Also, the simulated gain and radiation efficiency are provided.

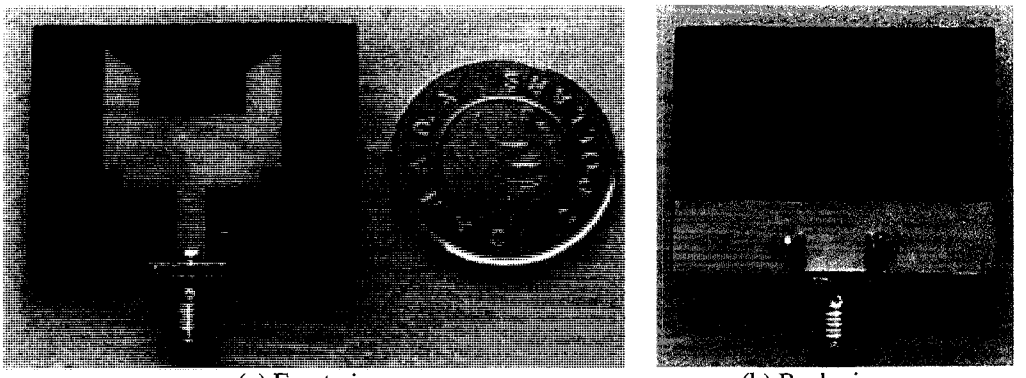

(a) Front view (b) Back view

Figure 4.20: The prototype of the double-beveled patch antenna

4.3.5.1 VSWR

The VSWR of the proposed antenna is measured. As depicted in Figure 4.21, the measured and simulated results are shown for comparison and indicate a reasonable agreement. The measured -10 dB return loss (VSWR<2) bandwidth of the antenna is approximately 9.74 GHz (3.00-12.74 GHz) and the antenna shows stable behaviors over the band. Thus, the measurement confirms the UWB characteristic of the double-beveled patch antenna as predicted in the simulation.

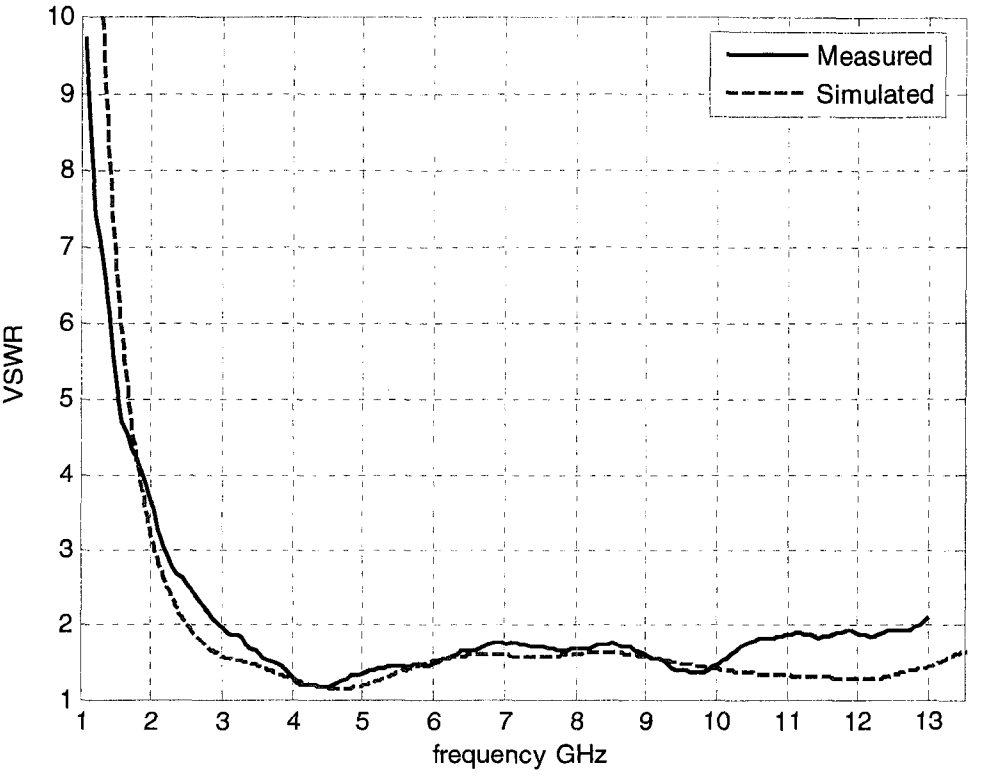

Figure 4.21: Simulated & measured VSWR

4.3.5.2 *Antenna Radiation Patterns*

The radiation characteristics of the proposed antenna are also investigated. The two dimensional radiation patterns presented here are taken at two sets of principle cuts, ϕ=0° and ϕ=90°. Referring to the coordinate system attached to the antenna geometry in Figure 4.14, the H-plane is the xz-plane and the E-plane is the yz-plane. Figures 4.22 and 4.23 illustrate the simulated and measured H-plane and E-plane radiation patterns respectively at 3.5, 5.5, 7.5 and 9.5 GHz. In general, the simulated and measured results are fairly consistent with each other at most of the frequencies but some discrepancies are noticed between them at higher frequencies especially in the E-plane due to the cable leakage current during the measurements and the intrinsic noise in the anechoic chamber.

Nevertheless, an analysis of the radiation pattern results shows that the proposed

antenna is characterized by omni-directional patterns in the H-plane for all in-band frequencies as in Figure 4.22. The measured *H*-plane patterns follow the shapes of the simulated ones well except at 9.5 GHz where there is very little difference.

For the E-plane patterns, Figure 4.23 shows that the simulated ones at low frequencies (3.5 and 5.5 GHz) form figure-of-eight patterns but at high frequencies, there are dips, especially at 9.5 GHZ. It is noticed that the measured patterns generally follow the simulated ones with some discrepancies.

In general, the double-beveled patch antenna shows an acceptable radiation pattern variation in its entire operational bandwidth since the degradation happens only for a small part of the entire bandwidth and it is not too drastic.

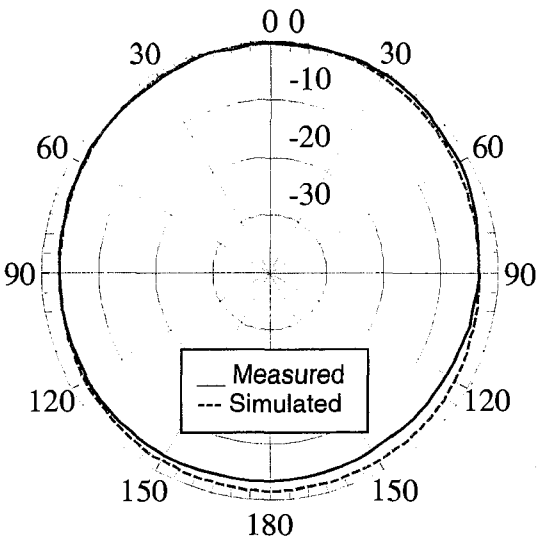

(a) H-plane at 3.5GHz

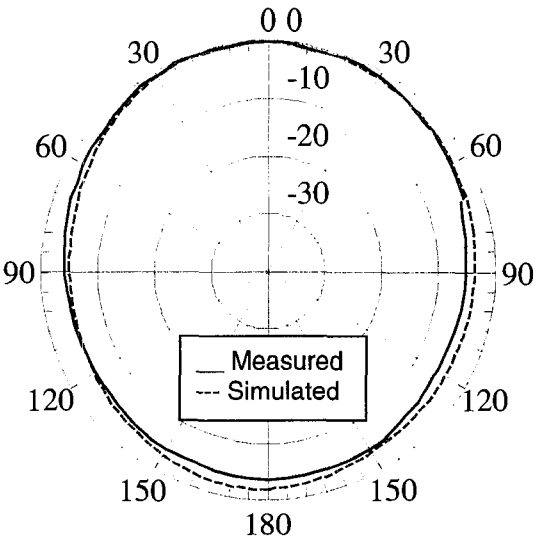

(b) H-plane at 5.5GHz

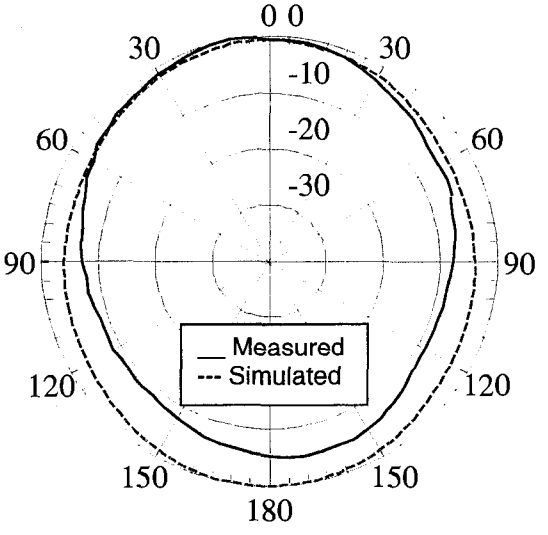

(c) H-plane at 7.5GHz

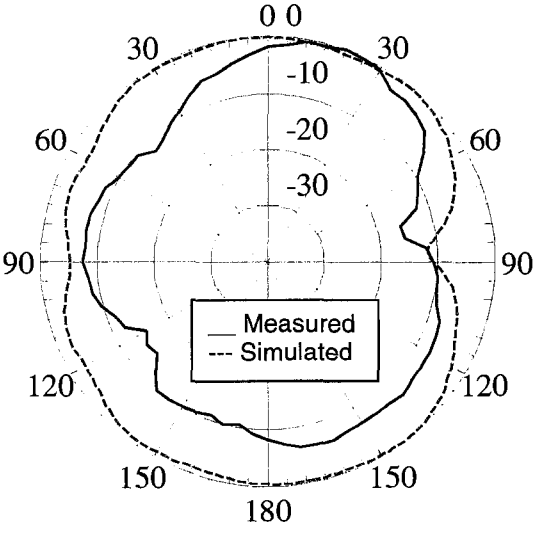

(d) H-plane at 9.5GHz

Figure 4.22: The simulated and measured radiation patterns in the H-plane at 3.5, 5.5, 7.5 and 9.5 GHz

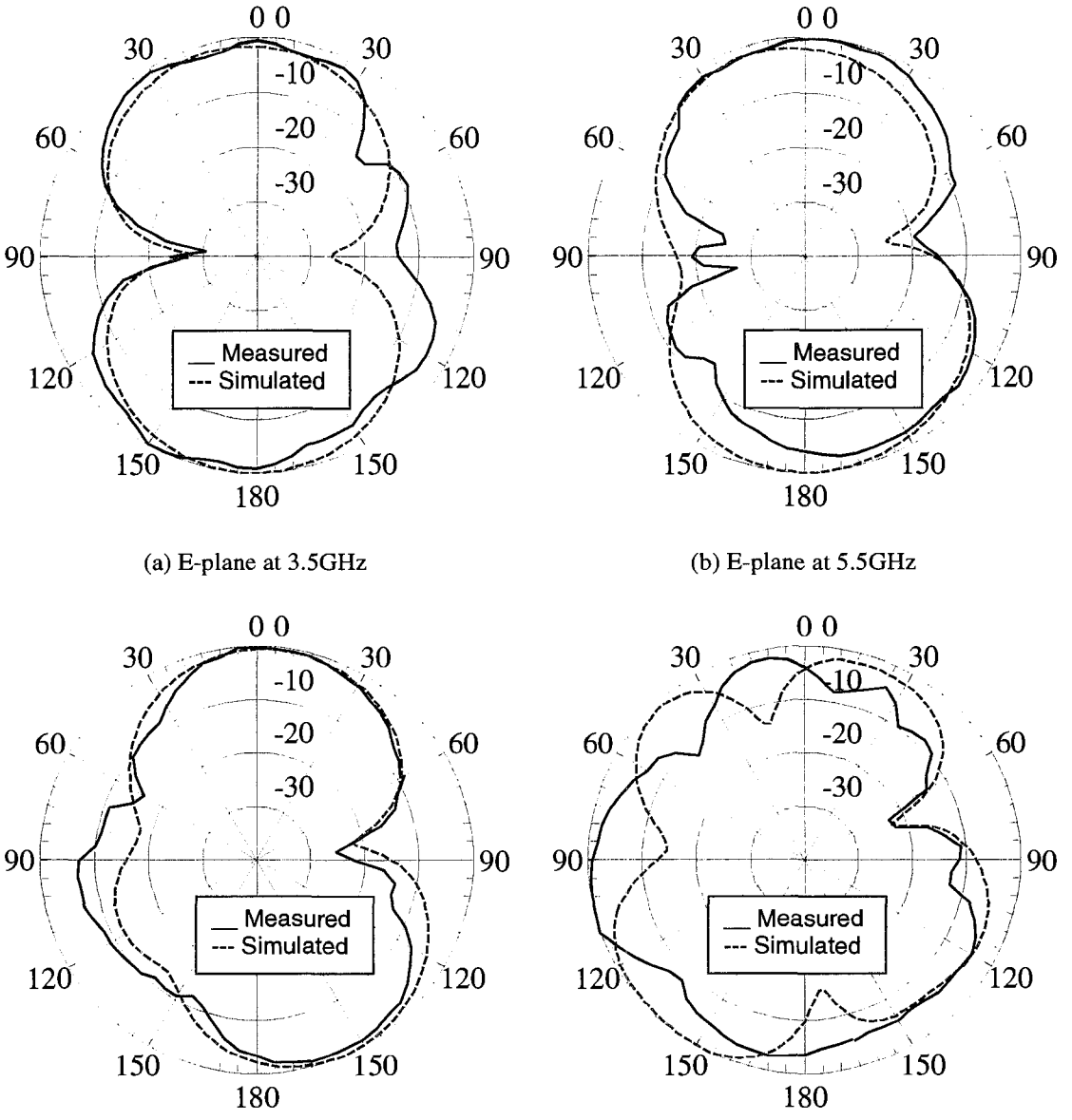

(a) E-plane at 3.5GHz

(b) E-plane at 5.5GHz

(c) E-plane at 7.5GHz

(d) E-plane at 9.5GHz

Figure 4.23: The simulated and measured radiation ratterns in the E-plane at 3.5, 5.5, 7.5 and 9.5 GHz

4.3.5.3 Gain and Radiation Efficiency

The gain and radiation efficiency versus frequency of the proposed antenna are also found to be suitable for the UWB communications and applications. The simulated antenna gain versus frequency is shown in Figure 4.24. It is greater than 3.4 dBi for all in-band frequencies and varies from 3.4 dBi to 6.1 dBi over the operating frequency range,

resulting in the maximum gain variation of 2.7 dB. The radiation efficiency is substantially high throughout the operational bandwidth of the antenna. Figure 4.25 shows that it is greater than 86 % in the entire operational bandwidth.

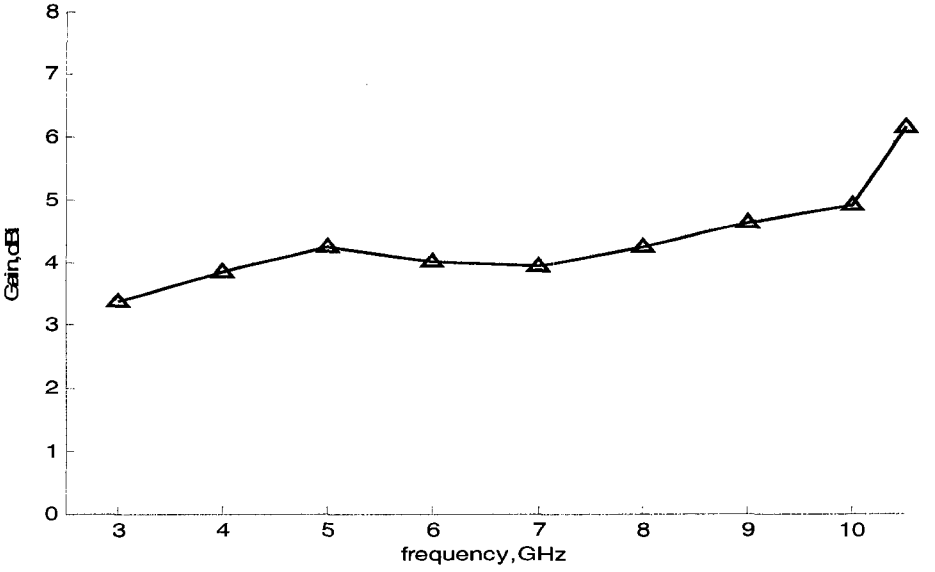

Figure 4.24: Simulated gain

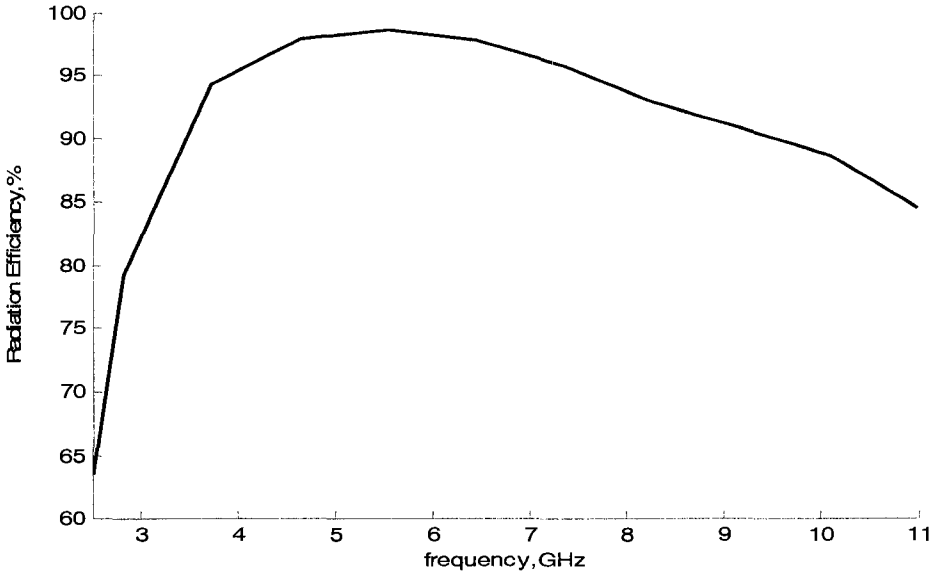

Figure 4.25: Radiation efficiency

4.4 The Band-Rejected Elliptical Patch Antenna

4.4.1 Overview

Over the allocated UWB frequency band, there are existing wireless local area network (WLAN) bands such as the 5.2-GHz (5150 - 5350 MHz) and 5.8-GHz (5725 - 5825 MHz) bands, which might interfere with UWB operations [122]. In order to avoid interference among these bands, UWB antennas with a frequency rejected function is desirable instead of using band-notched filter circuitry.

Thus, a band-rejected elliptical patch antenna with a notch cut and a U-like slot fed by a simple microstrip line is proposed [123]. It is designed and fabricated for UWB wireless communications with a stop-band notch in the 5-GHz WLAN band. This antenna is based on the elliptical antenna described in Section 4.2. In this design, we insert a U-like slot to obtain a band-notched function of 5.2/5.8 GHz. The operation bandwidth of the designed antenna is from 3.08 to 11.00 GHz with band rejection of 4.70 to 5.84 GHz. The proposed simple-shaped antenna provides a good radiation pattern and a relatively flat gain over the entire frequency band, excluding the rejected band.

In the following subsections, the design details and the related results will be presented and discussed. First, the antenna geometry and design process are explained. Then, the simulated and measured results, such as VSWR, radiation pattern, gain and radiation efficiency are provided and discussed.

4.4.2 Antenna Design

4.4.2.1 Design Process

The antenna is generated from the original design described in Section 4.2. Figure 4.26 depicts the design steps used to design the proposed antenna. After design the original antenna, the U-like slot is embedded beneath the notch cut in the elliptical patch to obtain the band-rejected characteristic of 5.2/5.8 GHz. The slot three parameters of the length, L_1, L_2, and L_3, are used to optimize the band-rejected performance. When the total length of the U-like slot is set to be about a half-wavelength at center of the desired rejected frequency band, a narrow frequency band can be filtered out while maintaining good matching over the rest of the UWB frequency band.

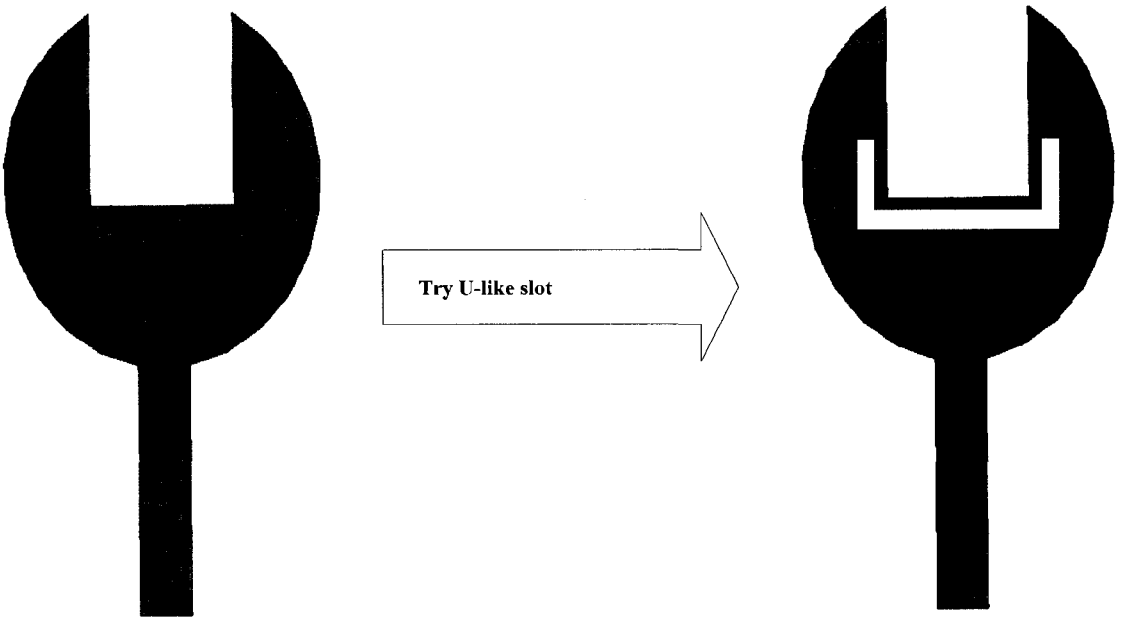

Figure 4.26: Flowchart for the design steps of the band-rejected patch antenna

4.4.2.2 Antenna Geometry

Figure 4.27 illustrates the geometry of the printed antenna as well as the Cartesian coordinate system.

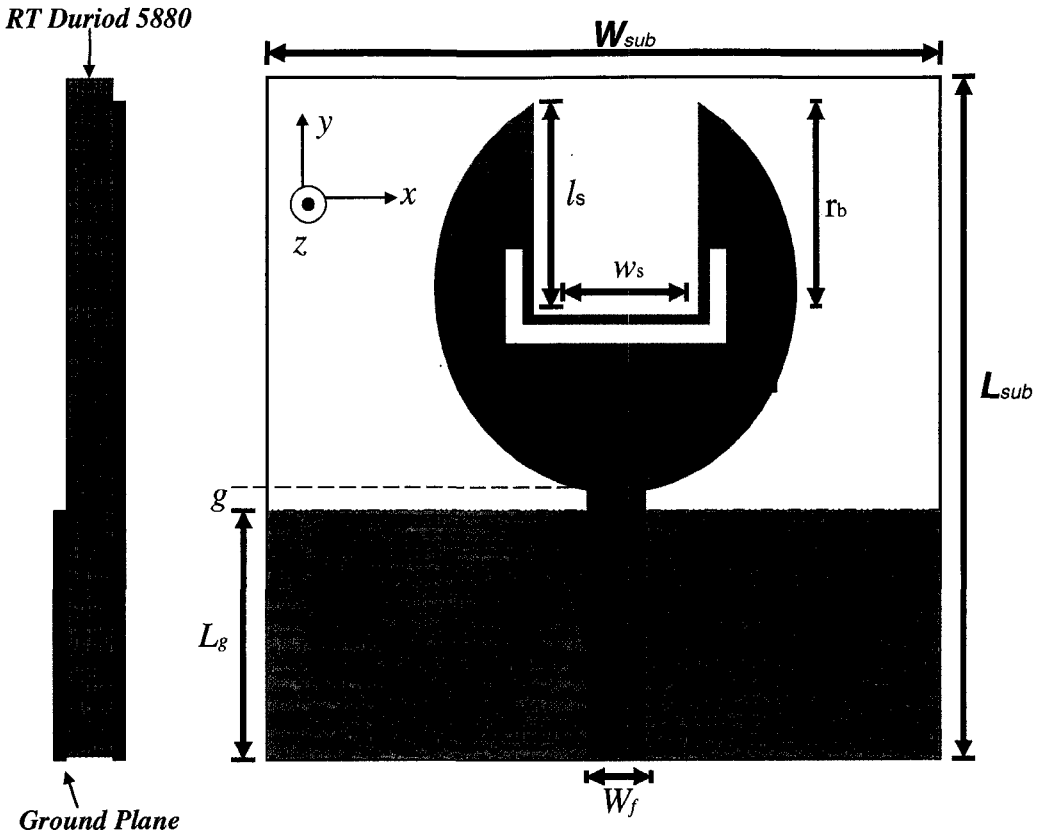

Figure 4.27: The geometry of the band-rejected elliptical patch antenna

It consists of an elliptical patch with notch cut and U-like slot as well as the partial ground plane. The Cartesian coordinate system (x,y,z) is oriented such that the bottom surface of the substrate lies in the x-y plane. All the parameters are the same as the original design parameters. Besides, the U-like slot is embedded beneath the notch cut in the elliptical patch to obtain the band-rejected characteristic. The slot three parameters of the length, L_1, L_2, and L_3, are used to optimize the band-rejected performance. The U-like slot has a uniform width of 1 mm, two vertical lengths of L_1= 4 mm and L_2= 4 mm and a horizontal length of L_3= 13 mm.

4.4.3 Results and Discussion

After taking into account the design considerations, the antenna is constructed as

shown in Figure 4.28 on Rogers RT/Duroid material using the following optimal parameters: L_{sub} =38 mm, W_{sub} =35 mm, r_a=11 mm, r_b=11.5, l_s =13 mm, w_s =10 mm, w_f =3.6, g=0.3, L_g=14.7 mm. L_1= 4 mm, L_2= 4 mm and L_3= 13 mm. The simulated and measured VSWR is presented along with the simulated radiation patterns in principle planes. Also, the simulated gain and radiation efficiency are provided.

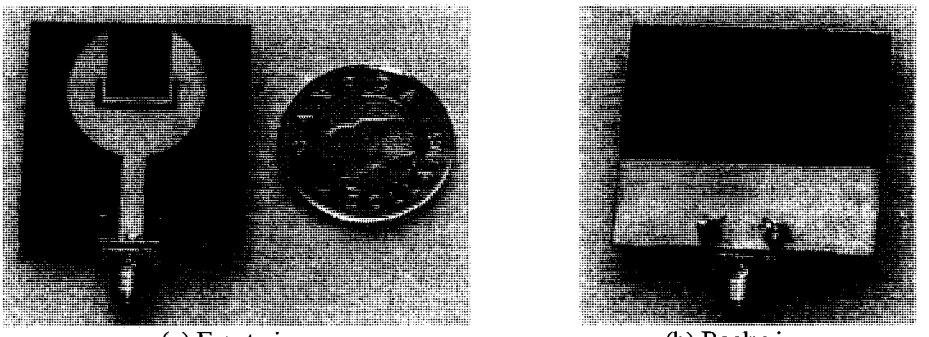

(a) Front view (b) Back view

Figure 4.28: The prototype of the band-rejected elliptical patch antenna

4.4.3.1 VSWR

Figure 4.29 shows the simulated and measured VSWR for the proposed antenna and the reference antenna (without the U- like slot). It clearly indicates that an UWB bandwidth (defined by 2:1 VSWR) covering 3.1–10.6 GHz is achieved for the reference antenna. For the proposed antenna with U-like slot, a bandwidth from 3.08 to 11.00 GHz with a sharp band rejection of 4.70 to 5.84 is obtained in the 5-GHz band, with small effects on other frequencies in the UWB bandwidth observed in the reference antenna. So, it is clear that the undesired band is tuned out while the wideband behavior of the antenna is maintained. Also, it is found that by adjusting the position and the length of the U-like slot to be about a half-wavelength at the center frequency of the desired rejected band, a destructive interference can be applicable, which results in the antenna being none-responsive at that frequency.

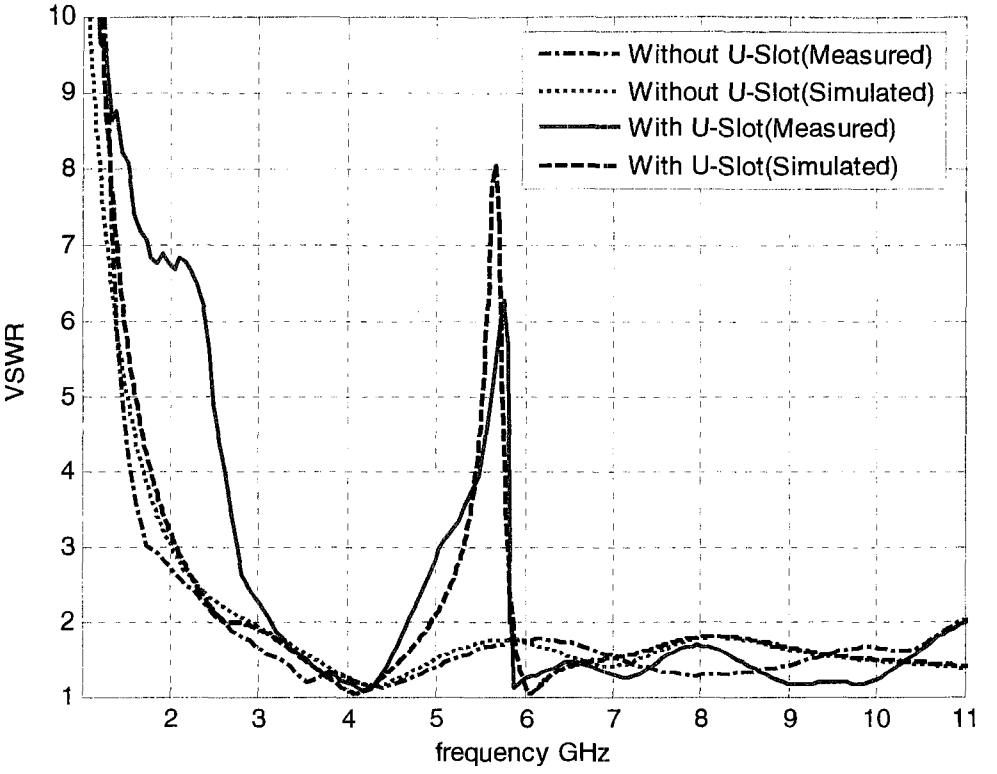

Figure 4.29: The simulated & measured VSWR

4.4.3.2 *Antenna Radiation Patterns*

The radiation characteristics of the proposed antenna are also investigated. The two dimensional radiation patterns presented here are taken at two sets of principal cuts, ϕ=0° and ϕ=90°. Referring to the coordinate system attached to the antenna geometry in Figure 4.26, the H-plane is the xz-plane and the E-plane is the yz-plane. Figure 4.30 illustrates the simulated H-plane and E-plane radiation patterns respectively at 3.5, 4.5, 7.5 and 10.5 GHz. The proposed antenna is characterized by an omni directional pattern in the H-plane while it is a quasi-omni directional pattern in the E-plane. It is obvious from these results that the radiation patterns are acceptable over the UWB bandwidth. Also, it is observed that the radiation patterns at other frequencies out of the notched frequency band

are about the same as those of the reference antenna.

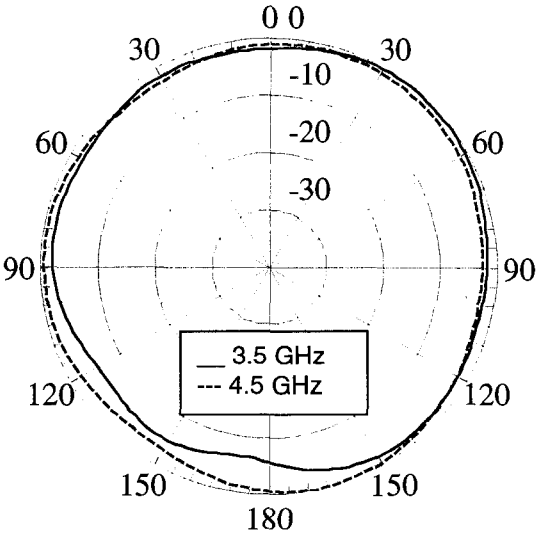

(a) H-plane (x-z) at 3.5 and 4.5 GHz.

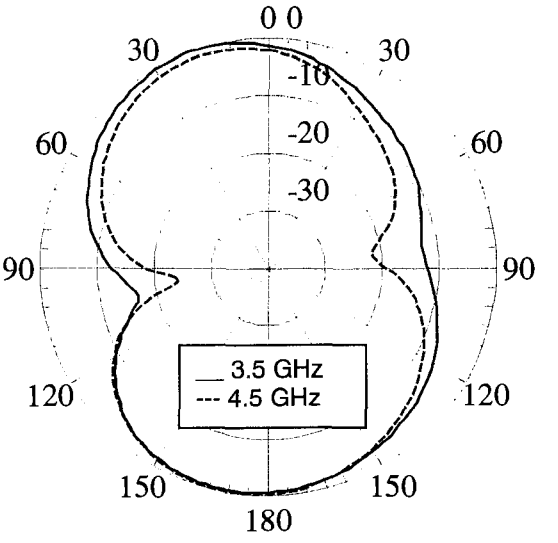

(c) E-plane (y-z) at 3.5 and 4.5 GHz.

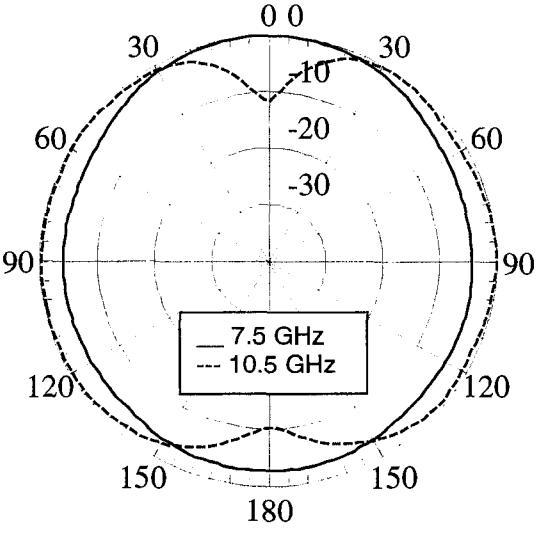

(b) H-plane (x-z) at 7.5 and 10.5 GHz.

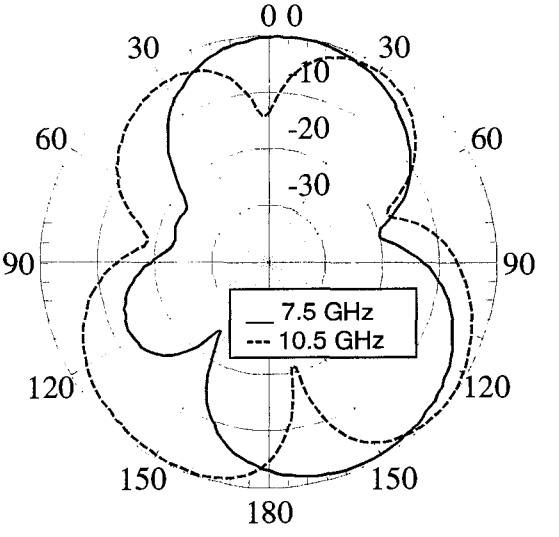

(d) E-plane (y-z) at 7.5 and 10.5 GHz.

Figure 4.30: The simulated radiation patterns in the H-plane and E-plane at 3.5, 4.5, 7.5 and 10.5 GHz

4.4.3.3 *Gain and Radiation Efficiency*

The gain and radiation efficiency versus frequency of the proposed antenna are also found to be suitable for the UWB communications and applications. The simulated antenna gain versus frequency is shown in Figure 4.31. It is greater than 3.6 dBi over the

operating frequency range while at the notched band, the antenna gain is sharply reduced due to the frequency rejected function. For other frequencies out of the notched frequency band, the antenna gain is about the same for the proposed and the reference antennas. The radiation efficiency is substantially high throughout the operational bandwidth of the antenna. Figure 4.32 shows that it is greater than 80 % in the entire operational bandwidth.

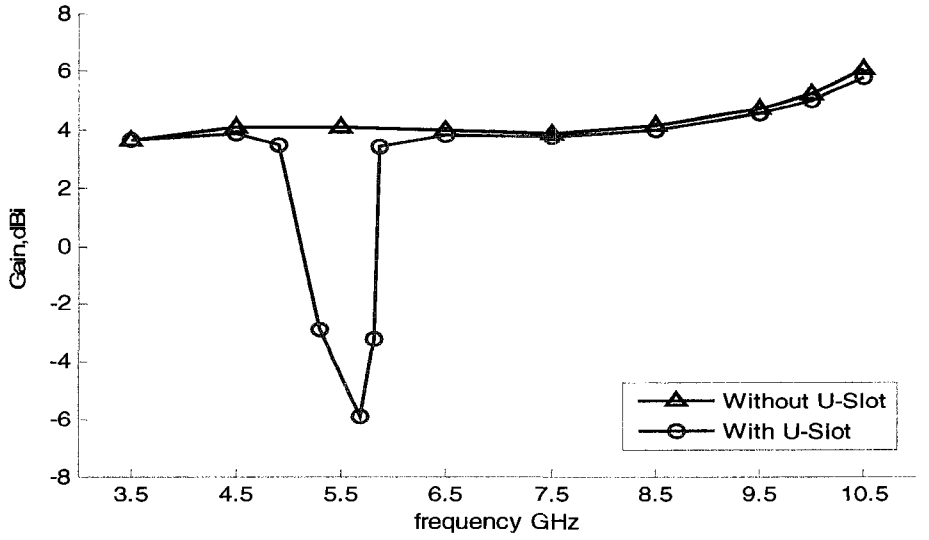

Figure 4.31: Simulated gain

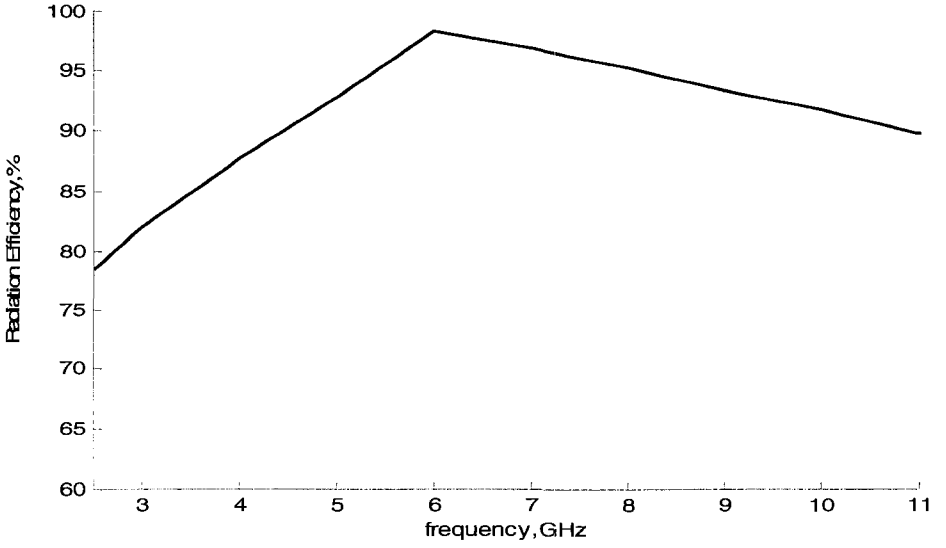

Figure 4.32: Radiation efficiency

4.5 Conclusion

In this chapter, three novel, small, low-cost and efficient UWB printed microstrip antennas are proposed for UWB wireless communications and applications. They are designed to satisfied frequency domain UWB requirements. The antennas are namely: the elliptical patch antenna, the double-beveled patch antenna and the band-rejected elliptical patch antenna.

The elliptical patch antenna operates over bandwidth of 140.9 % (2.65-10.80 GHz) with a flat gain of 2.5 dB variation and a minimum radiation efficiency of 85 %. The double-beveled patch antenna operates over bandwidth of 142.8 % (3.00-12.74 GHz) with a flat gain of 2.7 dB variations and a minimum radiation efficiency of 86 %. The band-rejected elliptical patch antenna operates over bandwidth from 3.08 to 11.00 GHz with band rejection of 4.70 to 5.84 GHz to filter out the band of 5.2/5.8 GHz. It provides a relatively flat gain greater than 3.6 dB over the operating frequency range, except at the notched band, in which the antenna gain is sharply reduced due to the frequency rejected function. Its radiation efficiency is greater than 85 % in most of the operational bandwidth. All antennas provide an acceptable radiation pattern over the entire frequency band. The table below shows a comparison of the three designed antennas.

Antennas	Bandwidth (GHz)	Radiation Patterns	Gain variations (dB)	Radiation efficiency (%)
Elliptical	8.15	Nearly omni-directional	2.5	85
Double-beveled	9.74	Nearly omni-directional	2.7	86
Band-rejected elliptical	7.92 excluding 1.14 as a notch	Nearly omni-directional	2.5	85

Table 4.1: Comparison of antennas characteristics

CHAPTER FIVE

Conclusion

5.1 Conclusion

In this thesis, five novel, small, low-profile, microstrip-fed printed UWB antennas are studied, analyzed, designed and implemented to satisfy UWB technology requirements. The design and analysis of the proposed printed antennas for UWB communications and applications in the 3.1-10.6 GHz bandwidth are pursued using the commercially available full wave simulation software HFSS. Because of their low cost, light weight and ease of implementation, these printed designs are desired in UWB wireless communication systems and applications, especially in portable devices and indoor applications such as wireless personal area networks (WPANs). These antennas are namely: the stepped-trapezoidal patch antenna, the trimmed notch-cut patch antenna, the elliptical patch antenna, the double-beveled patch antenna, and the band-rejected elliptical patch antenna. They are designed using different bandwidth-enhancement techniques to satisfy UWB bandwidth. Theses techniques are: the partial ground plane technique, the adjust of the gap between radiating element and ground plane technique, the steps

technique or cutting two notches in the radiating element, the beveling radiating element technique and the notch cut technique. The notch cut from the radiator is also used to miniaturize the size of the planar antennas.

In designing these antennas, the thesis focuses on UWB frequency domain characteristics such as the far field radiation patterns, bandwidth, gain and radiation efficiency. The design parameters of the antennas are also extensively analyzed in order to understand the antennas' operations to therefore achieve the optimal performance.

The stepped-trapezoidal patch antenna is composed of an isosceles trapezoidal patch with the circular-notch cut and two transition steps, fed by a microstrip line flushed on a partial ground plane. It operates over a bandwidth of 137.2 % (3.13-11.83 GHz). It provides a nearly omni-directional radiation pattern and a relatively flat gain over the entire frequency band with a maximum variation of 2.3 dB. The radiation efficiency is substantially high throughout the operational bandwidth at 94 % or higher in most of the operational bandwidth. Ohmic losses are not included in the calculated radiation efficiency.

The trimmed notch-cut patch antenna is composed of a planar rectangular patch with notch cut and a transition step fed by the microstrip line with the partial ground plane. It operates over a bandwidth of 132.1 % (3.1-10.6 GHz). It provides nearly omni-directional radiation patterns and relatively flat gain over the entire frequency band with a maximum variation of 1.2 dB. The radiation efficiency is substantially high throughout the operational bandwidth at 90 % or higher in most of the operational bandwidth.

The elliptical patch antenna is composed of a planar elliptical patch with notch cut fed by a microstrip line flushed on the partial ground plane. It operates over a bandwidth of 140.9 % (2.65-10.80 GHz). It provides omni-directional radiation patterns and

relatively flat gain over the entire frequency band with a maximum variation of 2.5 dB. The radiation efficiency is very high throughout the operational bandwidth at 88 % or more in most of the operational bandwidth.

The double-beveled patch antenna is composed of a symmetrical double-beveled planar patch antenna with notch cut fed by a microstrip line folded on the partial ground plane. It operates over a bandwidth of 142.8 % (3.00-12.74 GHz). It provides omni-directional radiation patterns and relatively flat gain over the entire frequency band with a maximum variation of 2.7 dB. The radiation efficiency is very high throughout the operational bandwidth which is greater than 86 % in the entire operational bandwidth.

The band-rejected elliptical patch is the same as elliptical patch antenna with the addition of a U-like slot fed by the simple microstrip line flushed on the partial ground plane. It is designed for UWB wireless communications with a stop-band notch in the 5-GHz WLAN band. Its operation bandwidth is from 3.08 to 11.00 GHz with a band rejection of 4.70 to 5.84 GHz to filter out the band of 5.2/5.8 GHz. It provides a good radiation pattern and a relatively flat gain over the entire frequency band, excluding the rejected band. It is greater than 3.6 dB over the operating frequency range while at the notched band, the antenna gain is sharply reduced due to the frequency rejected function. The radiation efficiency is high throughout the operational bandwidth which is greater than 85 % in most of the operational bandwidth.

All the antennas reported in this thesis share these design properties: they are fed by the 50 ohms-microstrip line flushed on the partial ground plane. They have feed gap and notch cut from the radiator. The notch cut is used to control the stability of the impedance matching bandwidth and to miniaturize the size of the planar antennas. It offers reduced patch size, more degree of freedom for design, extra space that could

accommodate other RF circuit elements. However, the parametric studies on the effect of the notch cut show that within a certain limit of the cutout size, the radiation properties do not change drastically. But beyond that limit, the notch cut highly affects radiation patterns at some bands of frequencies in the operational bandwidth.

It has been demonstrated numerically and experimentally that the proposed antennas are suitable for UWB technology. They can provide satisfactory frequency domain performance, including ultra wide bandwidth with nearly omni-directional radiation patterns, relatively flat gain and good radiation efficiency, which make them very suitable for the UWB wireless communications and applications.

This research has contributed to the research community with five technical papers published in five international conferences [116, 119, 120, 121, 123]. Also, to date, three journal letters have been submitted to different international technical journals to be considered for possible publication.

5.2 Future Work

Suggested future work can be pursued out in the following areas:

UWB systems transmit information at an extremely low power level that leads to a limit of the communication range. Therefore, high gain is required in order to enhance the quality of the transmission link and improve channel capacity. Consequently, the solution is an UWB antenna array configuration. In this thesis, the proposed UWB antennas reveal attractive characteristics for use in the array design. Their attractive characteristics include small element size, planar version, and ease of varying excitation amplitudes and phases

of the array elements due to microstrip feed. Thus, research and study of an UWB array comprised of one type of antenna proposed in this thesis could be carried out.

The proposed antennas in this thesis are suitable for portable devices. Therefore, the effect of theses devices on antenna performance is an important area to be investigated. In addition, the potential effects on human body should also be considered if the antennas are embedded in devices used near or by humans.

UWB systems occupy huge operational bandwidth and often utilize very short pulses for data transmission. UWB systems transmit narrow pulses rather than using a continuous wave carrier to communicate information. Therefore, an appropriate time domain performance is a key requirement for UWB antennas. Therefore, investigations and analysis are recommended to be carried out on the effect of the proposed antennas on the transmitted pulse to hence improve the time domain behavior by optimizing the antenna designs.

References

[1] "Ultra Wideband Radio in Multiple Access Communications," IEEE J. Sel. Areas Comn. Spl. Issue, Dec. 2002.

[2] "Ultra Wideband Technology: Enabling High-Speed Wireless Personal Area Networks," Intel White Paper, 2004.

[3] J. Liang, "Antenna Study and Design for Ultra Wideband Communication Applications," PHD Thesis, University of London, United Kingdom, July 2006.

[4] J. G. Proakis, "Digital Communications" New York: McGraw-Hill, 1989.

[5] C. E. Shannon, "A Mathematical Theory of Communication" Bell Syst. Tech. J., vol. 27, pp. 379-423, 623-656, July & October 1948.

[6] Federal Communication Commission, "First Report and Order, Revision of Part 15 of the Commission's Rules Regarding Ultra-Wideband Transmission System," FCC 02 48, 2002.

[7] L. Yang, G. Giannakis, "Ultra-Wideband Communications: An Idea Whose Time Has Come," IEEE Signal Processing Magazine, pp. 26-54, November 2004.

[8] D. Wentzloff, R. Blazquez, F. Lee, B. Ginsburg, J. Powell and A. Chandrakasan, "System Design Considerations for Ultra-Wideband Communication," IEEE Communications magazine, vol. 43, pp.114-121, August 2005.

[9] J. Taylor, "Introduction to ultra-wideband radar systems" CRC Press, Inc., 1995.

[10] G. Brzezina, "Planar Antennas in LTCC Technology for Ultra-Wideband Applications," M. A. Sc. Thesis, Carleton University, Canada, 2005.

[11] D. Barras, F. Ellinger, H. Jackel, and W. Hirt, "A Low Supply Voltage SiGe

LNA for Ultra-Wideband Frontends," IEEE Microwave and Wireless Components Letters, vol. 14, pp. 469-471, October 2004.

[12] A. Bevilacqua and A. Niknejad, "An Ultra-Wideband CMOS Low-Noise Amplifier for 3.1-10.6 GHz Wireless Receivers," IEEE Journal of Solid-State Circuits, vol. 39, pp. 2259-2268, December 2004.

[13] M. Tsai and H. Wang, "A 0.3-25 GHz Ultra-Wideband Mixer Using Commercial 0.18-/μm CMOS Technology," IEEE Microwave and Wireless Components Letters, vol. 14, pp. 522-524, November 2004.

[14] F. Lee, D. Wentzloff, and A. Chandrakasan, "An Ultra-Wideband Baseband Front-End," IEEE Radio Frequency Integrated Circuits (RFIC) Symposium, pp. 493-496, June 2004.

[15] J. Powell, "Antenna Design for Ultra Wideband Radio," M. A. Sc. Thesis, Massachusetts Institute of Technology, USA, May 2004.

[16] H. Harmuth and S. Rong, "Antenna for Nonsinusoidal Waves I. Radiators," IEEE Transactions on Electromagnetic Compatibility, vol. EMC-25, pp. 13-24, February 1983.

[17] I. Linardou, C. Migliaccio, J. M. Laheurte and A. Papiernik, "Twin Vivaldi Antenna Fed by Coplanar Waveguide," IEE Electronics Letters, vol.33, pp. 1835-1837, October1997.

[18] C. Balanis, "Antenna Theory Analysis and Design" John Wiley & Sons, Inc., 2005.

[19] S. Licul, J. Noronha, W. Davis, D. Sweeney, C. Anderson and T. Bielawa, "A Parametric Study of Time-Domain Characteristics of Possible UWB Antenna Architectures," IEEE 58th Vehicular Technology Conference, VTC 2003-Fall,

vol. 5, pp. 3110-3114, October 2003.

[20] Z. Chen, T. See and X. Qing, "Small Printed Ultra Wideband Antenna with Reduced Ground Plane Effect," IEEE Transactions on Antennas and Propagation, vol. 55, pp. 383-388, February 2007.

[21] N. Azenui, "Miniaturized Printed Circuit Antennas for Multi- and Ultra-Wide Band Applications," PHD Thesis, University of Illinois, USA, 2007.

[22] HFSS™, v10, Ansoft Corporation Software, Pittsburgh, PA, USA.

[23] K. Siwiak and D. McKeown, "Ultra-Wideband Radio Technology" John Wiley & Sons, Ltd., 2004.

[24] J. Belrose. "The Sounds of a Spark Transmitter:Telegraphy and Telephony," Adventures in CyberSound, http://newton.otago. ac.nz:808/~ursi/belrose/ spark.html.

[25] H. Schantz, "A Brief History of Ultra-Wideband Antennas," IEEE Conference on UWBST, pp. 209-213, November 2003.

[26] G. Aiello and G. Rogerson, "Ultra-wideband Wireless Systems," IEEE Microwave Magazine, pp. 36-47, June 2003.

[27] V. Rumsey, "Frequency Independent Antennas," IRE National Convention Record, vol. 5, pp. 114-118, March 1957.

[28] J. Dyson, "The Unidirectional Equiangular Spiral Antenna," IEEE Transactions on Antennas Propagation, vol. 7, pp. 329-334, October 1959.

[29] G. Ross, "A Time Domain Criterion for the Design of Wideband Radiating Elements", IEEE Transactions on Antennas Propagation, vol. 16, p. 355- 356, May 1968.

[30] G. Ross, "Transmission and Reception System for Generating and Receiving Base-

Band Duration Pulse Signals for Short Base-Band Pulse Communication System" U.S. Patent no. 3728632, April 1973.

[31] T. Barrett, "History of Ultra Wideband (UWB) Radar & Communications: Pioneers and Innovators," Progress in Electromagnetics Symposium 2000 (PIERS2000), USA, July 2000.

[32] Federal Communication Commission, "Part 15 - radio frequency devices," http://www.access.gpo.gov/nara/cfr/waisidx_00/47cfr15_00.html, 2005.

[33] I. Oppermann, M. Hamalainen and J. Iinatti, "UWB Theory and Applications" John Wiley & Sons, Ltd, 2004.

[34] N. Cravotta, "Ultrawideband: the Next Wireless Panacea?," EDN, www.edn.com, October 2002.

[35] W. Siriwongpairat, "Cross-Layer Design for Multi-Antenna Ultra-Wideband Systems," PHD Thesis, University of Maryland, 2005.

[36] Pulse Link, Inc, http://www.fantasma.net.

[37] K. Dotto, "Development of a Novel Ultra-Wideband Antenna and Prototype Scanner for Detection and Location of Voids in Wood," PHD Thesis, The University of British Columbia, 2005.

[38] M. Lapierre, "An Ultra Wideband Monopole/Dielectric Resonator Antenna," M. A. Sc. Thesis, Royal Military College of Canada, 2003.

[39] A. Petosa, "Antennas and Arrays Course Notes," Carleton University, 2002.

[40] G. Ramesh, "Microstrip Antenna Design Handbook" Artech House, 2001.

[41] G. Deschamps, "Microstrip Microwave Antennas," 3rd USAF Symposium on Antennas, 1953.

[42] H. Gutton and G. Baissinot, "Flat Aerial for Ultra High Frequencies," French

Patent no.70313, 1955.

[43] J. Howell, "Microstrip Antenna," IEEE International Antenna and Propagation Symposium, vol. 10, pp. 177-180, December 1972.

[44] H. Kazuhiro, H. Misao, "Analysis, Design, and Measurement of Small and Low-Profile Antennas" Artech House Inc., 1992.

[45] D. Pozar, "Microstrip Antennas," Proceedings of the IEEE, vol.80, pp. 79-91, January 1992.

[46] K. Kupta, G. Ramesh, I. J. Bahl, "Microstrip Lines and Slotlines" Artech House Inc. 1979.

[47] W. Choi, K. Chung, J. Jung and J. Choi, "Compact Ultra-Wideband Printed Antenna with Band-Rejection Characteristic," IEE Electronics Letters, vol.41, pp. 990-991, September 2005.

[48] K. Wong, Y. Chi, C. Su and F. Chang, "Band-Notched Ultra-Wideband Circular-Disc Monopole Antenna with an Arc-Shaped Slot," Microwave and Optical Technology Letters, vol. 45, pp. 188-191, May 2005.

[49] G. Lu, "Antenna and Synchronization Design Issues for the Ultra-Wideband Systems," PHD Thesis, the State University of New Jersey, USA, 2006.

[50] J. Hershey, "Wideband Antennas - a Short Survey," General Electric Company, 2000.

[51] S. Silver, "Microwave Antenna Theory and Design," UK: P. Peregrinus on behalf of the Institution of Electrical Engineers.

[52] Y. Mushiake, "Self-Complementary Antennas," IEEE Antennas and Propagation Magazine, vol. 34, pp. 23-29, December 1992.

[53] Y. Mushiake, "A Report on Japanese Developments of Antennas from Yagi-Uda Antenna to Self-Complementary Antennas," IEEE International Symposium on Antennas and Propagation, vol. 4, pp. 841-844, June 2003.

[54] D. Chen and H. Chen, "A CPW-Fed Dual-Frequency Monopole Antenna," IEEE Transactions on Antennas and Propagation, vol. 52, pp. 978-982, April 2004.

[55] Z. Liu, P. Hall and D. Wake, "Dual-Frequency Planar Inverted-F Antenna," IEEE Transactions on Antennas and Propagation, vol. 45, pp. 1451-1458, April 1997.

[56] A. Muscat and C. Parini, "Novel Compact Handset Antenna," 11th International Conference on Antennas and Propagation, vol. 1, pp. 336-339, April 2001.

[57] G. Lee, T. Chiou and K. Wong, "Broadband Stacked Shorted Patch Antenna for Mobile Communication Handsets," Asia-Pacific Microwave Conference, vol. 1, pp. 232-235, December 2001.

[58] A. Rudge, K. Milne, A. Olver and P. Knight, "The Handbook of Antenna Design" Peter Peregrinus Ltd., UK, 1982.

[59] M. Ammann and Z. Chen, "Wideband Monopole Antennas for Multi-Band Wireless Systems," IEEE Antennas and Propagation Magazine, vol. 45, pp. 146-150, April 2003.

[60] J. Ammann, "Square Planar Monopole Antenna," IEE National Conference on Antennas and Propagation, pp. 37-40, 30 March - 1 April 1999.

[61] N. Agrawall, G. Kumar, and K. Ray, "Wide-Band Planar Monopole Antennas," IEEE Transactions on Antennas and Propagation, vol. 46, pp. 294-295, February 1998.

[62] Z. Chen, "Experiments on Input Impedance of Tilted Planar Monopole Antenna," Microwave and Optical Technology Letters, vol. 26, pp. 202-204, August 2000.

[63] Z. Chen and Y. Chia, "Impedance Characteristics of Trapezoidal Planar Monopole Antennas," Microwave and Optical Technology Letters, vol. 27, pp. 120-122, October 2000.

[64] L. Smith, T. Starkie and J. Lang, "Measurements of Artimi's Antenna Designs," International Workshop on Ultrawideband Systems, Jiont with Conference on Ultrawideband Systems and Technologies, pp. 304-306, May 2004.

[65] G. Ruvio and M. Ammann, "A Compact Wide-Band Shorted Folded Antenna," IEEE International Workshop on Antenna Technology Small Antennas and Novel Metamaterials, pp. 84-87, March 2006.

[66] Z. Chen, M. Ammann, M. Chia and T. See, "Annular Planar Monopole Antennas," IEE Proceedings Microwaves, Antennas & Propagation, vol.149, pp. 200-203, August 2002.

[67] K. Kiminami, A. Hirata and T. Shiozawa, "Double-Sided Printed Bow-Tie Antenna for UWB Communications," IEEE Antennas and Wireless Propagation Letters, vol. 3, pp.152-153. 2004.

[68] G. Lu, S. Mark, I. Korisch, L. Greenstein and P. Spasojevic, "Diamond and Rounded Diamond Antennas for Ultrawide-Band Communications," IEEE Antennas and Wireless Propagation Letters, vol. 3, pp. 249-252, 2004.

[69] H. Schantz, "Planar Elliptical Element Ultra-Wideband Dipole Antennas," IEEE Antennas and Propagation Society International Symposium, vol. 3, pp. 44-47, June 2002.

[70] H. Schantz, "The Art and Science of Ultrawideband Antennas" Artech House Inc, 2005.

[71] M. Bataller, M. Fabrés, E. Daviu and A. Nogueira, "Overview of Planar Monopole Antennas for UWB Applications," Proceeding of EUCAP 2006, November 2006.

[72] J. Evans, M. Amunann, "Planar Trapezoidal and Pentagonal Monopoles with Impedance Bandwidths in Excess of 10:1" IEEE International Antenna and Propagation Symposium, vol. 3, pp.1558-1561, July 1999.

[73] M. Ammann, "Control of the Impedance Bandwidth of Wideband Planar Monopole Antennas Using A Beveling Technique," Microwave and Optical Technology Letters, vol. 30, pp. 229-232, July 2001.

[74] M. Ammann and Z. Chen, "An Asymmetrical Feed Arrangement for Improved Impedance Bandwidth of Planar Monopole Antennas," Microwave and Optical Technology Letters, vol. 40, pp.156-158, January 2004.

[75] J. Floc'h and L. Desclos, "Surface-Mounted Monopole Antenna," Microwave and Optical Technology Letters, vol. 16, pp. 349-352, December 1997.

[76] Z. Chen, M. Ammann, X. Qing, X. Wu, T.See, A. Cai, "Planar Antennas," IEEE Microwave Magazine, vol. 7, pp. 63-73, December 2006.

[77] M. Ammann and Z. Chen, "A Wide-Band Shorted Planar Monopole with Bevel," IEEE Transactions on Antennas and Propagation, vol. 51, pp. 901-903, April 2003.

[78] M. Ammann, "A Wideband Monopole for Reconfigurable Multiband Radio Terminals," IEEE International Symposium on Antennas and Propagation, vol. 1, pp. 170-173, July 2001.

[79] Z. Chen, M. Ammann, and M. Chia, "Broadband Square Annular Planar Monopoles," Microwave and Optical Technology Letters, vol. 36, pp. 449-454, March 2003.

[80] D. Valderas, J. Meléndez and I. Sancho, "Some Design Criteria for UWB Planar Monopole Antennas: Application to A Slotted Rectangular Monopole," Microwave and Optical Technology Letters, vol. 46, pp.6-11, July 2005.

[81] A. Cai, T. See, and Z. Chen, "Study of Human Head Effects on UWB Antenna," IEEE International Workshop on Antenna Technology (iWAT), pp. 310–313, March 2005.

[82] C. Huang and W. Hsia, "Planar Elliptical Antenna for Ultrawideband Communications," Electronics Letters, vol. 41, pp. 296-297, March 2005.

[83] S. Lee, J. Park, and J. Lee, "A Novel CPW-Fed Ultra-Wideband Antenna Design," Microwave Optical Technology Letters, vol. 44, , pp.393-396, 2005.

[84] S. Su, K. Wong, and C. Tang, "Ultra-Wideband Square Planar Monopole Antenna For IEEE 802.16a Operation In The 2–11GHz Band," Microwave Optical Technology Letters, vol. 42 pp. 463-466, 2004.

[85] E. Lee, P. Hall, and P. Gardner, "Compact Wideband Planar Monopole Antenna," Electronics Letters, vol. 35, pp.2157-2158, December 1999.

[86] E. Daviu, M. Fabres, M. Bataller, and A. Nogueira, "Wideband Double-Fed Planar Monopole Antennas," Electronics Letters, vol. 39, pp.1635-1636, November 2003.

[87] S. Honda, M. Ito, H. Seki, and Y. Jingo, "A Disc Monopole Antenna with 1:8 Impedance Bandwidth and Omnidirectional Radiation Pattern," IEEE International Symposium on Antennas and Propagation, pp.145-149, September 1992.

[88] M. Hammoud, P. Poey, and F. Colombel, "Matching the Input Impedance of a Broadband Disc Monopole," Electronics Letters, vol. 29, pp. 406-407, February 1993.

[89] G. Kumar, K. Ray, "Broadband Microstrip Antenna" Archtech House Inc., USA, 2003.

[90] M. Sanad, "Effect of Shorting Posts on Short Circuit Microstrip Antennas," IEEE International Symposium on Antennas and Propagation, vol. 2, pp. 794-797, June 1994.

[91] P. Anob, K. Ray, and G. Kumar, "Wideband Orthogonal Square Monopole Antennas with Semi-Circular Base," IEEE International Symposium on Antennas and Propagation, vol.3, pp.294-296, 2001.

[92] H. Schantz, "Introduction to Ultra-Wideband Antennas," IEEE Conference on UWBST, pp. 1-9, November 2003,

[93] H. Schantz, "Bottom Fed Planar Elliptical Ultra-Wideband Antennas," IEEE Conference on UWBST, pp. 219-223, November 2003.

[94] H. Schantz, "Radiation Efficiency of Ultra-Wideband Antennas," IEEE Conference on UWBST, pp. 351-355, May 2002.

[95] K. Wong, C. Wu and S. Su, "Ultrawide-Band Square Planar Metal-Plate Monopole Antenna with a Trident-Shaped Feeding Strip," IEEE Transactions on Antennas and Propagation, vol. 53, pp. 1262-1269, April 2005.

[96] C. Zhao, "Analysis on the Properties of a Coupled Planar Dipole UWB Antenna," IEEE Antennas and Wireless Propagation Letters, vol. 3, pp. 317-320, 2004.

[97] J. Powell, A. Chandrakasan, "Differential and Single Ended Elliptical Antennas for 3.1-10.6 GHz Ultra Wideband Communication," IEEE International Symposium on Antennas and Propagation, vol. 3, pp. 2935-2938, June 2004.

[98] C. Ying and Y. Zhang, "A Planar Antenna in LTCC for Single-Package Ultrawide-Band Radio," IEEE Transactions on Antennas and Propagation, vol. 53, pp. 3083-3093, September 2005.

[99] L. Jianxin, C. Chiau, C. Xiaodong and C. Parini, "Study of A Printed Circular Disc Monopole Antenna for UWB Systems," IEEE Transactions on Antennas and Propagation, vol. 53, pp. 3500-3504, November 2005.

[100] Z. Low, et al., "Low-Cost PCB Antenna for UWB Applications," IEEE Antennas and Wireless Propagation Letters, vol. 4. pp. 237-239, 2005.

[101] C. Marchais, et al., "Stripline Slot Antenna for UWB Communications," IEEE Antennas and Wireless Propagation Letters, vol. 5. pp. 319-322, 2006.

[102] S. Suh, W. Stutzman, W. Davis, "A New Ultrawideband Printed Monopole Antenna: The Planar Inverted Cone Antenna (PICA)," IEEE Transactions on Antennas and Propagation, vol. 52, pp. 1361- 1365, May 2004.

[103] M. Solis, H. Aguilar, "Ultra-Wideband Planar Monopole Antenna for Operation in the 3-20 GHz Band," VI th. International Symposium on Electromagnetic Compatibility and Electromagnetic Ecology (EMC-2005), pp. 97-100, June 2005.

[104] Z. Chen, "Novel Bi-Arm Rolled Monopole for UWB Applications," IEEE Transactions on Antennas and Propagation, vol. 53, pp. 672-677, February 2005.

[105] S. Choi, J. Park, S. Kim, J. Park, "A New Ultra-Wideband Antenna for UWB Applications," Microwave and Optical Technology Letters, vol. 40. pp. 399-401, 2004.

[106] S. Choi, H. Lee, K. Kwak, "Clover-Shaped Antenna for Ultra-Wideband Communications," Microwave and Optical Technology Letters, vol. 48, pp. 2111-2113, July 2006.

[107] J. Liang, C. Chiau, X. Chen and C. Parini, "Printed Circular Disc Monopole Antenna for Ultra-Wideband Applications," Electronics Letters, vol. 40, pp. 1246-1247, September 2004.

[108] N. Azenui and H. Yang, "Miniaturized Printed Circuit Board Antennas for Ultra-WideBand Applications," IEEE International Symposium on Antennas and Propagation, pp. 1639-1642, July 2006.

[109] C. Ying and Y. Zhang, "Integration of Ultra-Wideband Slot Antenna on LTCC Substrate," Electronics Letters, vol. 40, pp. 645-646, May 2004.

[110] E. Gazit, "Improved Design of the Vivaldi Antenna," IEE Proceedings, vol. 135, pp. 89-92, April 1988.

[111] E. Guillanton, J. Dauvignac, C. Pichot and J. Cashman, "A New Design Tapered Slot Antenna for Ultra-Wideband Applications," Microwave and Optical Technology Letters, vol. 19, pp.286-289, December 1998.

[112] J. Lee and J. Park, "Impedance Characteristics of Trapezoidal Ultra-Wideband Antennas with a Notch Function," Microwave and Optical Technology Letters, vol. 46, pp. 503-506, July 2005.

[113] Y. Kim and D. Kwon, "CPW-Fed Planar Ultra Wideband Antenna Having a Frequency Band Notch Function," Electronics Letters, vol. 40, pp. 403 – 405, April 2004.

[114] W. Lui, C. Cheng, Y. Cheng and H. Zhu, "Frequency Notched Ultra-Wideband Microstrip Slot Antenna with Fractal Tuning Stub," Electronics Letters, vol. 41, pp. 9-10, March 2005.

[115] M. Sadiku, "Numerical Techniques in Electromagnetics" CRC Press LLC., USA, 2001.

[116] A. Alshehri, A. Sebak and T. Denidni, "A Novel UWB Stepped-Trapezoidal Patch Antenna for Wireless Communications," The IASTED International Conference on Antennas, Radar and Wave Propagation (ARP 2008), USA, April 2008.

[117] R. DuHamel and F. Ore, "Logarithmic Periodic Antenna Designs," IRE National Convention Record, part 1, pp. 139-151, 1958.

[118] D. Kwon and Y Kim, "Suppression of Cable Leakage current for Edge-Fed Printed Dipole UWB Antennas Using Leakage-Blocking Slots," IEEE Antennas and Wireless Propagation Letters, vol. 5, pp.183-186, December 2006.

[119] A. Alshehri and A. Sebak, "A New Trimmed Notch-Cut Printed Antenna for UWB Wireless Application," 2008 European Electromagnetics International Conference (EUROEM 2008), Switzerland, July 2008.

[120] A. Alshehri and A. Sebak, "A New UWB Microstrip-Fed Planar Elliptical Patch Antenna for Wireless Communications," The 24th International Review of Progress in Applied Computational Electromagnetics (ACES 2008), Canada, April 2008.

[121] A. Alshehri and A. Sebak, "A Novel UWB Planar Patch Antenna for Wireless Communications," IEEE International Symposium on Antennas and Propagation, USA, July 2008.

[122] G. Schantz and G. Wolenec, "Ultra-Wideband Antenna Having Frequency Selectivity," U.S. Patent Publication no. 2003/0090436 A1, 2003.

[123] A. Alshehri and A. Sebak, "A Band-Rejected Printed Elliptical Antenna for UWB Wireless Communications," XXIX URSI General Assembly, USA, August 2008.